Technische Universität München
TUM School of Medicine and Health

The Effect of Vasoactive Intestinal Peptide on Intestinal Stem Cell Functions

Tatiana Agibalova

Vollständiger Abdruck der von der TUM School of Medicine and Health der Technischen Universität München zur Erlangung eines

Doctor of Philosophy (Ph.D.)

genehmigten Dissertation.

Vorsitz: Prof. Dr. Henning Wackerhage

Betreuer: Priv.-Doz. Dr. Moritz Middelhoff

Prüfende der Dissertation:

1. Prof. Dr. Dieter Saur
2. Prof. Dr. Dr. Ihsan Ekin Demir

Die Dissertation wurde am 25.07.2024 bei der TUM School of Medicine and Health der Technischen Universität München eingereicht und durch die TUM School of Medicine and Health am 20.09.2024 angenommen.

Parts of this thesis have been presented at the following conferences:

UEG week 2023, Copenhagen, Denmark

T. Agibalova, A. Ermolova, J. Wieland, I. E. Demir, D. Saur, B. Kohnke-Ertel, M. Quante, R. M. Schmid, and M. Middelhoff (2023). *The effect of vasoactive intestinal peptide on intestinal stem cell differentiation and activity.*

Visceral Medicine Congress 2021, Leipzig, Germany

T. Agibalova, J. Wieland, I. E. Demir, D. Saur, M. Quante, R. M. Schmid, and M. Middelhoff (2021). *Vasoactive intestinal peptide modulates intestinal stem cell activity and differentiation.*

Parts of this thesis have been submitted for publication:

T. Agibalova, A. Hempel, H. C. Maurer, M. Ragab, A. Ermolova, J. Wieland, C. Waldherr Ávila de Melo, F. Heindl, M. Giller, J. C. Fischer, M. Tschurtschenthaler, B. Kohnke-Ertel, R. Öllinger, K. Steiger, I. E. Demir, D. Saur, M. Quante, R. M. Schmid, and M. Middelhoff (2024). *Vasoactive intestinal peptide promotes secretory differentiation and mitigates radiation-induced intestinal Injury.* [Manuscript submitted to Stem Cell Research & Therapy].

Abstract

Intestinal stem cells (ISCs) are specialized cells that continuously regenerate the entire intestinal epithelial lining, ensuring the maintenance of intestinal homeostasis. The regulation of ISC proliferative activity and differentiation is modulated by a variety of signaling molecules within the ISC niche, including neuronal mediators secreted from the nerve fibers of the enteric nervous system as well as other non-neuronal sources.

In our study, we identified vasoactive intestinal peptide (VIP) as a potent modulator of stem cell behavior. VIP is a neuronal peptide widely distributed along the enteric nervous system and known for its wide range of effects, including regulation of intestinal motility, mucosal vasodilation, secretion, as well as modulation of immune cell functions. We assessed the impact of VIP on ISCs in homeostatic and injury conditions using a combination of *in vitro* organoid cultures and *in vivo* mouse models. Utilizing a model of murine intestinal organoids, we investigated the direct effects of VIP on intestinal epithelial cells and observed that VIP directs cellular differentiation towards secretory phenotype predominantly via the p38 MAPK pathway. Additionally, we found that VIP modulates epithelial proliferation as well as the number and proliferative activity of Lgr5-EGFP+ ISCs.

The regulation of ISCs is critical not only for maintaining intestinal integrity in homeostatic conditions but also for regenerating the epithelial lining after injury. Using an irradiation-based model of injury, we observed that irradiated Lgr5-EGFP+ ISCs became even more susceptible to modulations by VIP that resulted in the strong VIP-induced promotion of epithelial regeneration, improved cell survival, and reduced apoptosis *in vitro*. These effects translated into an *in vivo* model of abdominal irradiation, where intraperitoneal injections of VIP significantly mitigated radiation-induced intestinal injury and reduced inflammation in irradiated mice. This was further corroborated by alterations in cellular differentiation towards expansion of Lyz1+ Paneth cells in the intestinal epithelium of irradiated VIP-treated mice.

Taken together, our findings indicate a prominent role of VIP in modulating ISC behavior in intestinal homeostasis and its therapeutic potential to promote intestinal regeneration following acute irradiation injury.

Zusammenfassung

Intestinale Stammzellen sind spezialisierte Zellen, die kontinuierlich differenzierte Zellen des intestinalen Epithels generieren und darüber die Aufrechterhaltung der intestinalen Homöostase gewährleisten. Die proliferative Aktivität und Differenzierung intestinaler Stammzellen wird durch eine Vielzahl von Signalmolekülen innerhalb der Nische intestinaler Stammzellen modifiziert, einschließlich neuronaler Mediatoren, die von den Nervenfasern des enterischen Nervensystems sowie anderen nicht-neuronalen Quellen sezerniert werden.

In unserer Studie identifizierten wir vasoaktives intestinales Peptid (VIP) als einen potenten Modulator des Verhaltens von Stammzellen. VIP ist ein neuronales Peptid, das weit verbreitet entlang des enterischen Nervensystems vorkommt und für seine Vielzahl an Wirkungen bekannt ist, einschließlich der Regulation intestinaler Motilität, mukosaler Vasodilatation sowie epithelialer Sekretion und Modulation der Funktionen von Immunzellen. In der vorliegenden Arbeit untersuchten wir die Auswirkungen von VIP auf intestinale Stammzellen unter homöostatischen Bedingungen sowie nach akuter Gewebeschädigung mit Hilfe von *in vitro*-Organoidkulturen und *in vivo*-Mausmodellen. Unter Verwendung eines Modells muriner intestinaler Organoide untersuchten wir die direkten Effekte von VIP auf intestinale Epithelzellen und beobachteten, dass VIP die zelluläre Differenzierung überwiegend über den p38 MAPK-Weg in Richtung eines sekretorischen Phänotyps lenkt. Zusätzlich beobachteten wir, dass VIP die epitheliale Proliferation sowie die Anzahl und die proliferative Aktivität von Lgr5-EGFP+ intestinalen Stammzellen moduliert.

Die Regulierung von intestinalen Stammzellen ist nicht nur für die Aufrechterhaltung der intestinalen Integrität unter homöostatischen Bedingungen, sondern auch für die Regeneration des epithelialen Gewebes nach Verletzungen von entscheidender Bedeutung. Unter Verwendung eines strahlungsbasierten Verletzungsmodells beobachteten wir, dass bestrahlte Lgr5-EGFP+ intestinale Stammzellen noch anfälliger für Modulationen durch VIP wurden, was zu einer starken VIP-induzierten Förderung der epithelialen Regeneration, einer verbesserten Zellüberlebensrate und einer reduzierten Apoptose *in vitro* führte. Diese Effekte übersetzten sich in ein *in vivo*-Modell der abdominellen Bestrahlung, bei dem intraperitoneale Injektionen von VIP eine strahleninduzierte, intestinale Verletzung signifikant abmilderten und die Entzündungsreaktion bei bestrahlten Mäusen reduzierten. Dies wurde durch Veränderungen in der zellulären Differenzierung hin zur Expansion von Lyz1+ Paneth-Zellen im Darmepithel bestrahlter, VIP-behandelter Mäuse weiter bestätigt.

Zusammengefasst weisen unsere Ergebnisse auf eine wichtige Rolle von VIP bei der Modulation des Verhaltens intestinaler Stammzellen in intestinaler Homöostase hin und zeigen dessen therapeutisches Potenzial zur Förderung der intestinalen Regeneration nach akuten Bestrahlungsverletzungen auf.

Table of Contents

List of Figures

List of Tables

List of Abbreviations

ACTA1	Actin alpha 1
ARF	ADP-ribosylation factor
ATP	Adenosine Triphosphate
BCA	Bicinchoninic Acid
BMP	Bone Morphogenetic Protein
BSA	Bovine Serum Albumin
BrdU	Bromodeoxyuridine
CDKN1a	Cyclin-Dependent Kinase Inhibitor 1A
cDNA	Coding DNA
CFTR	Cystic Fibrosis Transmembrane Conductance Regulator
CNS	Central Nervous System
DAB	3,3'-Diaminobenzidine
DAG	Diacylglycerol
DCXR	Dicarbonyl and L-Xylulose Reductase
DMEM	Dulbecco's Modified Eagle Medium
DNA	Deoxyribonucleic Acid
DNBS	Dinitrobenzene Sulfonic Acid
DSS	Dextran Sulfate Sodium
EDTA	Ethylenediaminetetraacetic Acid
EdU	5-ethynyl-2’-deoxyuridine
EGF	Epidermal Growth Factor
EGFP	Enhanced Green Fluorescent Protein
ELISA	Enzyme-Linked Immunosorbent Assay
ENS	Enteric Nervous System
EPAC	Exchange Proteins Activated by cAMP
ERK	Extracellular Signal-Regulated Kinase
FACS	Fluorescence-Activated Cell Sorting
FBS	Fetal Bovine Serum
FDR	False Discovery Rate
FFPE	Formalin-Fixed Paraffin-Embedded
GHRH	Growth Hormone-Releasing Hormone
GI	Gastrointestinal

GLP-2	Glucagon-Like Peptide 2
GPCR	G-Protein Coupled Receptor
GSEA	Gene Set Enrichment Analysis
H&E	Hematoxylin and Eosin
HEPES	4-(2-hydroxyethyl)-1-piperazineethanesulfonic acid
IBD	Inflammatory Bowel Disease
IHC	Immunohistochemistry
IP3	Inositol 1,4,5-trisphosphate
IR	Ionizing Radiation
ISC	Intestinal Stem Cell
JNK	c-Jun N-terminal Kinase
JUP	Junction Plakoglobin
KO	Knockout
LGR5	Leucine-Rich Repeat-Containing G Protein-Coupled Receptor 5
LQ	Linear-Quadratic
LYZ1	Lysozyme 1
MAPK	Mitogen-Activated Protein Kinase
M3R	Muscarinic acetylcholine Receptor M3
MPTP	1-Methyl-4-Phenyl-1,2,3,6-Tetrahydropyridine
MUC2	Mucin 2
NES	Normalized Enrichment Score
NF-κB	Nuclear Factor Kappa-light-chain-enhancer of activated B cells
NO	Nitric Oxid
NPY	Neuropeptide Y
NHEJ	Non-Homologous End Joining
PACAP	Pituitary Adenylate Cyclase-Activating Polypeptide
PBS	Phosphate-Buffered Saline
PCA	Principal Component Analysis
PFA	Paraformaldehyde
PKA	Protein Kinase A
PKC	Protein Kinase C
PLD	Phospholipase D
PLC	Phospholipase C
qPCR	Quantitative Polymerase Chain Reaction
RNA	Ribonucleic Acid

RT	Room Temperature
SEM	Standard Error of Mean
SERT	Serotonin transporter
TBS	Tris-Buffered Saline
TNF-alpha	Tumor Necrosis Factor-alpha
TSO	Template Switch Oligo
TTX	Tetrodotoxin
TUNEL	Terminal deoxynucleotidyl transferase dUTP nick end labeling
UMIs	Unique Molecular Identifiers
VIP	Vasoactive Intestinal Peptide
WT	Wild-type
4-OHT	4-Hydroxytamoxifen

1. INTRODUCTION

1.1 Structure and functions of the small intestinal epithelium

The small intestinal epithelial barrier is essential for the optimal functioning of the human body, enabling digestion, nutrient absorption, protection against pathogens, and facilitating waste elimination. The epithelial lining of the small intestine is composed of villi, which are digit-like protrusions and pocket-like structures known as crypts. Each villus is covered with a single layer of epithelial cells that, in turn, have small protrusions on their apical membrane called microvilli. These formations significantly enhance the surface area available for nutrient uptake, thereby facilitating efficient nutrient absorption (Gehart & Clevers, 2019).

The intestinal epithelial lining is constantly affected by harsh conditions within the intestinal lumen, which include changes in pH levels or pathogens, as well as mechanical stress caused by the passage of food and bowel movements. The integrity of this barrier is maintained through a rapid turnover process, in which cells are constantly renewed to repair any damage. The intestinal epithelium is the most rapidly self-renewing tissue in the human body that achieves a complete renewal of its cellular layer within 4-5 days (Vermeulen & Snippert, 2014). This process of generating new cells relies on the activity of adult intestinal stem cells (ISCs) that continuously divide to create progenitor cells, which differentiate into all other specialized cell types, each with specific functions ranging from nutrient absorption and pathogen defense to cellular communication. ISCs reside at the bottom of crypts, which not only serve as physical protection from pathogens and luminal contents but also provide a specialized microenvironment that is rich in molecular signals and factors necessary for stem cell maintenance (Sailaja et al., 2016).

As ISCs divide, they give rise to daughter cells, which then move upwards from the base of the crypts into the transit-amplifying zone. The cells in this zone are characterized by their rapid division rate. After 2-3 rounds of division, cells begin to differentiate into specialized cell types that make up the intestinal epithelial lining. Following differentiation, mature cells continue their migration upwards along the villus until reaching the villus tip, where they undergo apoptosis and are shed into the lumen (Barker, 2014).

Around 90% of all intestinal epithelial cells are **enterocytes.** The primary function of these cells is the absorption of nutrients, water, and ions, as well as the uptake and processing of antigens. In addition, enterocytes play a pivotal role in maintaining the intestinal barrier, which

prevents pathogens and toxins from entering the bloodstream. The barrier function is achieved by tight junctions that can be dynamically regulated to ensure a balance between protective function and selective macromolecule transport (Snoeck et al., 2005).

Goblet cells are mucus-producing cells that are scattered among enterocytes and other cell types within the intestinal epithelium, comprising 8-10% of all epithelial cells in the intestinal lining. Goblet cells produce glycoproteins, known as mucins, which are the primary components of the mucus layer that covers the epithelial surface of the intestine. The mucus layer acts as a physical barrier that shields epithelial cells from pathogens, digestive enzymes, and food particles, thereby protecting them against damage and infection. Moreover, the compounds of the mucus layer are toxic to some bacteria, thereby contributing to the immune defense (Gustafsson & Johansson, 2022).

Enteroendocrine cells are specialized cells vital for cell-cell communication and interactions within the intestinal environment. These cells respond to various stimuli, including those from ingested food, secreted by pathogens, or produced by other cells, and orchestrate appropriate physiological responses. They release molecules that can be sensed by nerves, enter the bloodstream, or be detected by neighboring epithelial cells, thereby triggering changes in gut motility, blood flow, and secretion necessary for food absorption. Additionally, these cells can influence insulin release, regulate appetite, or induce vomiting through hormonal or neuronal pathways (Sternini et al., 2008).

Tuft cells serve as chemosensory cells and can be identified by a tuft of microvilli present on the apical membrane of cells. They can sense and respond to different chemical signals, including those released by pathogens. Upon activation by certain stimuli, tuft cells initiate an immune response by releasing cytokines and other signaling molecules that recruit and activate immune cells (Schneider et al., 2019).

Paneth cells are interspersed among ISCs at the base of intestinal crypts. Unlike many epithelial cell types, Paneth cells have a longer lifespan of about 60 days (Ireland et al., 2005). Paneth cells secrete factors such as Wnt3, Notch ligand Dll4, EGF, and TGF-alpha that are essential for ISC maintenance (Sato et al., 2011). Additionally, they secrete antibacterial components, such as lysozyme and cryptdins/defensins. These antimicrobials are crucial for preventing pathogen invasions into the crypts, thus contributing to the mucosal antimicrobial barrier (Bevins & Salzman, 2011).

1.2 Lgr5+ intestinal stem cells and the stem cell niche

Stem cells are defined by their ability to self-renew and give rise to differentiated progeny. Among the many identified markers for ISCs, Lgr5 (Leucine-rich repeat-containing G-protein coupled receptor 5) emerged as the most prominent and well-established marker for active ISCs. Lgr5+ ISCs are known for their high proliferative activity, dividing approximately every 24 hours (Barker et al., 2007).

In many tissues, stem cells undergo asymmetrical division, with one daughter cell retaining a stem cell character and the other destined to differentiate. In the intestine, however, stem cells give rise to two cells that have equal intrinsic abilities to become a stem cell – a process called symmetrical division. However, due to restricted space in the intestinal crypt, one cell will be displaced from the crypt and undergo differentiation (Snippert et al., 2010).

Each crypt contains multiple ISCs that constantly replace each other in a dynamic process. This ongoing replacement, driven by the limited space within the crypt, results in some ISCs being lost and replaced by the offspring of neighboring ISCs. Over time, typically within 1-6 months, one clone will stochastically replace other clones in a process defined as neutral drift (Lopez-Garcia et al., 2010).

Interestingly, the position of an Lgr5+ ISC within the crypt is crucial for its long-term viability and clonal formation potential. Cells located further away from the crypt bottom are more likely to be displaced and subsequently lost, reducing their chances of long-term clone formation. Specifically, ISCs near the crypt center are about three times more likely to colonize a crypt than those at the niche boundary (Ritsma et al., 2014). However, the retrograde movement of ISCs from the crypt border back to the crypt base, driven by Wnt signaling, also plays a significant role in determining the population of ISCs capable of creating clones that persist over time (Azkanaz et al., 2022).

Wnt signaling is a major component of the ISC niche, a specialized microenvironment characterized by its unique cellular composition, extracellular matrix, and signaling molecules that provide necessary support and signals for stem cell self-renewal and differentiation (Figure 1).

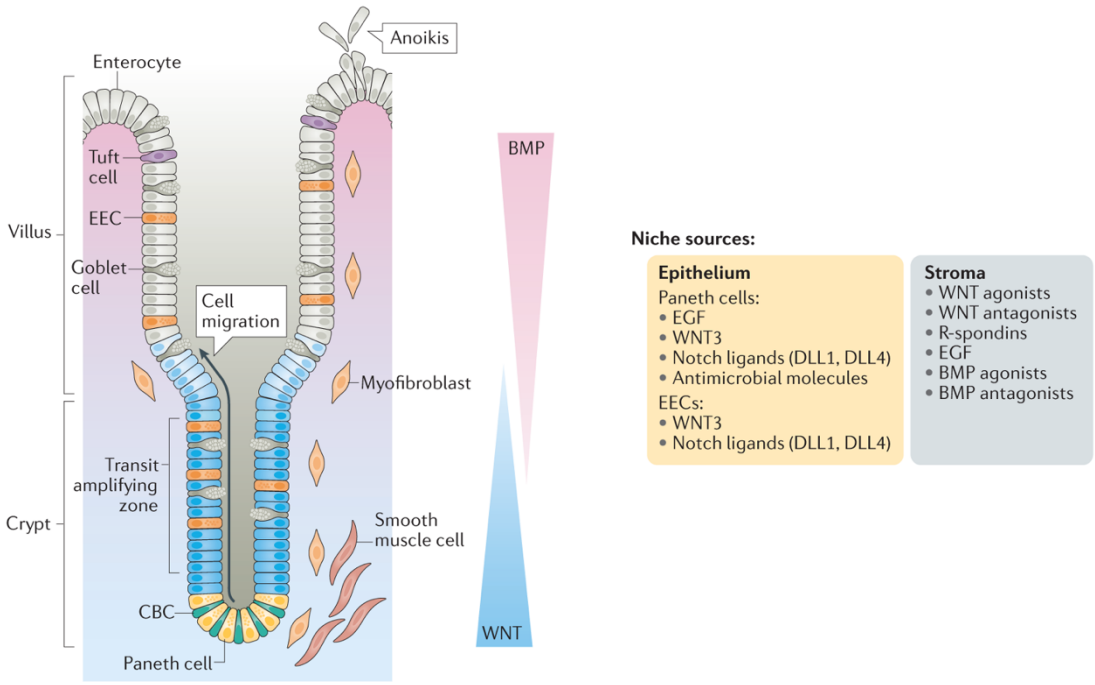

Figure 1. Schematic of the intestinal cell composition and regulatory signals in the stem cell niche.
Adapted from (Beumer & Clevers, 2021).

Wnt factors are typically produced by Paneth cells and mesenchymal cells surrounding crypts (Farin et al., 2012). R-spondin 1-4 are ligands originating from the stroma and signaling through the Wnt pathway. The presence of R-spondins, along with other Wnt ligands, prevents ISCs from undergoing their default fate of differentiation. Additionally, Wnt proteins are essential for maintaining R-spondin receptor expression, and R-spondin, in turn, drives the expansion of ISCs (Yan et al., 2017).

Paneth cells also provide Notch signals that are highly involved in the maintenance of ISCs (Pellegrinet et al., 2011). Blocking Notch signaling results in ISC depletion, which can be rescued by attenuation of Wnt signaling, thus demonstrating the interplay and opposing activities of Wnt and Notch signaling pathways. Notch signaling is crucial for regulating Wnt levels that enable the proper functioning of ISCs (Tian et al., 2015). Moreover, Notch signaling plays a distinct role in cell differentiation, negatively regulating the fate of secretory cells while promoting the development of absorptive cells (VanDussen et al., 2012).

Bone Morphogenetic Protein (BMP) signaling is another critical regulator within the ISC niche. Unlike Wnt and Notch signaling pathways, BMP signaling negatively regulates stem cell characteristics and promotes cell differentiation. Its activity increases in differentiated cells and

reaches its peak at the tips of the villi, creating a gradient essential for a balance between proliferation at the crypt base and differentiation as cells migrate upwards. This gradient is maintained by BMP signaling inhibitors that are secreted from mesenchymal cell populations, such as myofibroblasts and smooth muscle cells. These inhibitors specifically target BMP signaling to prevent premature differentiation at the crypt base, thereby preserving the potential of ISCs for self-renewal (McCarthy et al., 2020).

1.3 Intestinal stem cells and irradiation-induced injury

The gastrointestinal (GI) tract is extremely sensitive to irradiation (Ki et al., 2014). High doses of irradiation lead to the development of acute GI syndrome characterized by cell damage of the intestinal epithelial lining, resulting in a compromised intestinal barrier, infection, dehydration, and electrolyte imbalances (Kaur & Potten, 1986; Potten, 1990). One of the primary effects of irradiation is the induction of DNA double-strand breaks, which results in p53-mediated cell cycle arrest and massive apoptosis of cycling cells, reaching a peak at approximately 6 hours post-irradiation. The second wave of cell death, known as mitotic death, occurs as cells with unrepaired DNA attempt to re-enter the cell cycle (Kirsch et al., 2010).

Lgr5+ ISCs exhibit particular sensitivity to irradiation, compromising their ability to replenish cells lost in apoptosis (Metcalfe et al., 2014). Moreover, an aberrant signaling from the ISC niche, induced by irradiation, also contributes to impaired regeneration (Martinez et al., 2021). The persisting cell migration along the crypt-villus axis, massive cell death, and impaired functions of ISCs result in crypt shrinkage within 24-48 hours (Kaur & Potten, 1986; Potten, 1990).

Nevertheless, the intestine demonstrates a significant capacity to withstand and eventually recover from such damage, regenerating new crypts over time. Despite the vulnerability of Lgr5+ ISCs, their DNA repair mechanisms are more efficient than those in TA zone cells and differentiated cells. This difference is attributed to the fact that Lgr5+ ISCs effectively utilize homologous recombination in addition to non-homologous end joining (NHEJ) DNA repair (Hua et al., 2012). While the maintenance of the intestinal epithelium is still possible after the depletion of Lgr5+ cells under physiological conditions, the recovery after irradiation-induced injury entirely relies on Lgr5+ ISCs, highlighting that these cells are indispensable for intestinal tissue regeneration (Metcalfe et al., 2014; Tian et al., 2011).

The intestinal lining demonstrates a high level of cell plasticity in response to different injury conditions, including irradiation-induced injury. Different lineage-restricted progenitor cells or even fully committed Paneth cells can revert or dedifferentiate to a stem-like state. This allows them to acquire the ability to proliferate and replenish lost cells, thereby contributing to tissue repair and regeneration (Schmitt et al., 2018; Tetteh et al., 2016; Tian et al., 2011; S. Yu et al., 2018).

1.4 Enteric nervous system

The enteric nervous system (ENS) is the largest and most complex component of the peripheral nervous system that resides within the wall of the GI tract. It has a unique ability to function autonomously, regulating GI behavior independently of the input from the central nervous system (CNS). Despite this autonomy, the ENS maintains a dynamic interaction with the CNS through afferent and efferent fibers of the vagus nerve (Walsh & Zemper, 2019).

The ENS interacts with various intestinal cell types to modulate a wide range of processes, including motility, secretion, absorption, inflammation, and pain perception. It is organized into two main neural plexuses: the myenteric plexus located between the longitudinal and circular muscle layers, which primarily controls GI motility; and the submucosal plexus found in the submucosa, regulating enzyme secretion, blood flow, and absorption (Figure 2). The ENS comprises approximately 100 million neurons and secretes numerous neuronal mediators, most of which are identical to those found in the CNS (Nezami & Srinivasan, 2010; Rao & Gershon, 2016; Sharkey & Mawe, 2023).

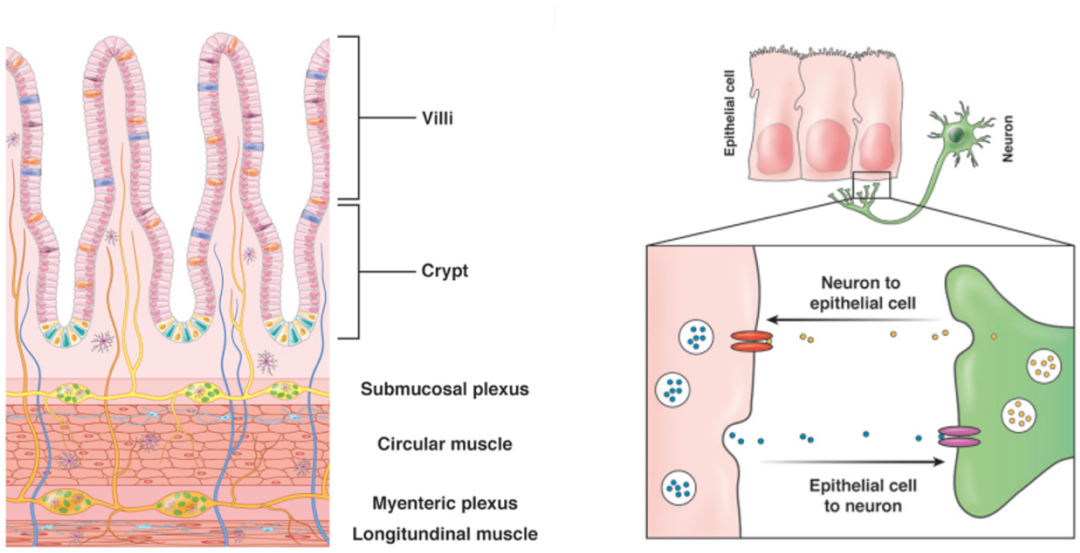

Figure 2. Anatomy of the intestinal epithelium and the enteric nervous system. Adapted from (Walsh & Zemper, 2019).

Several reports suggest that the ENS plays a significant role not only in regulating gut motility and secretion but also in modulating stem cell behavior that results in altered proliferation and differentiation. For example, antagonizing muscarinic acetylcholine receptors alters intestinal

differentiation, leading to a selective expansion of tuft cells. Additionally, cholinergic blockade induces a reduction in the Lgr5+ stem cell proliferative activity (Middelhoff et al., 2020). Cholinergic neurons also play a role in the gut healing process by activating nicotinic receptors on enterocytes, which help transition to homeostasis after injury (Petsakou et al., 2023).

Norepinephrine increases epithelial proliferation and wound healing via α2A adrenergic receptor. Sympathetic signaling through this receptor also stimulates stem cell functions and decreases differentiation (ten Hove et al., 2023).

Serotonin has been implicated in upregulation of cell proliferation within intestinal crypts (Tutton, 1974). Furthermore, serotonin re-uptake transporter knock-out (SERT KO) mice showed significantly taller villi, deeper crypts, and increased enterocyte proliferation. However, there were no significant differences in cellular composition along the villi between SERT KO and wild-type genotypes (Tackett et al., 2017). Notably, it has been shown that serotonin-induced mucosal growth and cell turnover of the intestinal epithelium are mediated by serotonin of neuronal origin rather than serotonin originating from enteroendocrine cells of the mucosa. These effects on the murine mucosa, however, were shown to be indirect and caused by serotonergic activation of cholinergic neurons (Gross et al., 2012).

Substance P is known to induce the proliferation of cytokine pre-treated human epithelial cells in the colon. This effect is predominantly mediated through the activation of NK-1 receptor (NK1R), as demonstrated by the complete blockade of Substance P-induced proliferation in a cytokine-treated cell by an NK1R-specific antagonist (Goode et al., 2003). In more detail, the activation of NK1R results in the stimulation of EGFR and MAPK signaling pathways via a metalloprotease-dependent mechanism, which, in turn, promotes colonic cell proliferation (Koon et al., 2004).

The research on Neuropeptide Y (NPY) has been primarily focused on its role in secretion, immune modulation, and gut motility. It has been shown, however, that NPY also significantly induces the expression of villin, an early marker of cell differentiation, that could be linked to its role in enhancing migration and reducing adhesion in small intestinal cells (Lee et al., 2005).

1.5 Vasoactive intestinal peptide and its receptors

Vasoactive intestinal peptide (VIP) is a 28-amino acid peptide that was first isolated from the porcine small intestine and identified as a substance inducing vasodilation and regulating arterial blood pressure (Said & Mutt, 1972). Subsequent research revealed that VIP is involved in a variety of physiological processes in the CNS, pancreas, lungs, and intestines (Dickson & Finlayson, 2009). Given its wide-ranging biological effects, VIP is currently being explored as a therapeutic agent for several conditions, such as inflammatory bowel disease (IBD), sepsis, diabetes, and pulmonary diseases, including COVID-19 (Abad et al., 2012; Deng et al., 2010; Sanlioglu et al., 2012; Zhong et al., 2023).

VIP belongs to a family of structurally similar peptides that includes pituitary adenylate cyclase-activating polypeptide (PACAP), secretin, glucagon, and growth hormone-releasing hormone (GHRH). Notably, VIP shares a significant sequence homology with PACAP, demonstrating a 68% similarity (Langer et al., 2022). It is synthesized in nerves as well as in immune cells, such as lymphocytes (Leceta et al., 1996), and its expression has also been detected in certain cancer cells where it can function in an autocrine manner (I. H. Rao et al., 2023).

VIP primarily interacts with the VIPR1 and VIPR2 (also known as VPAC1 and VPAC2, respectively), as well as PAC1 receptors that are widely distributed throughout the body and can activate a broad range of signaling pathways. These receptors belong to class B of the secretin-like G-protein coupled receptors (GPCR) and respond to molecules of different sizes. While the VIPR1 and VIPR2 display a similar affinity for both VIP and PACAP, the PAC1 receptor predominantly binds to PACAP, showing a significantly lower affinity for VIP (Langer et al., 2022). VIPR1 is more abundant in the brain, T-lymphocytes, liver, lungs, and intestines, whereas VIPR2 is found in the hippocampus, brain stem, spinal cord, and smooth muscles. Interestingly, VIPR1 was reported to be overexpressed in the majority of human tumors, including colon, breast, lung, thyroid, and prostate cancers. In contrast, the overexpression of VIPR2 was detected only in a few cancers, like leiomyomas and GI stromal tumors. Additionally, VIPR signaling was associated with tumor progression of a certain number of malignancies, making VIP receptors promising targets for cancer diagnostics and therapy (Tang et al., 2014).

Upon VIP binding, the receptor undergoes a conformational change that results in the interaction of the intracellular loop of the receptor with the G-protein. This triggers multiple downstream signaling cascades, such as cAMP production, protein kinase A (PKA) and

phospholipase C (PLC) activation, inositol phosphate turnover, as well as activation of the MAPK and NF-κB pathways (Figure 3) (Tang et al., 2014).

One of the most common outcomes of cAMP accumulation is the activation of PKA. This kinase phosphorylates numerous target proteins, leading to diverse cell responses, such as stimulation and differentiation of neuronal stem cells, as well as neuroblast differentiation. This signaling also stimulates secretion and proliferation of pituitary cells via activating the extracellular signal-regulated kinase (ERK) phosphorylation. In different cancer cell lines, PKA promotes cell proliferation and cell survival via the ERK pathway, and in the immune system, it mediates the anti-inflammatory properties of VIP by regulating cytokine production. Apart from PKA, cAMP can also activate exchange proteins activated by cAMP (EPAC), which induces anti-inflammatory transcription factors (Langer et al., 2022; Lu et al., 2022).

VIP binding to the receptor can also activate PLC through the $G_{i/o}$ and $G_{q/11}$ proteins, leading to the formation of diacylglycerol (DAG) and inositol 1,4,5-trisphosphate (IP3). This results in the activation of protein kinase C (PKC) by DAG and calcium release from the endoplasmic reticulum by IP3. This pathway is responsible for cell migration, secretion of neurotransmitters, and glial cell differentiation.

The PKA and PKC-dependent activation of mitogen-activated protein kinases (MAPK) by VIP includes the activation of ERK1/2, JNK, and p38 MAPK pathways. These pathways are involved in the regulation of cell proliferation, differentiation, survival, and inflammation.

VIP can also induce phosphatidyl inositol 3 kinase (PI3K) activation, leading to Akt phosphorylation. The PI3K-Akt signaling pathway plays a role in insulin secretion by pancreatic cells, as well as neuroendocrine cell differentiation. Additionally, VIP can stimulate phospholipase D (PLD) independently of G protein through the activation of ADP-ribosylation factor (ARF) (Langer et al., 2022; Lu et al., 2022; Tang et al., 2014).

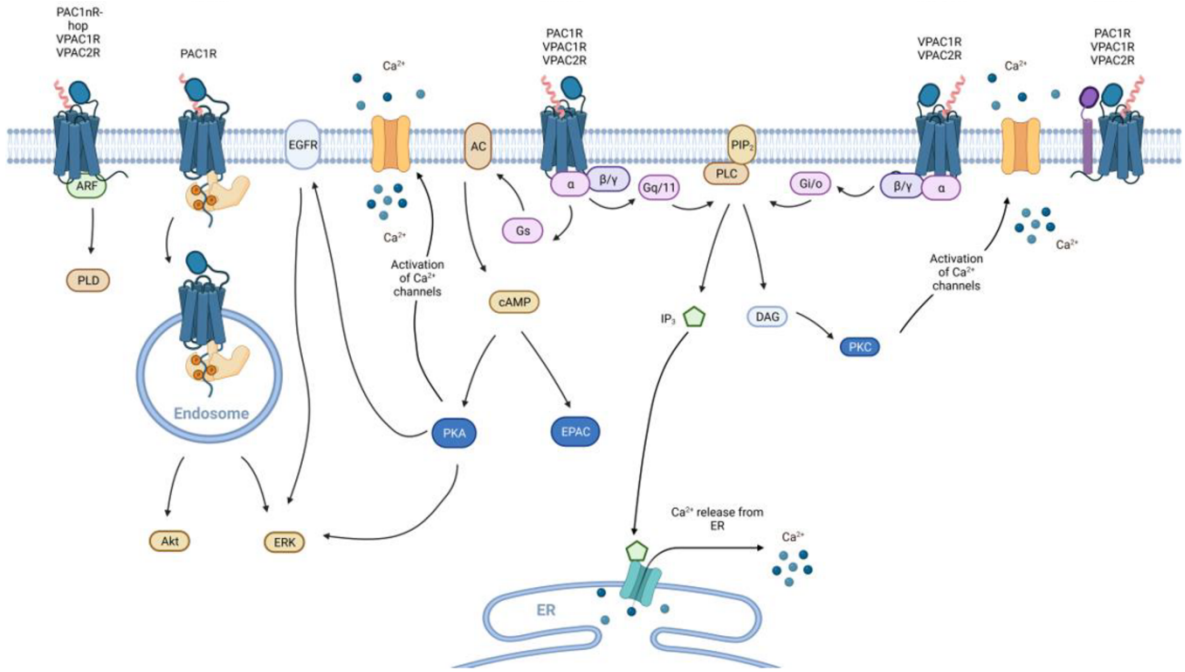

Figure 3. Molecular mechanisms of VIP signal transduction.
Adapted from (Lu et al., 2022).

1.6 VIP in the regulation of intestinal epithelial cell types

In the intestinal epithelium, VIP primarily acts through the VIPR1 receptor, gene expression of which is around 300-fold higher than that of VIPR2 and PAC1 in the murine mucosa. The highest expression level of VIPR1 is detected in the murine proximal colon, followed by the distal colon and jejunal and ileal segments of the small intestine (Jayawardena et al., 2017). In the human small intestine, the expression of VIPR1 at both gene and protein levels was detected in all epithelial compartments along the crypt-villus axis, with the highest expression in the basal portion of the crypts, where immunoreactivity was predominantly confined to the plasma membrane (Haber et al., 2017; Schulz et al., 2004). Also, mRNA expression of VIP was reported in the bottom of crypts in human colonic mucosa, yet with no detectable protein product (Jönsson et al., 2012).

Several knockout (KO) studies have reported abnormalities in the small bowel of VIP KO mice. Specifically, these mice demonstrate significantly increased villus length and crypt depth, along with a reduction in mucus secretion, thickened muscle layers, and impaired GI transit (Lelievre et al., 2007; Wu et al., 2015; Yusta et al., 2012). Molecular analysis revealed reduced levels of Lysozyme, Defcr-rs1, Cryptdin 5, and RegIII-alpha mRNA transcripts in Paneth cells from the VIP KO jejunum (Yusta et al., 2012). Furthermore, VIP KO mice show a marked decrease in the numbers of Muc2+ goblet cells in the colon; this phenotype, however, can be rescued by VIP administration (Wu et al., 2015). Additionally, VIP deficiency induces increased proliferation in intestinal crypts of the small intestine of VIP KO mice (Yusta et al., 2012). This pattern of increased proliferation is also observed in mice deficient in VIPR1, suggesting a crucial role of VIPR1 signaling in regulating intestinal cell growth and function (Fabricius et al., 2011).

Several studies have also explored the direct effects of VIP on the intestinal epithelium. For instance, VIP enhanced Muc2 gene expression in human colonic epithelial cells via activation of the p38 and MEK/ERK signaling pathways (Hokari et al., 2005). In addition, blocking VIP receptors *ex vivo* has been shown to reduce goblet cell numbers in an organotypic slice of the murine ileum (Schwerdtfeger & Tobet, 2020). A co-culture model consisting of a human submucosa with the submucosal plexus and a human colonic epithelial monolayer has identified VIP as an anti-proliferative mediator. In this study, electrical activation of submucosal neurons maintained monolayer organization and decreased cell proliferation. Both tetrodotoxin (TTX) and a VIP receptor antagonist blocked these effects, leading to an increased proportion of proliferating cells and greater cell density. Conversely, VIP treatment

in the presence of TTX reproduced the originally observed anti-proliferative effects (Toumi et al., 2003).

Other effects of VIP on intestinal epithelial cells include stimulating molecular transport across enterocyte membranes and regulating epithelial permeability. VIP activates ion channels and transporters crucial for electrolyte and fluid secretion (Banks et al., 2005). For instance, in the murine duodenum, VIP induces HCO_3^- secretion by activating the cystic fibrosis transmembrane conductance regulator (CFTR) in a protein kinase A-dependent manner, while in the ileum and the colon, it increases the secretion of Cl^- and HCO_3^- (Iwasaki et al., 2019). In addition, VIP promotes transcellular calcium transport in colonic cells *in vitro* (Rodrat et al., 2022). In colitis models, VIP plays a critical role in maintaining intestinal barrier integrity by increasing the expression of the junctional proteins claudin-3 and claudin-4 (Morampudi et al., 2015; Seo et al., 2019). Furthermore, VIP prevents the translocation of tight junction proteins, such as zonula occludens-1, occludin, and claudin-3, from the lateral membrane to the cytoplasm in *Citrobacter rodentium*-induced colitis (Conlin et al., 2009).

1.7 VIP in pathological conditions of the gastrointestinal tract

VIP has been proposed as a potential pharmacological target for various GI pathological conditions due to its ability to alleviate symptoms and modify disease progression. The colonic mucosa of patients undergoing irradiation therapy exhibits an elevated expression of VIP, which coincides with the occurrence of inflammatory and repair processes (Höckerfelt et al., 2000). Furthermore, evidence from experimental mouse models of intestinal inflammation and infection demonstrates that VIP KO mice appear more susceptible to injury (Wu et al., 2015; H. B. Yu et al., 2021).

Various mechanisms contribute to the protective effects of VIP. For instance, VIP alleviates epithelial apoptosis and mitochondrial damage primarily by lowering oxidative damage in *Citrobacter rodentium*-infected colonic cells (Maiti et al., 2018). Another study demonstrates that in mice infected with the same pathogen, VIP promotes the recruitment of group 3 innate lymphoid cells that contribute to host-defense mechanisms (H. B. Yu et al., 2021). In a mouse model of Crohn's disease, VIP downregulates inflammatory and Th1-driven autoimmune responses, thereby effectively mitigating the symptoms of trinitrobenzene sulfonic acid (TNBS)-induced colitis (Abad et al., 2003). Similarly, VIP and its analogues not only decrease inflammation but also increase the expression of tight junction proteins in models of necrotizing enterocolitis or TNBS-induced colitis (Seo et al., 2019; Xu et al., 2018). Regulation of tight junction proteins and intestinal permeability by VIP has also been demonstrated during enteropathogenic *Escherichia coli* infection of colonic cell monolayers (Morampudi et al., 2015).

Although many studies highlight the beneficial effects of VIP signaling in various colitis models, some findings are contradictory. For instance, female VIP KO mice exhibited resistance to dextran sulfate sodium (DSS)-induced colitis (Yusta et al., 2012). Similarly, resistance to this type of colitis was observed in cases where VIP was genetically deleted or its receptors were pharmacologically blocked (Vu et al., 2014).

VIP has also been studied in the context of colon cancer. Inhibition of VIP signaling reduced cell proliferation in a colonic cancer cell line and reduced the tumor volume, staging, lymphocyte infiltrate, and the number of dysplastic crypts *in vivo* (Levy et al., 2002). Moreover, VIPR antagonist treatment of CT26 tumor-bearing mice also reduced tumor growth. This reduction occurred more due to the increased polarization and phagocytosis of macrophages rather than a direct effect of VIP signaling on tumor cells (Kittikulsuth et al., 2023).

Aims of the study

The initial aim of this study was to identify neuronal mediators that can directly regulate the activity of intestinal stem cells. After identifying VIP as a crucial regulator of stem cell functions, the primary objective became to explore the role of VIP in modulating the behavior of ISCs under conditions of stress and homeostasis, using intestinal organoids as a model system.

The next objective was to elucidate how VIP influences cellular differentiation, which is a critical aspect of ISC behavior. This involves exploring key VIP signaling pathways to determine the mechanisms through which VIP modulates cellular differentiation.

Additionally, the study aims to characterize the direct effects of VIP on the ISC pool and its proliferative activity by evaluating the progeny pool of these ISCs, as well as assessing the overall impact of VIP on cell proliferation.

Furthermore, this study will evaluate the therapeutic potential of VIP, investigating its role as either a preventive or mitigative agent to enhance recovery in intestinal tissues damaged by irradiation. These investigations are expected to provide significant insights into the direct regenerative effects of VIP on intestinal epithelial cells, alongside its known impact on immune cells, potentially leading to the development of novel clinical approaches.

Finally, by conducting experimental analyses on mice, including molecular analyses and histological examinations, this research aims to clarify how results obtained *in vitro* can be applied *in vivo*. This comprehensive approach not only addresses significant scientific questions but also offers insights into the field of regenerative medicine.

2. METHODS

2.1 Animals

2.1.1 Animal lines and husbandry

All animal experiments were approved by the District Government of Upper Bavaria (Regierung von Oberbayern) and performed in accordance with the German Animal Welfare and Ethical Guidelines of the Klinikum rechts der Isar, TUM, Munich, Germany.

Female and male adult mice were aged between 6 and 12 weeks at the time of sacrifice. C57Bl6/J (Strain #000664), *Lgr5*-eGFP-IRES-CreER^{T2} (Strain #008875), *R26*R-LSL-TdTomato (Strain #007909) mice were obtained from the Jackson Laboratory (USA). For lineage tracing experiments, *Lgr5*-EGFP-IRES-CreER^{T2} were crossed with *R26*R-LSL-TdTomato mice to obtain *Lgr5*-EGFP-IRES-CreER^{T2}+/- *R26*R-LSL-TdTomato+/- progeny.

All mice were maintained and bred under specific pathogen-free conditions and provided with the standard chow diet (ssniff, Spezialdiäten GmbH, Soest, Germany) and water *ad libitum* in the animal facility of Klinikum rechts der Isar of Technische Universität München. At the time of weaning (3 weeks after birth), mice were assigned specific Lab IDs via ear clipping. The clipped ear tissues were used for subsequent genotyping to identify the presence of specific genes.

2.1.2 DNA extraction and genotyping

The clipped ear tissues were lysed in 200 µl of DirectPCR® Lysis Reagent Tail (31-102-T, Peqlab) supplemented with 2 µl Proteinase K (03115828001, Roche) overnight at 55°C at 300-500 rpm in a ThermoMixer F1.5 (Eppendorf). The samples were then heated to 85°C for 1 hour to inactivate the enzyme and stored at 4°C prior to the analysis.

For each gene, 9 µl of the PCR Master mix (Table 1) were mixed with 1 µl of tissue lysate used as a DNA input.

Table 1. PCR Master mix

Ingredient	**Volume, µl**
Distilled water	2x(Number of samples+2)

GoTaq® Green Master Mix (M7422, Promega)	5x(Number of samples+2)
Primers (10 mM each primer)	2x(Number of samples+2)

Genotyping primers were ordered from Sigma-Aldrich as 100 μM stock solutions in dH20 and kept at -20°C for long-term storage. For genotyping, primers were mixed accordingly and diluted with distilled water to a concentration of 10 μM. The primer sequences are listed in Table 2.

Table 2. PCR primer sequences

Primer	**Sequence (5´-3´)**	**Product, base pairs**
Lgr5CreERT-eGFP common forward	CTG CTC TCT GCT CCC AGT CT	WT: 298 MT: 174
Lgr5CreERT-eGFP WT reverse	ATA CCC CAT CCC TTT TGA GC	
Lgr5CreERT-eGFP MT reverse	GAA CTT CAG GGT CAG CTT GC	
LSL-TdRed MT forward	CTG TTC CTG TAC GGC ATG G	WT: 297 MT: 196
LSL-TdRed MT reverse	GGC ATT AAA GCA GCG TAT CC	
LSL-TdRed WT forward	AAG GGA GCT GCA GTG GAG TA	
LSL-TdRed WT reverse	CCG AAA ATC TGT GGG AAG TC	

PCR reactions were performed in a Thermal Cycler (T100, Biorad) with parameters outlined in Table 3.

Table 3. PCR reaction conditions

Lgr5CreERT-eGFP				**LSL-TdRed**		
	Temperature	Duration	Cycles	Temperature	Duration	Cycles
Initialization	94ºC	3 min	1x	95ºC	3 min	1x
Denaturation	94ºC	30 sec	35x	95ºC	30 sec	35x
Annealing	58ºC	40 sec		61ºC	1 min	
Extension	65ºC	1 min		72ºC	1 min	
Final elongation	65ºC	3 min	1x	72ºC	3 min	1x
Final hold	10ºC	∞		10ºC	∞	

To prepare a 2.5% agarose gel for electrophoresis, 7.5 g of agarose (Biozym, Hess. Oldendorf) was dissolved in 300 ml of TAE buffer (840004, Biozym) by heating in a microwave oven. After the agarose was shortly cooled at room temperature (RT), 15 μl of ROTI®GelStain (Roth) was added to the agarose solution. The solution was then poured into an electrophoresis chamber (Bio-Rad) and allowed to solidify. Electrophoresis of the PCR products was performed at a constant voltage of 120 V for 60-90 minutes, and a 100 bp ladder (N0467L, BioLabs) was added to the gel for the band size estimation. The results were visualized under UV light on a Gel Doc™ XR system (EX/EM 312/516-518 nm) (Bio-Rad) using Quantity One software (Bio-Rad).

2.2 Tissue processing

2.2.1 Sample collection

Mice were euthanized by an overdose of isoflurane (798-932, cp-pharma) and cervical dislocation at the age of 6-12 weeks. The small intestine was removed from the body, and its length was measured using a ruler. The small intestine was divided into three equal parts, and the middle segment was identified as the jejunum. The proximal 2-3 cm of the jejunum were used for histological analysis. Additionally, two small pieces of the jejunum (3 mm each) were

placed on tissue paper to remove excess water, weighed, snap-frozen in liquid nitrogen, and stored at -80°C for subsequent ELISA analysis. The rest of the jejunum was used for crypt collection.

For histological analysis, the intestine was cut open, preserved in a Swiss roll configuration using a cotton-tipped applicator (11969, Lohmann&Rauscher), and placed into a histological cassette (7-0009, neoLab) for overnight incubation in 4% (v/v) paraformaldehyde (PFA) (MRI Apotheke). On the following day, the cotton-tipped applicators were removed, and the intestinal rolls were cut into 2 halves and replaced into new histological cassettes (7-0014, neoLab). The dehydration of the samples was achieved by incubation in ethanol solutions of increasing concentrations, xylene, and paraffin using an S300 tissue processing unit (Leica). The dehydrated samples were then embedded in paraffin, cooled, and stored at RT.

2.2.2 Immunohistochemical (IHC) analysis

For the preparation of paraffin sections, the paraffin blocks were first pre-cooled at -20°C for approximately 1 hour and then sectioned with a MICROM HM355S microtome (Thermo Fisher Scientific). The 3.5 μm tissue sections were then mounted on SUPERFROST® (ULTRA) PLUS microscope slides (Thermo Fisher Scientific) and air-dried overnight at RT. The slides were heated to 60°C for 1 hour to increase tissue attachment to the glass surface and then incubated in Roti®Histol (Roth) for 2 x 10 minutes, followed by rehydration in ethanol (Otto Fischar GmbH & Co) of descending concentration (100%, 96%, 70%) and distilled water (2 x 3-5 minutes each).

After deparaffinization and rehydration, the slides were boiled in citrate buffer (1.00244.1000, Merck) for 15 minutes for antigen retrieval and then cooled down at RT. For the next steps, the slides were transferred to a humidified chamber (2-1879, neoLab), and tissue sections were encircled with a PAP pen (S2002, Dako). Endogenous peroxidase was blocked with 3% (v/v) hydrogen peroxide (1.08597.1000, Merck) for 15 minutes in the dark at RT, followed by three 5-minute washes with PBS (0890.1, Roth). Tissue permeabilization and blocking of unspecific binding were achieved by incubating the slides with 3% (w/v) BSA (9418, Sigma-Aldrich) in PBST (PBS; 0890.1, Roth with 0.025% Triton X-100; T8787, Sigma-Aldrich) supplemented with 4 drops/ml of Streptavidin from the Streptavidin/Biotin blocking kit (SP-2002, Vector labs) and 5% (v/v) goat serum (SP-1000, Vector labs). Primary antibodies (see Table 4) diluted in 3% (w/v) BSA in PBST were mixed with 4 drops/ml of Biotin from the Streptavidin/Biotin blocking kit and added to the slides after removal of the blocking solution and incubated overnight at 4ºC in a humidified chamber.

Table 4. Antibodies used in IHC(p)

Antigen	Dilution or concentration	Article number	Manufacturer
VIPR1	1:500	PA3-113	Thermo Fisher Scientific
NPY1R	2 μg/ml	HPA029903	Sigma-Aldrich
5-HTR4	1:200	PA5-75300	Thermo Fisher Scientific

Following three 5-minute washes with PBST, the secondary biotinylated goat-anti-rabbit antibodies (1:500, BA-1000, Vector labs) were applied and incubated on the slides for 30 minutes at RT. Next, the avidin-biotin peroxidase complex (PK-6100, Vector labs) was prepared and added to the samples according to the manufacturer's instructions. Staining was developed using the DAB kit (SK-4100, Vector labs), and cell nuclei were counterstained with hematoxylin (1.05175.2500, Merck). Finally, the slides were dehydrated with ascending ethanol series and Roti-Histol, mounted in Pertex embedding medium (41-4012-00, Medite), and covered with coverslips (MENZEL-Gläser, e.g., BB024032A1, Thermo Fisher Scientific). Image acquisition was achieved on a Zeiss AxioImager.A1 microscope.

2.2.3 Histopathological evaluation

The sectioning, staining, and pathological scoring of irradiated murine intestines were performed by the Institute of Pathology, Technical University of Munich.

Intestinal tissues embedded in paraffin were sectioned, deparaffinized, and stained according to a standard hematoxylin and eosin (H&E) protocol, followed by a histopathological evaluation by an experienced, blinded pathologist. The evaluation employed a scoring system that ranged from 0 (equivalent to germ-free mice without inflammation) to 12 (highly inflamed) and included several parameters, such as immune cell infiltrate, epithelial damage, and mucosal architecture/atypia.

2.2.4 Immunofluorescent analysis

For the immunofluorescent analysis, paraffin sections were deparaffinized, rehydrated, and subjected to antigen retrieval, as described in the 2.2.2 section. The blocking step involved

incubating the sections in 3% (w/v) BSA (9418, Sigma-Aldrich) in PBST for 1 hour at RT, followed by the incubation with primary antibodies diluted in 3% (w/v) BSA in PBST (Table 5). After overnight incubation with primary antibodies at 4ºC, the sections were washed three times with PBST and then incubated with Goat anti-Rabbit IgG (H+L) Highly Cross-Adsorbed Secondary Antibody, Alexa Fluor™ 594 (1:1000, A-11037, Thermo Fisher Scientific) for 1 hour at RT. The sections were washed three times with PBS, mounted with VECTASHIELD® Antifade Mounting Medium with DAPI (H-1200-10, Vector labs) and the coverslips were sealed to the slides using a nail polish. The analysis was performed using a Leica SP8 confocal microscope.

Table 5. Antibodies used in immunofluorescent analysis

CHRM3	1:500	ab126168	abcam
NK1R	1:100	ATR-001	alomone labs
LYZ1	1:200	PA5-16668	Thermo Fisher Scientific

For visualization of Lgr5-EGFP+ cells in the intestines of *Lgr5*-EGFP-IRES-CreER^{T2} mice, the tissues were preserved in O.C.T™ (OCT) Compound (Tissue-Tek®). In this case, the PFA-fixed intestines were briefly washed with PBS and then replaced into 30% (w/v) sucrose (S0389, Sigma-Aldrich) solution overnight at 4ºC. On the following day, the intestines were replaced into cryomolds (4566, Tissue-Tek®) filled with the OCT and transferred to -80 ºC freezers for long-term storage. These cryo blocks were moved to -20ºC a day before the sectioning to equilibrate to a temperature suitable for cutting. CryoStar NX70 cryostat (Thermo Fisher Scientific) was used to create 5 μm sections that were mounted on SUPERFROST® (ULTRA) PLUS microscope slides (Thermo Fisher Scientific) and air-dried at RT. The sections were washed three times for 5 minutes with PBS, mounted with VECTASHIELD® Antifade Mounting Medium with DAPI (H-1200-10, Vector labs), and the coverslips were sealed to the slides using nail polish. The analysis was performed using a Leica SP8 confocal microscope.

2.2.5 ELISA analysis

Snap-frozen tissue pieces were overlaid with 200 μl of Dulbecco's phosphate-buffered saline (DPBS) (14190094, Thermo Fisher Scientific), homogenized using a SilentCrusher M (Heidolph) until no tissue remnants were visible, and then centrifuged for 5 minutes at 5000g.

The supernatants were then preserved for further analysis at -80ºC. VIP and TNF-alpha levels were measured using the Mouse VIP (Competitive EIA) ELISA Kit (LS-F4059, LSBio) and the Mouse TNF Alpha (Sandwich ELISA) ELISA Kit (LS-F5192, LSBio), respectively, according to the manufacturer's instructions. Data were acquired on a FLUOstar Omega microplate reader (BMG Labtech), and concentrations were obtained using a sigmoidal 4PL function in GraphPad Prism version 10. The obtained concentrations were normalized to the tissue weights.

2.2.6 Crypt collection for the flow cytometry

For intestinal crypt isolation, the murine jejunum was minced into small pieces using scissors and transferred to a 50 ml tube (227261, Greiner). This was followed by extensive washing rounds with DPBS until the supernatant looked clear. The DPBS was then removed, and the tissue pieces were overlaid with 10 mM EDTA (AM9260G, Thermo Fisher Scientific) in DPBS, followed by incubation on ice for 15 minutes. After a gentle shaking for 10 seconds, the 10 mM EDTA solution was renewed, and the tubes were replaced on a shaking platform for the next 15 minutes of incubation on ice. This was followed by another round of manual shaking for 10 seconds, renewal of EDTA solution, and incubation of the tubes on the shaking platform for an additional 30 minutes. The crypt release was achieved by vigorous pipetting with 10% (v/v) Fetal Bovine Serum (FBS) (10500064, Thermo Fisher Scientific) in DPBS using a 10 ml serological pipette (607180, Greiner), and crypts were collected by passing through a 70 μm EASYstrainer™ cell strainer (542070, Greiner). The crypts were centrifuged for 5 minutes at 300g and resuspended in 1 ml TrypLE™ Express Enzyme (12605010, Thermo Fisher Scientific) for single-cell dissociation. The reaction was then stopped by adding 5 ml of 10% (v/v) FBS in DPBS, and the crypt dissociation into single cells was further enhanced by passing the crypt solution through a 10 ml syringe (4606108V, B Braun) with a 20G needle (4665791, B Braun). The cells were pelleted and resuspended with the LIVE/DEAD™ Fixable Violet Dead Cell Stain Kit (1:1000, L34964, Thermo Fisher Scientific) and CD326 (EpCAM) Antibody (1:400, 17-5791-82, Thermo Fisher Scientific) for 20 minutes at 4°C. The cell suspension was washed once, resuspended in the FACS buffer (DPBS containing 1 mM EDTA and 1% (v/v) FBS), and replaced into Falcon® 5 mL Round Bottom Polystyrene Test Tube, with Cell Strainer Snap Cap (352235, Corning). Flow cytometry analysis was performed using BD FACS Canto II (BD Bioscience), and the data were analyzed using Flo Jo v.10.8.1 software. The gating strategy is presented in Figure 4.

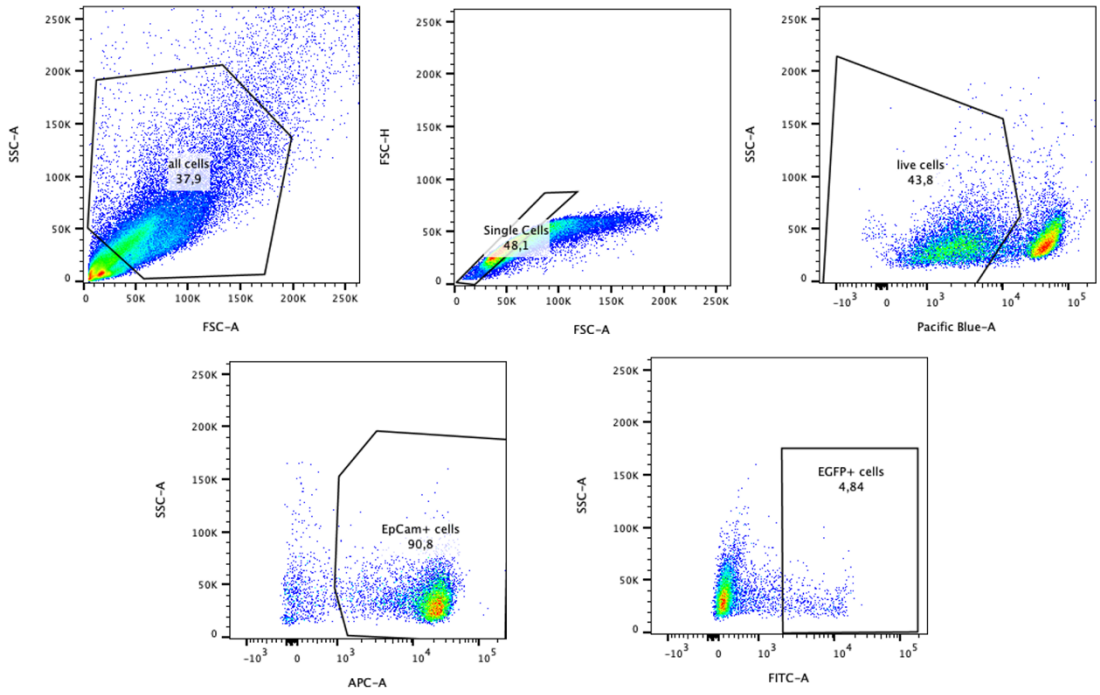

Figure 4. Gating strategy for Flow cytometry analysis of Lgr5-EGFP+ cells isolated from the murine jejunum.

2.3 Mouse experiments

2.3.1 Drug treatment *in vivo*

To study the effects of VIP *in vivo, Lgr5*-EGFP-IRES-CreER^{T2} mice of both sexes and at 6-12 weeks of age received daily intraperitoneal injections (i.p.) of VIP (human, rat, mouse, rabbit, canine, porcine) (1911, Tocris) at a dosage of 750 µg/kg (100 µl per mouse) for five consecutive days. To antagonize VIP signaling *in vivo*, Vasoactive Intestinal Peptide Fragment 6-28 (V4508, Sigma-Aldrich) was administered at a dosage of 500 µg/kg (100 µl per mouse) through daily i.p. injections for five consecutive days. Control mice were injected with 100 µl of sterile distilled water. The injections were performed using 1 ml syringes (9161406V, B Braun) and needles (4665457, B Braun). Following 24 hours after the last injection, the mice were sacrificed and processed as described in section 2.2.6.

2.3.2 Lineage tracing

Lineage tracing was induced in *Lgr5*-EGFP-IRES-CreER^{T2}/*R26*R-LSL-TdTomato mice with a single dose of tamoxifen (T5648, Sigma-Aldrich) administered via oral gavage, followed by daily i.p. injections of 750 µg/kg VIP over five consecutive days. To prepare the tamoxifen solution, 80 µl of 100% ethanol (9065.3, Roth) was added to 20 mg of tamoxifen and heated

to 55°C until the tamoxifen was dissolved. Then, 920 µl of MIGLYOL® 812 (3274, Caelo) was added to the mixture and heated to 55°C. Each mouse received 150 µl of the tamoxifen (3 mg) solution using a 1 ml syringe (9161406V, B Braun) with a reusable oral gavage needle.

2.3.3 Irradiation

For *in vivo* irradiation experiments, female *Lgr5*-EGFP-IRES-CreER^{T2} mice aged 7-9 weeks were used. Mice were exposed to abdominal irradiation following anesthesia with medetomidine (0.5 mg/kg), midazolam (5 mg/kg), and fentanyl (0.05 mg/kg) administered intraperitoneally. To maintain body temperature and prevent eye dryness, anesthetized mice were kept on a heating pad before and after irradiation, and their eyes were protected with an eye cream. Mice were subjected to 12 Gy irradiation using a CIX2 X-Ray Irradiator (Xstrahl) (195 kV, 15 mA, 0.5 mm copper filter) at 488 mm table height and a dose rate of 1.33 Gy/min (45 seconds per 1 Gy). During irradiation, mice were fixed on a plastic tray and shielded with lead plates, exposing to irradiation only the abdominal area. Anesthesia was reversed by atipamezole (2.5 mg/kg), flumazenil (0.5 mg/kg), and naloxone (1.2 mg/kg) applied subcutaneously. VIP treatment was performed daily over a span of three consecutive days starting 72 hours post-irradiation. Mice were injected intraperitoneally with 100 µl of either vehicle (sterile water) or VIP at a dose of 750 µg/kg. The body weights of mice were recorded just before the irradiation procedure and then monitored daily until the end of the experiment.

2.4 Organoid culture

2.4.1 Organoid isolation

The intestinal crypts were isolated from the murine jejunum as described in section 2.2.6. All the steps, starting from the crypt release by pipetting, were performed under sterile conditions to avoid the risk of contamination of the organoid culture. The isolated crypts were pelleted and resuspended in 5 ml of 10% (v/v) FBS in DPBS. A 10 µl portion of the crypt suspension was transferred to a glass slide and inspected under a microscope to estimate the crypt number. The crypts were pelleted again, carefully mixed with a corresponding volume of ice-cold Matrigel® (354230, Corning®), so that 50 µl of Matrigel®, containing 500-1000 crypts, was plated into each well of a 24-well plate (83.3922.005, Sarstedt). After the Matrigel® was allowed to solidify, 380-500 µl of the pre-warmed complete growth medium was added to each Matrigel® dome.

The growth medium was prepared using Advanced DMEM/F12 Reduced Serum Medium (12634010, Gibco) supplemented with 1% (v/v) GlutaMAX (100x) (35050061, Gibco), 1 (v/v) % HEPES (15630080, Gibco), 1 % (v/v) Penicillin-Streptomycin (15140122, Gibco) and was stored at 4°C for long-term use.

For organoid culture, 40 ml of the growth medium was transferred to a 50 ml tube, supplemented with additional growth factors listed in Table 6, and was used over 1 week.

Table 6. Complete growth medium

Component	Concentration	Article number	Manufacturer
B27 (100x conc.)	1x	17504044	Thermo Fisher Scientific
N2 (50x conc.)	1x	17502048	Thermo Fisher Scientific
N-acetyl cysteine (NAC)	1 mM	A7250	Sigma-Aldrich
Noggin	100 ng/ml	250-38	PeproTech
murine R-Spondin-1 (produced in-house using Cultrex HA-R-Spondin1-Fc 293T Cells, 3710-001-01, Bio-Techne)	500 ng/ml		
recombinant murine EGF	50 ng/ml	315-09	PeproTech

Murine R-Spondin-1 was produced using Cultrex HA-R-Spondin1-Fc 293T Cells (3710-001-01, Bio-Techne) according to the manufacturer's protocol. The cells were thawed, transferred to a T25 cell culture flask (83.3910.302, Sarstedt), and maintained in an incubator in the Basal growth medium (DMEM High Glucose (10313021, Gibco), 10% (v/v) FBS, 1% (v/v) Penicillin-Streptomycin, 1% (v/v) GlutaMAX). After passaging, the cells were selected by maintaining them in the Basal growth medium supplemented with 300 μg/ml Zeocin™ (45-0430, Thermo Fisher Scientific) for at least five days. After the selection step, the medium was changed back

to the Basal growth medium, and the cells were sequentially passaged into larger culture vessels to expand cell numbers. Once the cells reached 80% confluence, the medium was changed to the Conditioned medium (CD 293 Medium (11913019, Gibco), 1% (v/v) GlutaMAX). After 7-10 days in culture, the supernatant was collected, centrifuged at 3000g for 15 minutes, and filtered through a 0.2 μm filter (17845-ACK, Sartorius). HA-R-Spondin1-Fc was purified using the Fc tag via Protein A Agarose Purification at the Protein Expression and Purification Facility of the Institute of Structural Biology, Helmholtz Zentrum München. The concentration of purified R-spondin-1 was determined using the Pierce™ BCA Protein Assay Kit (23225, Thermo Fisher Scientific).

2.4.2 Treatment of organoids

Organoids were stimulated with compounds listed in Table 7 alone or in combination with 100 nM VIP (1911, Tocris). The medium of untreated and treated samples was changed daily.

Table 7. Compounds used for *in vitro* treatments

Drug	**Concentration**	**Article number**	**Manufacturer**
SB202190	10 μM	1264	Tocris
PD98059	20 μM	1213	Tocris
JNK-inhibitor II	20 μM	420119	Sigma-Aldrich
BMS-345541	1 μM	B9935	Sigma-Aldrich
Stausporine	0.02 μM	S1421	Selleckchem
Prucalopride	100 nM	SML1371	Sigma-Aldrich
GR73632	100 nM	1669	Tocris
BMS-345541	1μM	S8044	Selleckchem
QNZ	1 μM	ab141588	abcam

Lineage tracing was induced by treatment of organoids with 1 μM (Z)-4-Hydrotamoxifen (4-OHT) (H7904, Sigma-Aldrich) daily for either 72 hours or 48 hours, along with VIP treatment.

2.4.3 Growth measurement

Starting 24 hours post-plating, 8-10 images of each biological replicate were taken using AxioVision software via Zeiss Axiovert 200M microscope (5x magnification). Fiji software (version 2.1.0/1.53c) was used to count and measure the size of viable organoids. The average size for each sample was calculated using the average measurements of 5-35 organoids.

2.4.4 Irradiation of organoids

Organoids were exposed to 6 Gy of X-rays using a CIX2 X-Ray Irradiator (Xstrahl), set at 195 kV, 15 mA with a 0.5 mm copper filter, at a table height of 488 mm. The dose rate was 1.33 Gy/min, corresponding to 45 seconds per 1 Gy.

2.4.5 Organoid survival assay

Isolated crypts were mixed into a 70% Matrigel® suspension and plated in a volume of 40 μl of Matrigel® per well, eight wells per dose. During this step, the suspension was frequently resuspended to ensure a homogeneous distribution of crypts across all wells. After a 24-hour incubation, the plates were irradiated with doses of 2 Gy, 4 Gy, 6 Gy, 8 Gy, or sham-irradiated (0 Gy), and the organoids were allowed to grow for 168 hours. To assess the growth rate and phenotypic changes, the images of each well were taken daily starting 24 hours post-plating.

At 168 hours post-irradiation, the total count of viable organoids in each well was performed as described in Section 2.4.3. The resulting organoid counts were used to find the average viable organoid count per well for each dose.

GraphPad Prism 8.0.2 software was used to generate the survival curve according to the Linear-Quadratic (LQ) model. Organoid survival was analyzed using the formula designed by K. H. Chadwick and H. P. Leenhouts (McMahon, 2019):

$$SF = e^{-(\alpha * X + \beta * X^2)}$$

SF: the fraction of survived organoids,

X: the X-ray dose in Gy,

$\alpha * X$: the linear component of the organoid radiation-induced death,

$\beta * X^2$: the quadratic component of the organoid radiation-induced death.

The α/β ratio was determined by the GraphPad 8.0.2 software analysis.

The survival fraction was determined using the following formula (Buch et al., 2012):

$$\mathrm{SF} = \mathrm{PE}[n\ \mathrm{Gy}]/\mathrm{PE}\ [0\ \mathrm{Gy}],$$

SF: survival fraction,

PE [n Gy]: plating efficiency for the dose of interest,

PE [0 Gy]: plating efficiency for the unirradiated samples.

To determine the plating efficiency for each dose, the following formula was applied:

$$PE = Average\ organoid\ count\ per\ well\ at\ 192\ h * \frac{100}{average\ formed\ organoid\ count\ at\ 24\ h}.$$

The average formed organoid count at 24 hours was estimated using Fiji software (version 2.1.0/1.53c) from images taken 24 hours post-plating. The viable organoids were counted in each image, and the average of all images per sample was multiplied by 4 to represent the average count of formed organoids.

2.4.6 Immunofluorescence *in situ*

Immunostaining of organoids was performed in 24-well plates. The medium was removed from each well, followed by a rinse with DPBS. Matrigel® domes were then incubated with 4% (v/v) PFA on a shaker for 20 minutes at RT. After a brief rinse with DPBS, the organoids were subjected to a 2-hour incubation at RT in a solution containing 3% (w/v) BSA (9418, Sigma-Aldrich) and 0.1% (v/v) Triton X-100 (T8787, Sigma-Aldrich) in DPBS for both blocking and permeabilization. Then, organoids were stained overnight at 4°C with the polyclonal anti-lysozyme 1 rabbit primary antibody (1:200, PA5-16668, Invitrogen) or with the MUC2 Polyclonal Antibody (1:200, PA5-79702, Thermo Fisher Scientific). After three washing steps with DPBS, the organoids were incubated with anti-IgG Rabbit Alexa Fluor 596 secondary antibody (1:1000, A-11012, Invitrogen) overnight on a shaker at 4°C. Before imaging, the Matrigel® domes were transferred to a *µ*-slide 8 Well (80826, ibidi) and covered with 50 *µ*L of the VECTASHIELD® Antifade Mounting Medium with DAPI (H-1200-10, Vector labs) for the nuclear counterstaining. Imaging was performed by recording z-stacks of entire organoids using a Leica SP8 confocal microscope equipped with a 40x HC PL APO Oil objective lens.

2.4.7 Preparation of Formalin-Fixed Paraffin-Embedded Samples and Sections

For fixation and embedding of organoids for Formalin-Fixed Paraffin-Embedded (FFPE) sections, disinfected round glass coverslips (72231-10, Electron Microscopy Sciences) were inserted into a 24-well plate prior to plating the organoids. At the end of the experiments, the organoids were fixed, as described in Section 2.4.6. After a short rinse with DPBS, the glass coverslips with the Matrigel® domes were transferred to Bio-Net histology cassettes (09-0403, Langenbrinck GmbH) and washed in 70% ethanol before overnight dehydration with a S300 tissue processing unit (Leica). On the following day, the organoids were scraped off the coverslips into embedding forms using a scalpel, embedded in paraffin, cooled, and stored at RT. The FFPE blocks were then processed for immunostaining using VIPR1 antibody (1:500, PA3-113, Thermo Fisher Scientific), as described in Section 2.2.2.

2.4.8 qPCR analysis

Organoids were extracted from Matrigel® by incubating them with Corning® Cell Recovery Solution (354253, Corning) for 10 minutes on ice, followed by mechanical disruption of Matrigel® using pipetting. They were then pelleted and resuspended in RLT Lysis buffer (1015762, Qiagen) supplemented with 1% (v/v) β-Mercaptoethanol (M3148, Sigma-Aldrich). RNA was isolated using the Maxwell® 16 LEV simplyRNA kit (AS1280, Promega) according to the manufacturer's instructions and RNA concentrations were measured with a NanoDrop™ 2000 Spectrophotometer (Thermo Fisher Scientific). The amount of RNA used for each reverse transcription reaction was determined based on the lowest RNA concentration among each sample set. cDNA was synthesized using the QuantiTect Reverse transcription kit (205314, Qiagen) and then diluted with nuclease-free water at a 1:2 ratio.

qPCR reactions were set up in a total volume of 10 μl per reaction in LightCycler® 480 Multiwell Plate 96 (04729692001, Roche) and contained 1 μl of cDNA, 1 μl of primer mix, 3 μl of nuclease-free water and 5 μl of the Compound 1 of LightCycler® 480 SYBR Green I Master (04887352001, Roche). Primers were ordered from Sigma-Aldrich as 100 μM stock solutions in dH20 and kept at -20°C for long-term use. For qPCR reactions, primers were mixed accordingly and diluted with nuclease-free water to a concentration of 10 μM. The primer sequences are listed in Table 8.

Target gene expression levels were evaluated using a qTOWER^3 Real-time PCR Thermal Cycler (AnalytikJena) with the following parameters: 95°C for 5 minutes, followed by 46 cycles of 95°C for 10 seconds, 55°C for 20 seconds, and 72°C for 10 seconds. Relative quantitative

gene expression was determined via second derivative analysis followed by the ΔΔCT method using *Hmbs* gene expression for endogenous normalization.

Table 8. Primers used for qPCR analysis

Gene	Primer	Sequence
Hmbs	Forward	5'-TTGGAAACACCCTGGAAACC-3'
	Reverse	5'-TGAATTCCTGCAGCAGCTCATCC-3'
Lys1	Forward	5'-GGAATGGATGGCTACCGTGG-3'
	Reverse	5'-CATGCCACCCATGCTCGAAT-3'
Muc2	Forward	5'-AACATCTCAGGGCCGAAA-3'
	Reverse	5'-TGCGCTTGGAGTGATAGAAA-3'
Clca1	Forward	5'-GATCGCTCAGCACTCCAT-3'
	Reverse	5'-GAGCCATTCATCCATTGGTTA-3'
Dclk1	Forward	5'-AGTACATTCGGACCCTCTCTC -3'
	Reverse	5'-CGTACCAGTCAAGGTGTGCTT-3'
NeuroD	Forward	5'-ATGGCGATGAAAGCGGTGTG-3'
	Reverse	5'-TGCACTGGTACAGCCTTGTGT-3'
Acta1	Forward	5'-CCAAAGCTAACCGGGAGAA-3'
	Reverse	5'-CCCCAGAATCCAACACGA-3'
Gnai2	Forward	5'-GGGTGCTGGCTGAGGATGA -3'
	Reverse	5'-TCCTTCTTGTTGAGGAAGAG-3'
Jup	Forward	5'-CCTGTGGACTCTGCGCAAT-3'
	Reverse	5'-GACCAGGATCTTCAGCACACTCT-3'

Dcxr	Forward	5’-CAGGTTGTGGCGGTGAG-3’
	Reverse	5’-TGGATGACAGCCCGAAGA-3’
Cdkn1a	Forward	5’-GCAAAGTGTGCCGTTGTC -3’
	Reverse	5’-AGACCAATCAGCGCTTGG-3’
Ccng1	Forward	5’-TGGGAAGTCAGGGAAGATGG-3’
	Reverse	5’-TGCGAGCTGCTAAAGGTGAA-3’

2.4.9 RNA sequencing

Library preparation for bulk-sequencing of poly(A)-RNA was done as described previously (Parekh et al., 2016). Briefly, barcoded cDNA of each sample was generated with a Maxima RT polymerase (Thermo Fisher Scientific) using oligo-dT primer containing barcodes, unique molecular identifiers (UMIs), and an adaptor. 5'-Ends of the cDNAs were extended by a template switch oligo (TSO), and full-length cDNA was amplified with primers binding to the TSO-site and the adaptor. NEB UltraII FS kit was used to fragment cDNA. After end repair and A-tailing, a TruSeq adapter was ligated, and 3’-end-fragments were finally amplified using primers with Illumina P5 and P7 overhangs. In comparison to Parekh et al. (Parekh et al., 2016), the P5 and P7 sites were exchanged to allow sequencing of the cDNA in read1 and barcodes and UMIs in read2 to achieve a better cluster recognition. The library was sequenced on a NextSeq 500 (Illumina) with 65 cycles for the cDNA in read1 and 19 cycles for the barcodes and UMIs in read2. Data was processed using the published Drop-seq pipeline (v1.0) to generate sample- and gene-wise UMI tables (Macosko et al., 2015). Reference genome (GRCm38) was used for alignment. Transcript and gene definitions were used according to the GENCODE M25.

Genome-wide differential gene expression analysis was calculated using the DESeq2 R package (Love et al., 2014) for RNA-Seq count data. A false discovery rate (FDR) of ≤ 0.05 was considered significant. Designs accounted for mouse identifier (where appropriate) and treatment, respectively. Principal component analysis was carried out using the plotPCA function from DESeq2. Genome-wide differential gene expression signatures, as represented by Wald statistics per gene, were interrogated by gene set enrichment analysis (GSEA)

(Korotkevich et al., 2021; Subramanian et al., 2005) using modules 'c2.cp', 'c3.tft.gtrd', 'c6.all' and 'h.all' from the MSigDb version 7.4 (Liberzon et al., 2015). GEO accession is available as GSE261001 (https://www.ncbi.nlm.nih.gov/geo/query/acc.cgi?acc=GSE261001)

2.4.10 Flow cytometry and cell sorting

Organoids were harvested from Matrigel® and then incubated with TrypLE™ Express Enzyme (12605010, Thermo Fisher Scientific) for 10 minutes at 37°C to obtain a single cell solution. After the enzyme reaction was stopped by adding PBS containing 10% (v/v) FBS, the cells were pelleted and resuspended with the Pierce BCA (1:1000, L34964, Thermo Fisher Scientific) for 20 minutes at 4°C for live-dead discrimination. The cell suspension was washed once with DPBS, resuspended in FACS buffer (DPBS containing 1 mM EDTA and 1% (v/v) FBS), and transferred to a Falcon® 5 mL Round Bottom Polystyrene Test Tube, with Cell Strainer Snap Cap (352235, Corning). Flow cytometry analysis was performed using a BD FACS Canto II (BD Bioscience), and cell sorting was carried out using a BD FACSAria Fusion (BD Bioscience). Lgr5-EGFP+ population was detected in the FITC channel (488 nm laser, 530/30 filter). Flow cytometry data were analyzed using FlowJo v.10.8.1 software. The example of the gating strategy is presented in Figure 5.

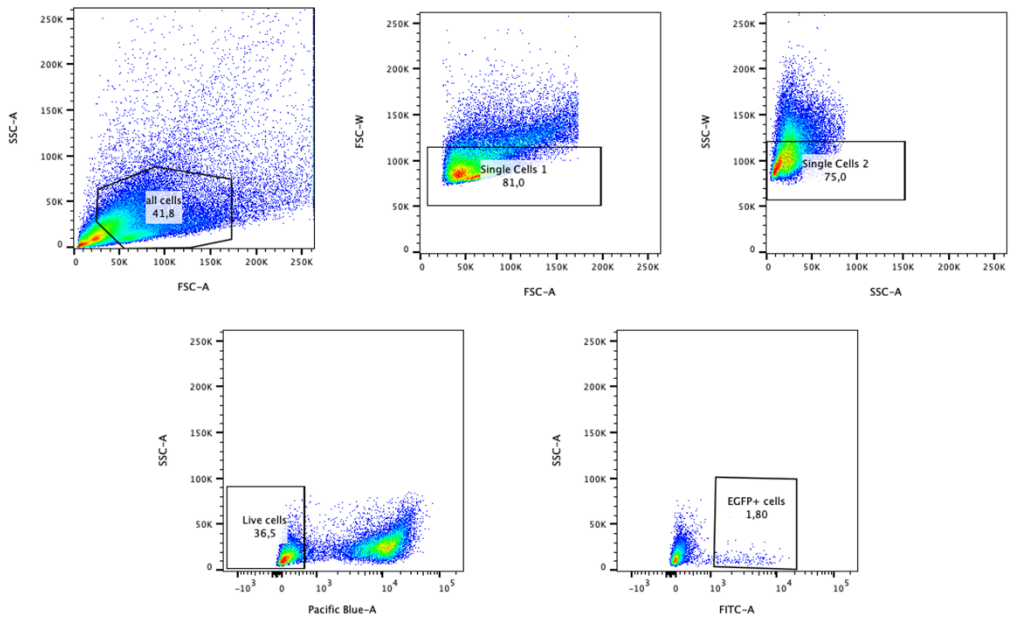

Figure 5. Gating strategy for Flow cytometry analysis of Lgr5-EGFP+ cells isolated from the intestinal organoids.

2.4.11 Cell proliferation analysis

To assess cell proliferation, organoids were incubated for 2 hours at 37°C in the incubator with the corresponding growth medium containing 10 μM EdU reagent (Click-iT EdU Alexa Fluor 647 Flow Cytometry Assay kit, C10424, Invitrogen). After the incubation, the organoids were released from the Matrigel® domes and dissociated into a single-cell suspension using TrypLE™ Express Enzyme. They were then stained for live/dead discrimination with the LIVE/DEAD™ Fixable Violet Dead Cell Stain Kit (1:1000, L34964, Thermo Fisher Scientific) for 20 minutes at 4°C. Fixation, permeabilization, and the Click-iT reaction were carried out according to the manufacturer's instructions. The population of cells that incorporated the EdU reagent was measured in the APC channel (640 nm laser, 660/20 filter). The results were processed using FlowJo v.10.8.1 software.

2.4.12 Cell survival analysis

For luminescent analysis, organoids were plated in black-walled 24-well cell culture plates (4445, Corning). Cell viability was assessed using the CellTiter-Glo® 3D Cell Viability Assay (G9681, Promega), according to the manufacturer's instructions. Before the analysis, the medium was removed, and 200 μl of CellTiter-Glo® 3D reagent was added to each well. The plate was then vigorously shaken on an orbital shaker for 5 minutes, followed by a 25-minute incubation at 37°C to induce cell lysis. The luminescent signal was subsequently detected using a FLUOstar Omega microplate reader (BMG Labtech).

2.4.13 TUNEL assay

Cell apoptosis was evaluated using the APO-BrdU™ TUNEL Assay Kit, with Alexa Fluor™ 488 Anti-BrdU (A23210, Invitrogen). Organoids were extracted from the Matrigel® domes and dissociated into a single-cell suspension, then fixed using 1% (v/v) PFA. After washing with DPBS, cells were incubated with ice-cold 70% (v/v) ethanol overnight at -20°C. DNA labeling and staining were performed according to the manufacturer's instructions. The population of cells positive for BrdU was measured in the FITC channel (488 nm laser, 530/30 filter). The results were analyzed using FlowJo v.10.8.1 software.

2.4.14 Western Blot

Organoids were harvested from Matrigel® and then lysed in RIPA lysis buffer (R0278, Sigma-Aldrich), supplemented with cOmplete EDTA-free Protease Inhibitor Cocktail (05056489001, Roche) and PhosSTOP™ (04906837001, Roche). The lysis was conducted on ice with gentle

agitation for 30 minutes, followed by centrifugation at 15000g for 15 minutes at 4°C. The resulting supernatants were either stored at -80°C or processed immediately. Protein concentrations were quantified using the Pierce BCA Protein Assay Kit (23225, Thermo Fisher Scientific) according to the manufacturer's instructions.

For further analysis, samples were adjusted to equal concentrations with RIPA buffer, mixed with Laemmli buffer (300 mM Tris-HCl, pH 6.8, 10% (w/v) SDS, 50% (v/v) glycerol, 0.05% (w/v) bromophenol blue, 5% (v/v) β-mercaptoethanol), and heated to 95°C for 5 minutes. Samples and size standards (26619, Thermo Fisher Scientific) were loaded onto the SDS–polyacrylamide gel prepared, as indicated in Table 9.

Table 9. SDS-polyacrylamide gel preparation

(2x gels in 1.5 mm plates)			Stacking gel	Separating gel
Component	Manufacturer	Article N	Volume	Volume
dH_2O			2.7 ml	7.9 ml
Acrylamide	Serva	10688.01	670 µl	6.7 ml
Tris-HCl	Roth	5429.2	500 µl; 0.5 mM, (pH6.8)	5 ml; 1.5 mM, (pH8.8)
TEMED	Roth	2867.3	8 µl	16 µl
10% (w/v) SDS	Roth	CN30.2	40 µl	200 µl
10% (w/v) APS	Sigma-Aldrich	248614	40 µl	200 µl

SDS-polyacrylamide gel electrophoresis was performed using a Mini-Protean® 3 Cell System and a Mini Trans-Blot Cell (Bio-Rad). The gel tank was placed on ice and filled with a running buffer (25 mM Tris-HCL, 192 mM glycine, 0.1% (w/v) SDS). The voltage was set to 80 V for 30 minutes and then increased to 120 V for another 60-90 minutes until the dye front reached the bottom of the gel. Proteins were transferred onto a 0.2 µm nitrocellulose blotting membrane (10600001, GE Healthcare) at 100 V for 90 minutes in a transfer buffer (25 mM Tris-HCl, 192 mM glycine, 20% (v/v) methanol) on ice.

The membranes were blocked with 5% (w/v) BSA (9418, Sigma-Aldrich) containing 0.01% (v/v) Tween® 20 (P9416, Sigma-Aldrich) in tris-buffered saline (1244.1, Roth) for 1 hour at RT. Following the blocking step, the membranes were incubated overnight at 4°C with either Phospho-p38 MAPK (Thr180/Tyr182) Antibody (1:1000, 9211, Cell Signaling), p38 MAPK Antibody (1:1000, 9212, Cell Signaling), NF-κB p65 Polyclonal Antibody (1:250, 51-0500, Thermo Fisher Scientific) or Phospho-NF-κB p65 (Ser536) (93H1) Rabbit mAb (1:1000, 3022, Cell Signaling). After three washing steps, the membranes were incubated with horseradish peroxidase-conjugated anti-rabbit secondary antibody (1:50,000, NA934VS, GE Healthcare) for 1 hour at RT and developed using the Amersham ECL Prime Western Blotting Detection Reagent (RPN2232, Cytiva). β-Actin was detected using Anti-β-Actin–Peroxidase antibody (1:50,000, A3854, Sigma-Aldrich) and served as a loading control.

2.5 Statistical analysis

Statistical analysis was performed using GraphPad Prism 10 Software. Data were generally presented as mean ± standard error of the mean (SEM) unless specified otherwise. Differences between groups were assessed using Student's t-test, one-way ANOVA, and two-way ANOVA. For *in vitro* experiments, paired comparisons were used. A p-value of < 0.05 was considered statistically significant, with significance denoted as follows: *$p < 0.05$, **$p < 0.01$, ***$p < 0.001$, ****$p < 0.0001$; not significant results were marked as ns ($p > 0.05$). Statistical details and numbers of biological replicates (n) are provided in the legends accompanying each figure.

3. RESULTS

3.1 Neuronal mediators

Accumulating evidence suggests that neuronal mediators may play a significant role in regulating intestinal stem cell behavior (Goode et al., 2003; Middelhoff et al., 2020; Tackett et al., 2017). A pioneering study by Haber et al., employing single-cell RNA sequencing, revealed the expression of receptors of different neuronal mediators in various cell types of the intestinal epithelium (Figure 6). This data demonstrates that receptors for several neuronal mediators such as *Vipr1, 5-Htr4* serotonin receptor, *Chrm3* (Cholinergic receptor muscarinic 3), and *Tacr1* substance P receptor are expressed in stem and early progenitor cells, suggesting an impact on stem cell functions.

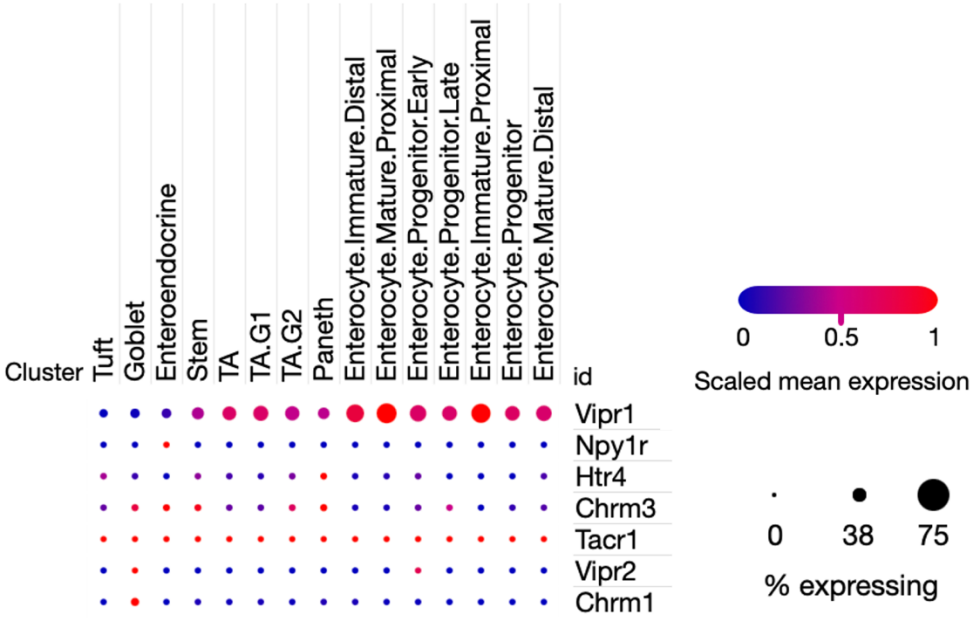

Figure 6. Gene expression of neuronal mediator receptors in different cell types of the intestinal epithelium.
Based on the single-cell RNA sequencing data set from (Haber et al., 2017). Created with a visualization tool of the Single Cell Portal by the Broad Institute (https://singlecell.broadinstitute.org/single_cell/study/SCP44/small-intestinal-epithelium).

We selected several receptors with the highest gene expression according to the published dataset (Figure 6) and performed immunohistochemical and immunofluorescent analyses to verify the presence of the protein product in the jejunal tissue of the small intestine in adult wild-type mice. Our analysis revealed prominent expression of muscarinic acetylcholine receptor M3 (M3R) not only in the villi but also in the crypt region (Figure 7a), aligning with the gene expression data. The presence of this receptor in the crypt region is consistent with the reported involvement of M3R in stem cell regulation (Middelhoff et al., 2020). Interestingly, Vipr1 and 5-Htr4 were also highly present within the crypt regions, indicating their potential role in regulating stem cell functions (Figure 7b and c). In contrast, Nk1r expression was more sporadic, detected in isolated cells within both villi and crypts (Figure 7d), while Npy1r protein expression was barely detectable in the murine small intestinal tissue (Figure 7e).

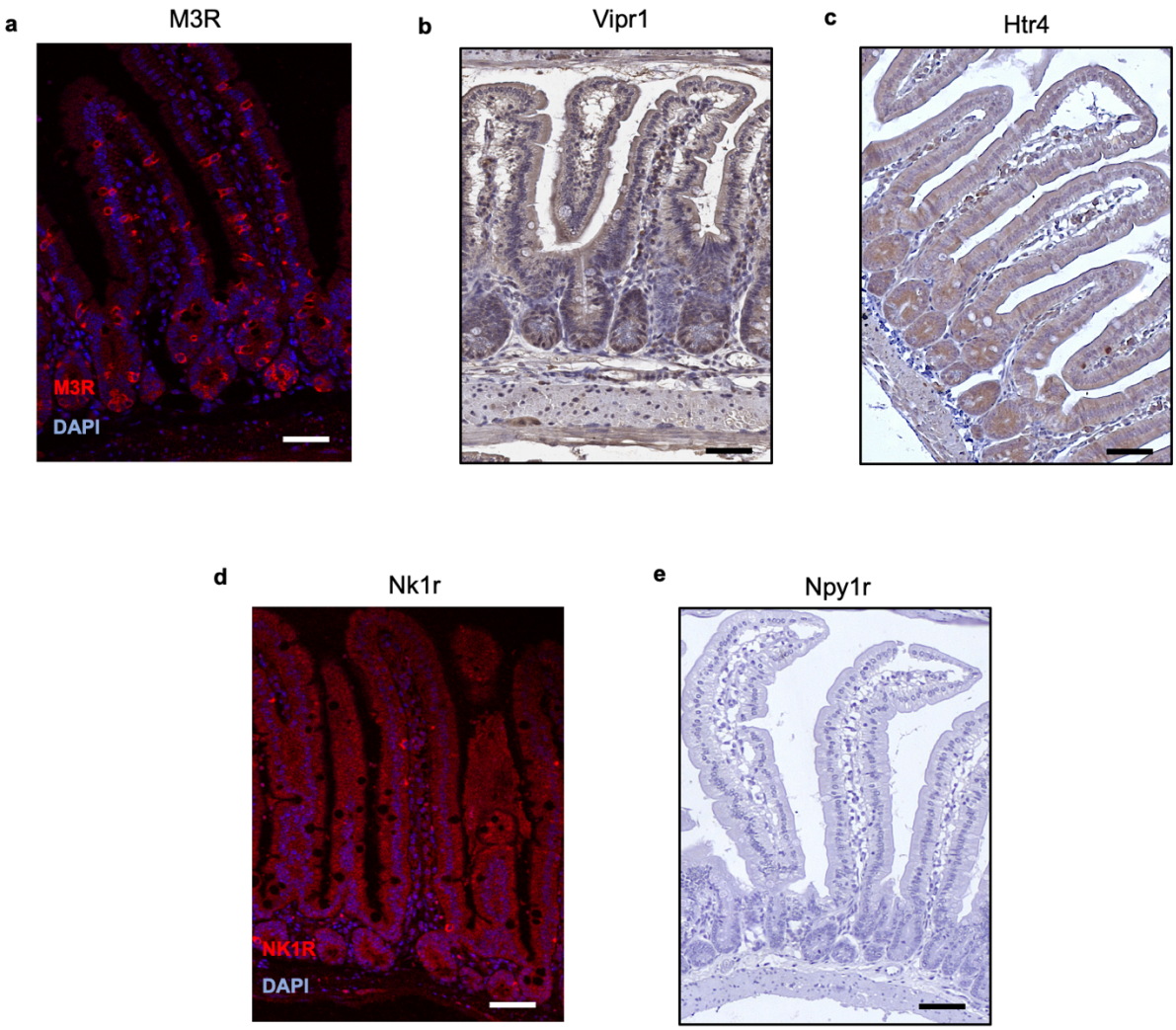

Figure 7. Neuronal mediator receptors in the epithelium of the murine small intestine.

a, Immunofluorescent analysis of muscarinic acetylcholine receptor M3 (M3R). **b,** Immunohistochemical analysis of vasoactive intestinal peptide receptor 1 (Vipr1). **c,** Immunohistochemical analysis of serotonin receptor 4 (5-Htr4). **d,** Immunofluorescent analysis of substance P receptor (Nk1r). **e,** Immunohistochemical analysis of neuropeptide Y receptor type 1 (Npy1r). Scale bars, 100 μm.

Intestinal organoids have emerged as a powerful tool for studying the complex dynamics and molecular mechanisms within the intestinal epithelium. Their ability to replicate the complex structure and cellular diversity of the intestinal epithelium has greatly facilitated advanced research in disease modeling and drug discovery (Angus et al., 2020). Therefore, to investigate the effects of neuropeptides on the intestinal epithelium, we developed an organoid-based *in vitro* model. In this model, we isolated organoids from jejunal crypts of wild-type mice and allowed them to recover from the isolation stress for 24 hours. Then, organoids were exposed to a specific receptor agonist for the next 72 hours before proceeding to the analysis (Figure 8a).

Unlike Npy1r, which was barely detectable by our IHC analysis, receptors for serotonin and substance P were highly present in the murine mucosa, including the crypt region (Figure 7c and Figure 7d). This led us to investigate whether these neuronal mediators exert an effect on progenitor cells, resulting in altered cell differentiation. To address this, intestinal organoids were treated with either prucalopride (serotonin 5-HTR4 receptor agonist) or GR73632 (substance P NK1R receptor agonist) and subsequently subjected to qPCR analysis to assess the gene expression of epithelial differentiation markers, such as *Lys1* (Paneth cell marker), *Muc2* and *Clca1* (goblet cell marker), *Dclk1* (tuft cell marker), and *NeuroD* (enteroendocrine cell marker).

The analysis has shown that neither prucalopride nor GR73632 affected the gene expression of epithelial differentiation markers in treated organoids (Figure 8b). Similarly, bulk RNA sequencing analysis of organoids treated with prucalopride or GR73632 did not show significant changes in transcriptional profiles, as evident from the PCA plot (Figure 8c).

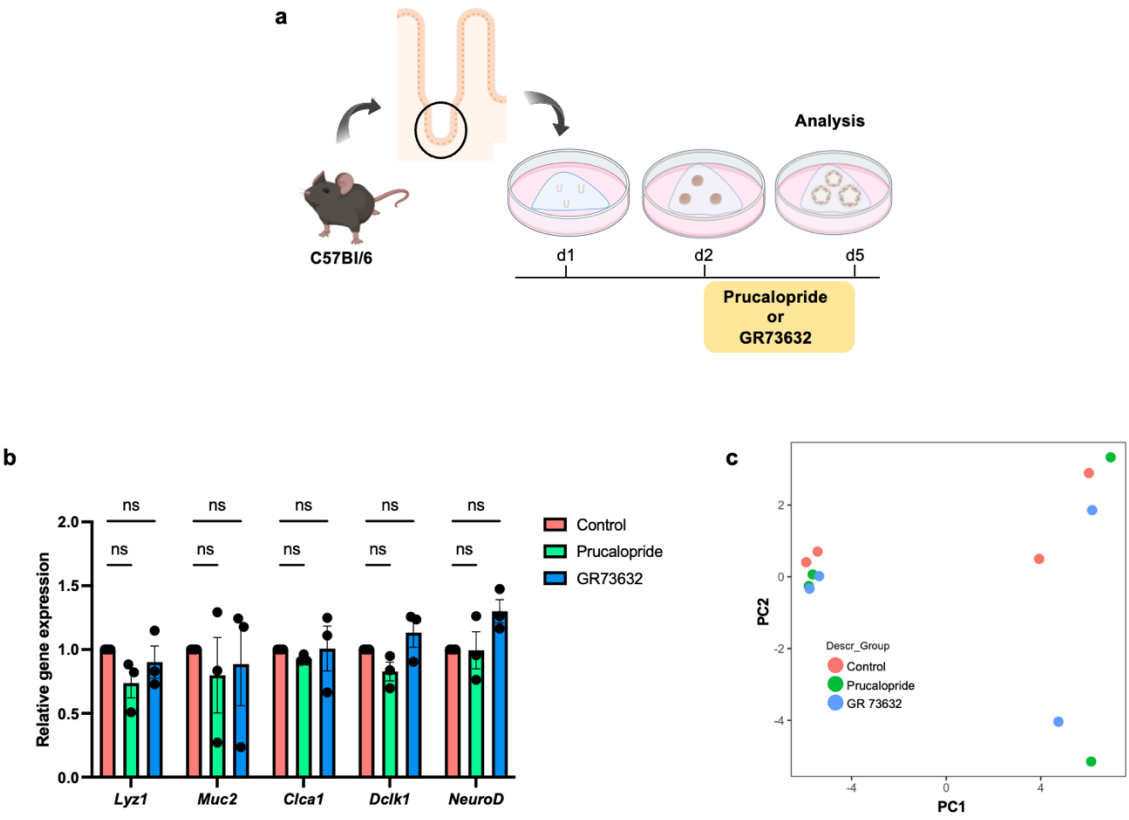

Figure 8. Serotonin and Substance P receptor agonists do not significantly change the gene expression of intestinal organoids.

a, Experimental setup and treatment scheme. **b**, qPCR analysis of differentiation markers upon indicated agonist treatments (n=3 per group). ns = not significant. **c**, Principal component analysis of transformed count data from the bulk RNA sequencing of control and treated intestinal organoids (n=4 per group). Data are shown as mean ± SEM. n = number of biological replicates. Statistical analysis was performed using two-way ANOVA (**b**).

3.2 VIP in homeostasis

3.2.1 Establishment of VIP treatment protocol *in vitro*

VIP is another prominent neuronal mediator that is highly present in the ENS. Its effects in the small intestine are primarily mediated through VIPR1, which is highly present along the villus-crypt axis, with significant expression in the crypt zone, as determined by the IHC analysis (Figure 7b). To establish and optimize our *in vitro* model (Figure 9a), we first verified the expression of VIPR1 on organoid membranes (Figure 9b) and determined the optimal VIP concentration by tracking organoid growth over time (Figure 9c). Notably, a subset of organoids treated with VIP acquired a cystic phenotype after treatment onset, reflecting the activation of intracellular mechanisms triggered by VIP treatment (McCauley et al., 2020) (Figure 9d). The concentration of 100 nM of VIP showed the most prominent effect at 72 hours after treatment onset and was used in all further experiments.

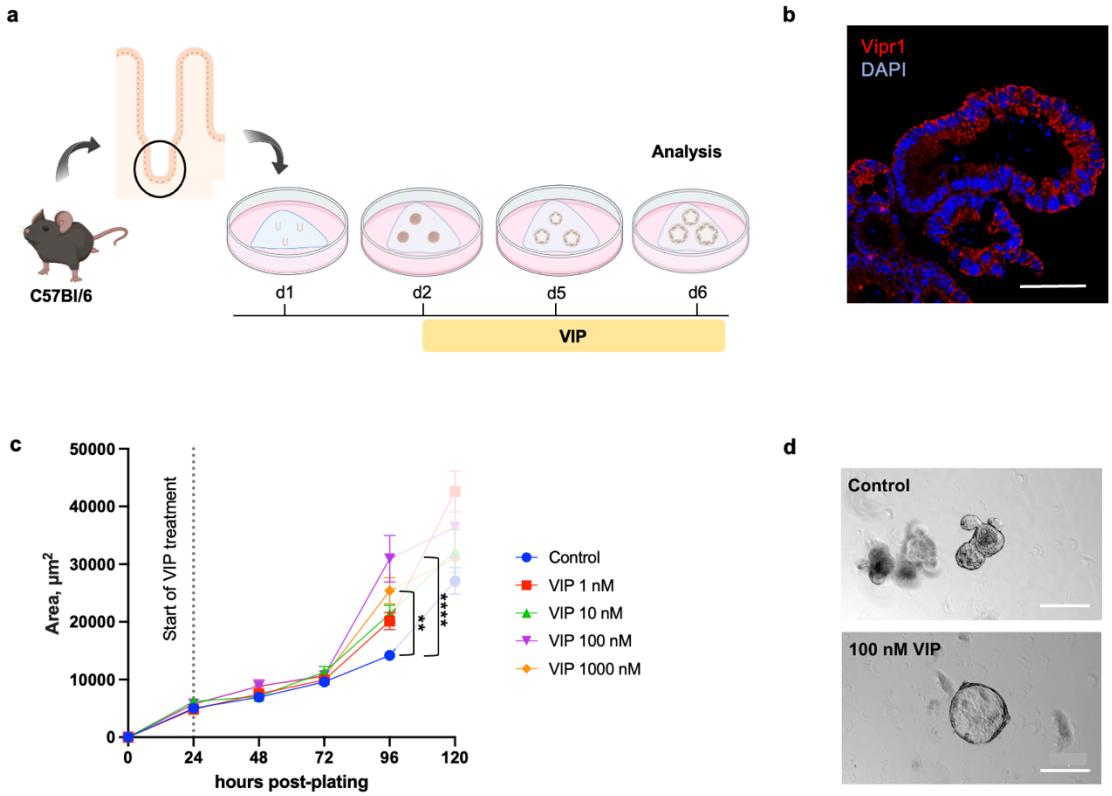

Figure 9. Characterization of VIP treatment *in vitro.*
a, Experimental setup and treatment scheme. **b,** Immunofluorescent analysis of Vipr1 in intestinal organoids (Scale bar, 50 μm). **c**, Organoid growth represented by

the mean organoid area in μm^2 measured for 5 days after plating. The organoids that were isolated from crypts pooled together from two biological replicates. Data are shown as means ± SEM (n=15-20 organoids per VIP dose per time point). **d**, Organoid phenotype following 72h of VIP treatment (Scale bars, 50 μm). **p < 0.05, **p < 0.01, ***p < 0.001, ****p < 0.0001.* Statistical analysis was performed using two-way ANOVA (**c**).

3.2.2 VIP treatment and cellular differentiation

To investigate the effect of VIP on intestinal epithelial cells, organoids were allowed to establish from murine intestinal crypts *in vitro* for 24 hours and then subjected to a 72-hour treatment with 100 nM VIP before being harvested for analysis (Figure 10a). Bulk RNA sequencing of control and VIP-treated organoids provided initial insights into the potential impact of VIP treatment. PCA plots revealed a prominent separation of samples treated with VIP from untreated samples, showing a clear change in transcriptional profiles induced by VIP (Figure 10b). Further analysis showed that VIP-treated organoids were enriched for signaling pathways such as TNF-alpha/NF-κB, epithelial-mesenchymal transition, and inflammatory response (Figure 10c), further pointing to significant changes in gene transcription induced by VIP. Moreover, the transcriptional signature of several differentiated cell types mostly related to the secretory lineage, such as goblet cells, tuft cells, and Paneth cells, also appeared to be upregulated (Figure 10d). To validate this further, we conducted qPCR analysis on the most common differentiation markers of epithelial cell types and observed an increase in gene expression for Paneth (*Lyz1*) and goblet cell markers (*Clca1, Muc2*), whereas markers for tuft cells (*Dclk1*) and enteroendocrine cell types (*NeuroD*) remained unchanged (Figure 10e). Immunofluorescent analysis, in turn, revealed the expansion of Lyz1+ Paneth cells in VIP-treated organoids (Figure 10f). Although VIP treatment did not induce statistically significant changes in the numbers of Muc2+ goblet cells, the trend towards expansion of these cells appeared clear (Figure 10g).

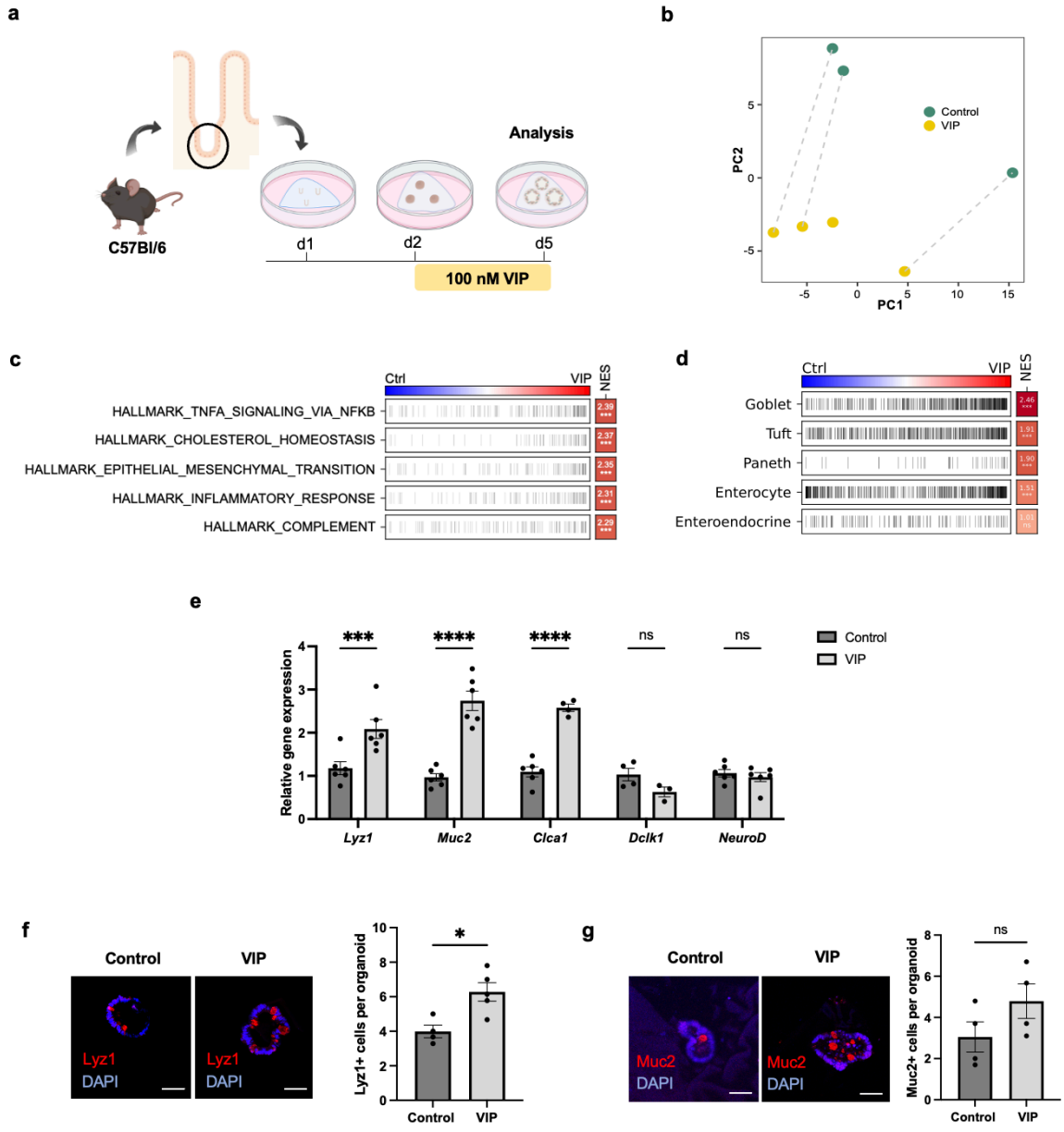

Figure 10. VIP drives cell differentiation towards secretory phenotype.

a, Experimental setup and treatment scheme. **b**, Principal component analysis of transformed count data from the bulk RNA sequencing of control and VIP-treated whole intestinal organoids. n=3 (Control), n=4 (VIP). **c, d,** Hallmark gene-set enrichment analysis of differential gene expression in VIP-treated organoids; Ctrl = control, NES = normalized enrichment score. n=3 (Control), n=4 (VIP). **e,** qPCR analysis of differentiation markers of Paneth cells (*Lyz1*), n=6 (Control), n=6 (VIP); goblet cells (*Muc2, Clca1*) n=6 (Control), n=4-6 (VIP); tuft cells (*Dclk1*) n=4 (Control), n=3 (VIP); enteroendocrine cells (*NeuroD*) n=6 (Control), n=6 (VIP) upon VIP treatment. **f,** Immunofluorescent analysis of Lyz1 staining in control and VIP-treated organoids (Scale bars, 50 μm). n=4 (Control), n=5 (VIP). **g,** Immunofluorescent analysis of Muc2 staining in control and VIP-treated organoids (Scale bars, 50 μm). n=4 (Control), n=4 (VIP). *$*p < 0.05$, $**p < 0.01$, $***p < 0.001$, $****p < 0.0001$.* Data are shown as means ± SEM, n = number of biological

replicates. Statistical analysis was performed using two-way ANOVA (**e**) and paired Student's *t*-test (**f, g**).

3.2.3 Signaling pathways mediating VIP-induced cell differentiation

Having established that VIP treatment affects cell differentiation, we next investigated the specific signaling pathway that could mediate the observed changes. Bulk RNA sequencing analysis had previously identified the TNF-alpha/NF-κB pathway as one of the most prominently upregulated hallmark pathways in VIP-treated organoids (Figure 10c). We, therefore, hypothesized that the NF-κB pathway could be involved in altering cellular differentiation downstream of VIP signaling. To confirm the activation of this pathway, we performed a Western blot analysis focusing on a key activation marker within the NF-κB pathway: phosphorylation of NF-κB p65. This analysis revealed a trend towards increased phosphorylation of NF-κB p65 in VIP-treated organoids, although the observed trend did not reach statistical significance, likely due to the small sample size (Figure 11a). Next, we inhibited the NF-κB pathway using one of two different inhibitors: NF-κB inhibitor BMS-345541 or QNZ concomitant to VIP treatment (Figure 11b). Although neither of the NF-κB inhibitors significantly abrogated the VIP-induced effects, as evidenced by qPCR analysis (Figure 11c), the BMS-345541 inhibitor showed a trend towards mitigating the upregulation of the Paneth cell marker *Lyz1* and the goblet cell marker *Clca1*. To further investigate this, we performed immunostaining for Lyz1, yet similarly detected no reversal of the VIP-induced phenotype upon co-treatment with the BMS-345541 inhibitor (Figure 11d).

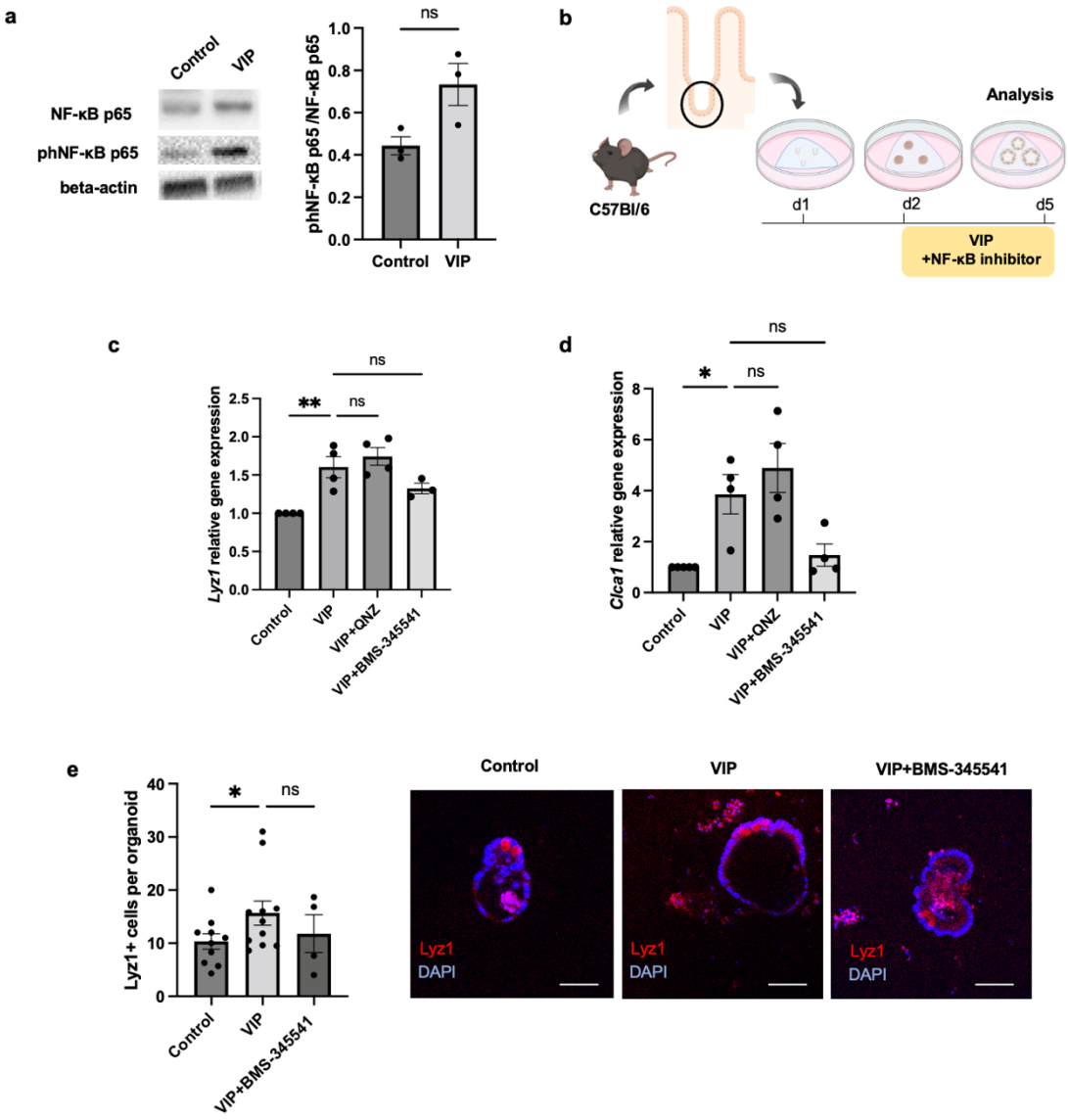

Figure 11. NF-κB pathway does not mediate VIP-induced secretory cell differentiation in organoids.

a, Experimental setup and treatment scheme. **b,** Western blot analysis showing a trend towards NF-κB signaling activation upon VIP treatment (n=3 per group). **c**, qPCR analysis of *Lyz1* differentiation marker in VIP-treated organoids in the presence of NF-κB signaling inhibitors, n=4 (Control), n=4 (VIP), n=4 (VIP+QNZ), n=3 (VIP+ BMS-345541). **d,** qPCR analysis of *Clca1* differentiation marker in VIP-treated organoids in the presence of NF-κB signaling inhibitors (n=4 per group). **e,** Quantification of Lyz1+ cells per organoid revealed by immunofluorescent staining following BMS-345541 inhibitor co-treatment (Scale bars, 50 μm), n=10 (Control), n=11 (VIP), n=4 (VIP+BMS-345541). **p < 0.05, **p < 0.01, ***p < 0.001, ****p < 0.0001.* Data are shown as means ± SEM, n = number of biological replicates. Statistical analysis was performed using paired Student's *t*-test in (**b**) and one-way ANOVA (**c-e**).

To examine additional signaling pathways that could be involved in VIP-mediated changes to epithelial cell differentiation, we subjected organoids to distinct inhibitors that target potential downstream signaling effectors of VIP simultaneous to VIP treatment. These inhibitors included p38 MAPK inhibitor SB202190, MEK1 MAPK inhibitor PD98059, c-Jun N-terminal kinase inhibitor II, and PKC inhibitor Staurosporine. Our analysis indicated that the upregulation of markers associated with secretory cell differentiation, as assessed by qPCR analysis in VIP-treated organoids, was most effectively diminished by co-treatment with the p38 MAPK inhibitor SB202190 and the MEK1 MAPK inhibitor PD98059 (Figure 12a). This suggested a significant role of the MAPK pathway in mediating the effect of VIP on cell differentiation. In line, the immunoblot analysis revealed the upregulation of p38 MAPK phosphorylation at Thr180/Tyr182 in VIP-treated organoids (Figure 12b), indicating p38 MAPK activation by VIP (Raingeaud et al., 1995). In contrast, inhibition of the c-Jun and PKC pathways had only minimal or no effect on VIP-induced differentiation at the transcript level (Figure 12a). To further confirm the role of the MAPK pathway in VIP-mediated changes to cell differentiation, we performed immunofluorescent analysis and quantified Lyz1+ cells in organoids following co-treatments with SB202190 or PD98059. The analysis showed that the expansion of Lyz1+ cells induced by VIP treatment was significantly reduced by the addition of the p38 MAPK inhibitor SB202190 but not by the MEK1 MAPK inhibitor PD98059 (Figure 12c). This data suggests a significant modulation of secretory cell differentiation by VIP, mediated by VIP-induced intracellular p38 MAPK activation.

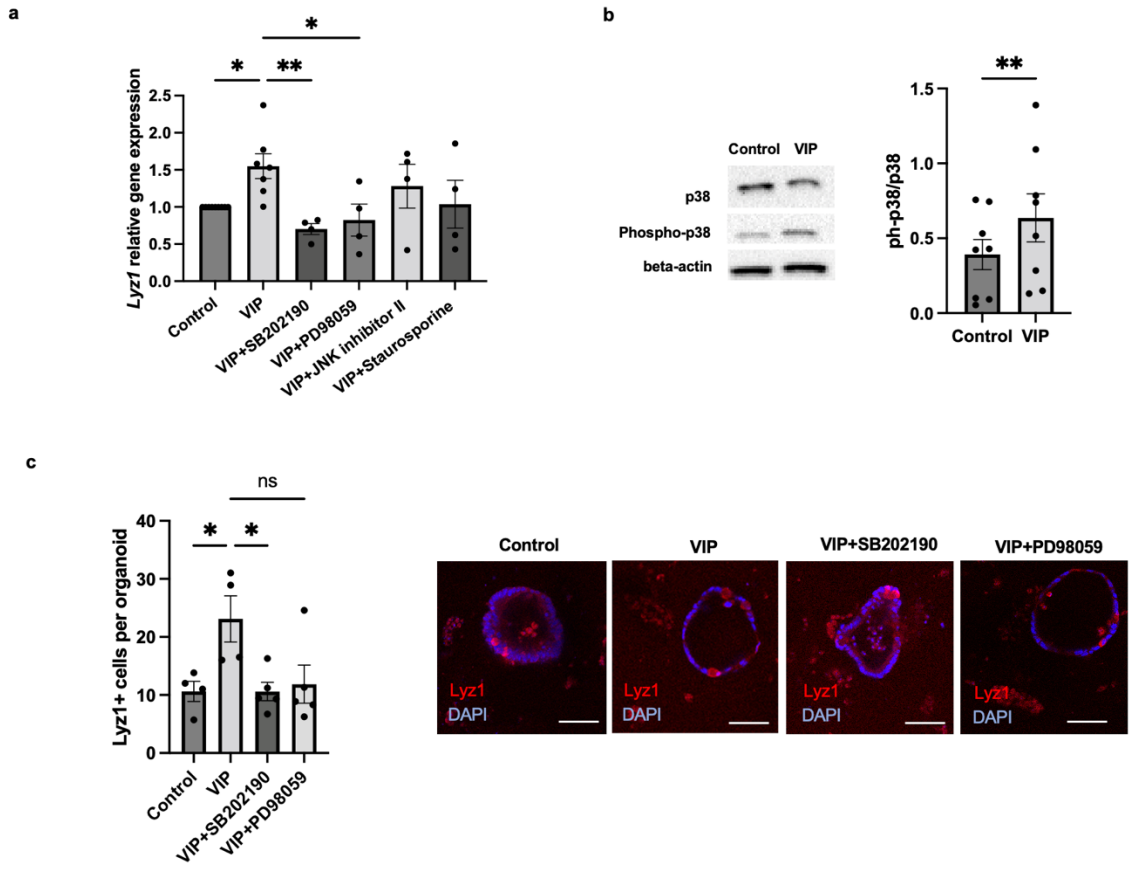

Figure 12. VIP-induced secretory phenotype is driven by intracellular p38 MAPK activation.
a, qPCR analysis of *Lyz1* differentiation marker in VIP-treated organoids in the presence of inhibitors targeting potential downstream signaling pathways. n=8 (Control), n=8 (VIP), n=4 (VIP+SB202190), n=4 (VIP+PD98059), n=4 (VIP+JNK inhibitor II), n=4 (VIP+Staurosporine). **b,** Western blot analysis showing p38 MAPK pathway activation upon VIP treatment (n=8 per group). **c,** Representative images of Lyz1 immunofluorescent analysis and quantification of Lyz1+ cells per organoid following co-treatments with indicated inhibitors (Scale bars, 50 μm; n=4 per group). **p < 0.05, **p < 0.01, ***p < 0.001, ****p < 0.0001.* Data are shown as means ± SEM, n = number of biological replicates. Statistical analysis was performed using paired Student's *t*-test in (**b**) and one-way ANOVA (**a, c**).

3.2.4 The effect of VIP on Lgr5+ intestinal stem cells

In view of the prominent effect on cellular differentiation induced by VIP, we further investigated whether VIP directly affects ISC numbers and their proliferative activity. For this purpose, we derived organoids from *Lgr5*-EGFP-IRES-CreER^{T2} reporter mice that harbor the *Lgr5*-EGFP-IRES-CreER^{T2} "knock-in" allele. This modification disrupts *Lgr5* gene function and drives the expression of enhanced green fluorescent protein (EGFP) and the CreER^{T2} protein

from the endogenous *Lgr5* locus (Barker et al., 2007). As a result, Lgr5+ ISCs are labeled with a fluorescent signal in mouse tissues, as well as in derived organoids (Figure 13a). To assess the numbers of Lgr5-EGFP+ ISC, we subjected organoids to 72 hours of VIP treatment followed by flow cytometry analysis (Figure 13b). The analysis showed an increase in the Lgr5+ ISC fraction induced by VIP treatment, indicating a direct effect of VIP on Lgr5-EGFP+ ISC dynamics (Figure 13c).

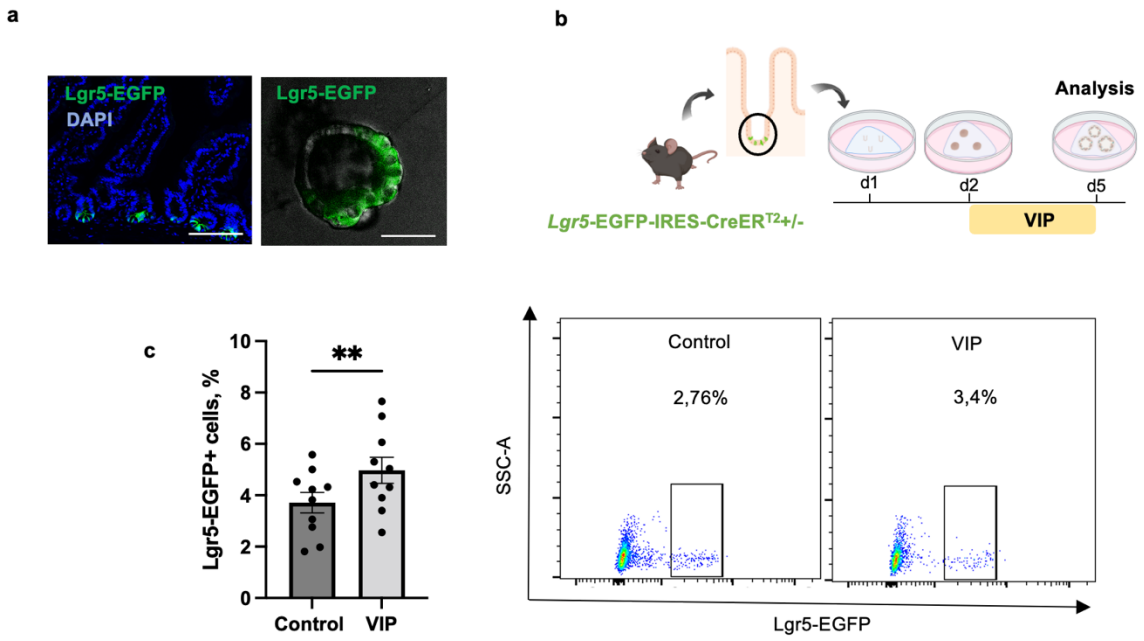

Figure 13. VIP modulates Lgr5-EGFP+ ISC number *in vitro*.
a, Intestinal tissue of *Lgr5*-EGFP-IRES-CreER^{T2} reporter mice (right image, scale bar=200 μm) and organoids derived from *Lgr5*-EGFP-IRES-CreER^{T2} reporter mice (left image; scale bar=50 μm). **b,** Experimental setup and treatment scheme. **c,** Quantification of Lgr5-EGFP+ ISCs in VIP-treated organoids by Flow cytometry (n=10 per group). *$p < 0.05$, **$p < 0.01$, ***$p < 0.001$, ****$p < 0.0001$. Data are shown as means ± SEM, n = number of biological replicates. Statistical analysis was performed using paired Student's *t*-test (**c**).

Furthermore, to delve deeper into the potential effect of VIP on ISC proliferative activity, we derived organoids from *Lgr5*-EGFP-IRES-CreER^{T2}/*R26*R-LSL-TdTomato mice (Madisen et al., 2009). *R26*R-LSL-TdTomato mice produce an mRNA encoding tandem dimer of red fluorescent Tomato (tdTomato) protein that is not translated unless the Cre-mediated excision removes a transcriptional stop signal flanked by loxP sites. As a result, all daughter cells of

Lgr5-EGFP+ ISCs in *Lgr5*-EGFP-IRES-CreER^{T2}/*R26*R-LSL-TdTomato mice acquire the fluorescent tdTomato signal following activation of Cre.

We induced the Cre activity in organoids derived from *Lgr5*-EGFP-IRES-CreER^{T2}/*R26*R-LSL-TdTomato mice by treating them with 4-OHT over 72 hours simultaneous to VIP treatment (Figure 14a). Our findings indicate that VIP significantly reduces the number of Lgr5-EGFP+ ISC progeny (Figure 14b), suggesting an impact of VIP on ISCs and their generation of daughter cells. This observation also coincided with a marked decrease in the proportion of proliferating cells in VIP-treated organoids, as revealed by the EdU proliferation assay, which detects cells undergoing DNA synthesis (Figure 14c).

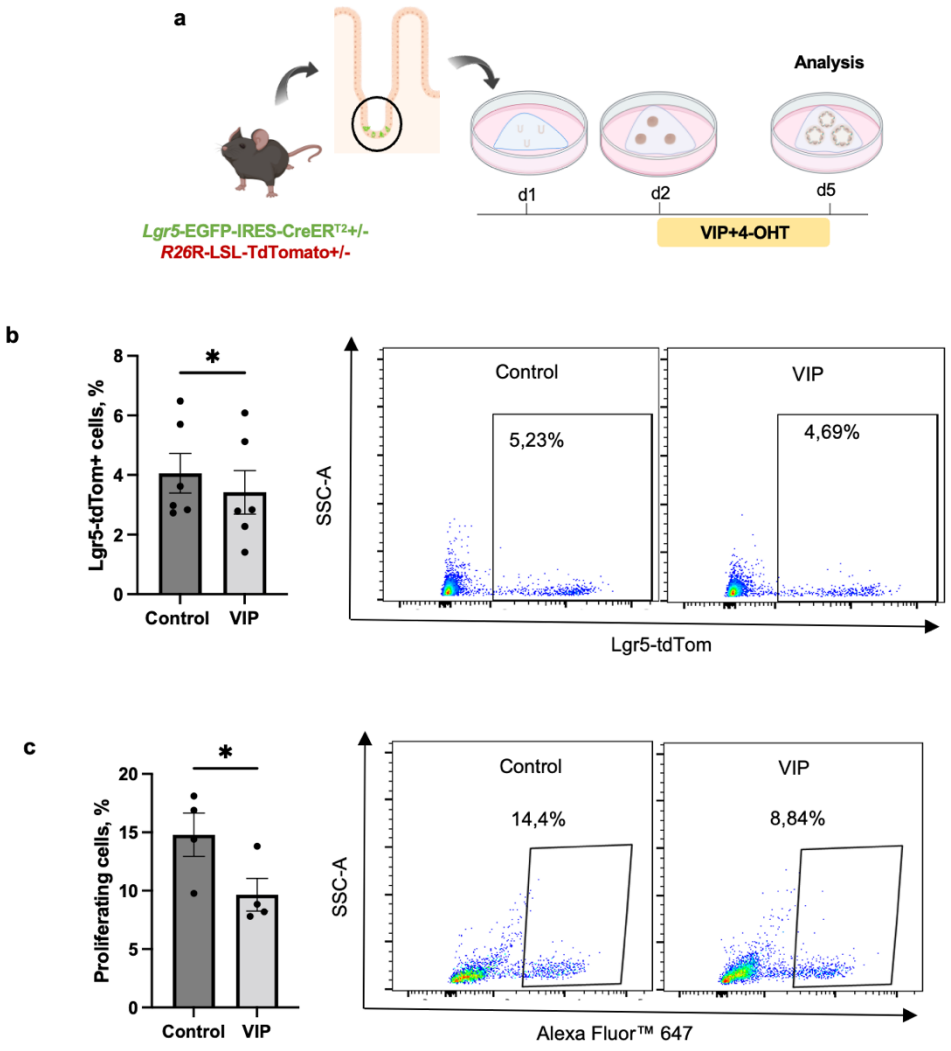

Figure 14. VIP reduces Lgr5-EGFP+ ISC progeny *in vitro.*
a, Experimental setup and treatment scheme. **b,** Analysis of Lgr5-EGFP+ ISC progeny following VIP treatment (n=6 per group). **c,** Analysis of cellular proliferation

by EdU assay following VIP treatment (n=4 per group). **p < 0.05, **p < 0.01, ***p < 0.001, ****p < 0.0001.* Data are shown as means ± SEM, n = number of biological replicates. Statistical analysis was performed using paired Student's *t*-test (**b, c**).

To further investigate the effects of VIP treatment on Lgr5-EGFP+ ISCs, we performed bulk RNA sequencing analysis of these cells isolated from both VIP-treated and untreated organoids derived from *Lgr5*-EGFP-IRES-CreER^{T2} reporter mice. This analysis revealed a distinct separation between treated and untreated Lgr5-EGFP+ ISCs in PCA plots, highlighting the profound effect of VIP on these cells (Figure 15a).

In treated Lgr5-EGFP+ ISCs, VIP induced a notable upregulation of genes associated with 'apical junction' and 'mitotic spindle' pathways – hallmark gene sets known for their roles in cell-cell adhesion and cell division, respectively (González-Mariscal et al., 2020; Prosser & Pelletier, 2017). Additionally, genes within the 'G2M checkpoint' pathway, crucial for cell cycle control and DNA damage repair (Yam et al., 2022), were also upregulated. These gene expression patterns support the observed expansion of Lgr5-EGFP+ ISCs following VIP treatment (Figure 15b).

The comparison with our bulk RNA sequencing data from whole VIP-treated organoids (see Figure 10c) further revealed that the transcriptional profiles associated with proliferation (upregulated 'mitotic spindle' and 'G2M checkpoint' hallmark pathways) clearly clustered with the isolated Lgr5-EGFP+ ISCs (Figure 15c). In contrast, pathways like the 'TNF-alpha/NF-κB signaling' pathway and 'epithelial-mesenchymal transition' were associated with the VIP effect on whole organoids (i.e., non-Lgr5-EGFP+ cell types), thus indicating that VIP may induce compartment-specific transcriptional changes in intestinal epithelial cells (Figure 15c).

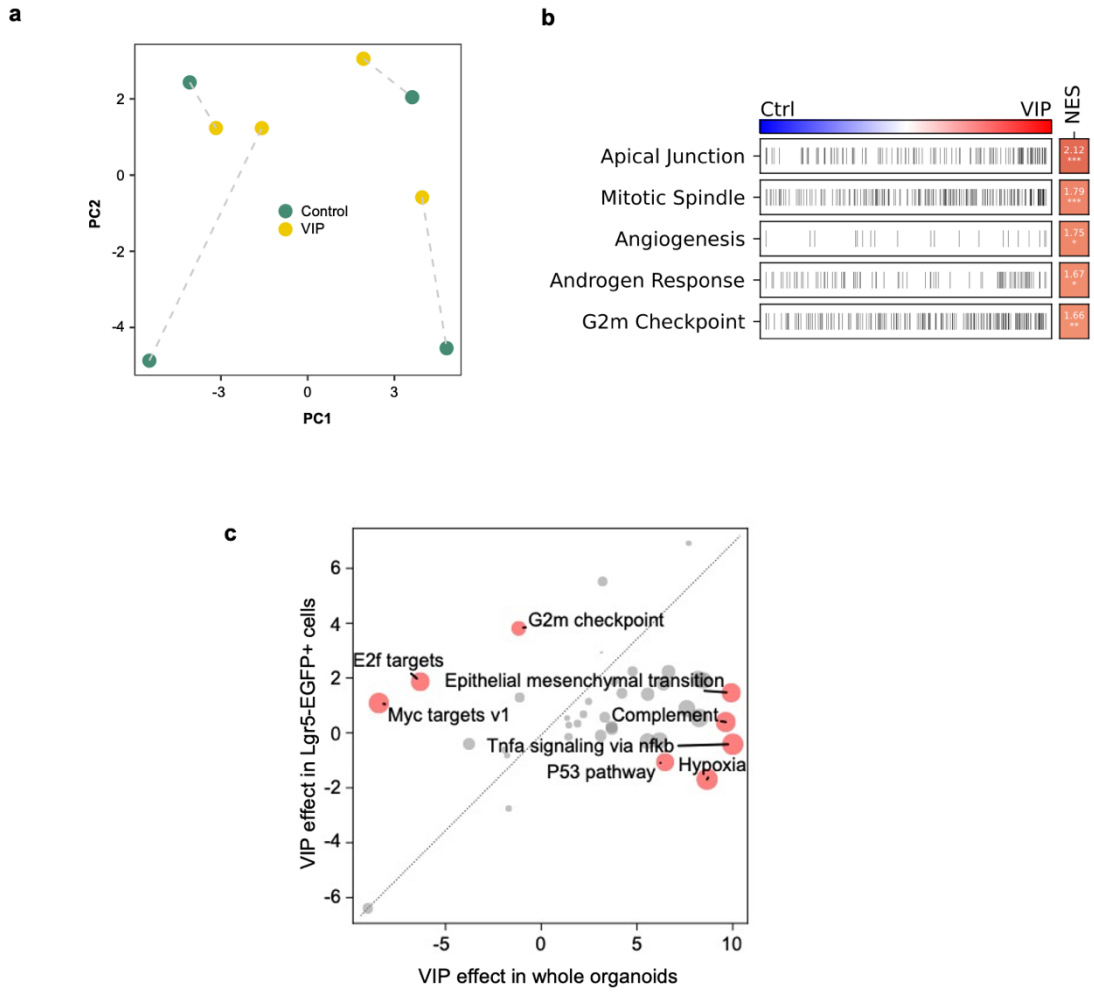

Figure 15. Gene expression profiles of Lgr5-EGFP+ ISCs in organoids following VIP treatment.

a, Principal component analysis (PCA) of transformed count data from bulk RNA sequencing of Lgr5-EGFP+ ISCs isolated from intestinal control organoids and organoids treated with VIP (n=4 per group). **b,** Hallmark gene-set enrichment analysis of differential gene expression in Lgr5-EGFP+ ISCs isolated from VIP-treated organoids; Ctrl = control, NES = normalized enrichment score. **c,** VIP-induced differential upregulation of hallmark pathways in Lgr5-EGFP+ ISCs compared to treated whole organoids.

3.3 VIP in injury conditions

3.3.1 Irradiation-based injury model

Considering the significant impact of VIP on Lgr5-EGFP+ ISCs under normal physiological conditions, we aimed to explore whether VIP could modulate cell regeneration following injury. Since Lgr5-EGFP+ ISCs have been described to be essential for intestinal regeneration after irradiation-induced damage (Metcalfe et al., 2014), we developed an irradiation-based injury model that involved the exposure of intestinal organoids to a single dose of ionizing irradiation.

To identify an appropriate irradiation dose for our injury model, we first assessed the radiosensitivity of intestinal organoids. This was done by exposing the organoids to various doses of ionizing irradiation 48 hours post-plating, a time point chosen to allow for recovery after stress associated with the isolation procedure. The survival of organoids was then monitored over the next 8 days. Based on these data, we generated a survival curve and determined the organoid radiosensitivity as 4.75±0.05 Gy, which represents a dose required to ensure the survival of 37% of all organoids (Figure 16a). Furthermore, by analyzing changes in organoid size over time, we detected a dose-dependent size reduction following irradiation (Figure 16b). A dose of 6 Gy was chosen for all subsequent experiments as a point that exceeds the established radiosensitivity threshold, presenting a more challenging yet survivable condition for the organoids and enabling the study of repair mechanisms without causing complete cell death.

To explore the potential impact of VIP on the intestinal epithelium under conditions of injury, we designed two experimental models. These models aimed to investigate VIP as a preventive agent by adding VIP to the organoid cultures before irradiation or as a therapeutic agent by treating organoids with VIP post-irradiation (Figure 16c).

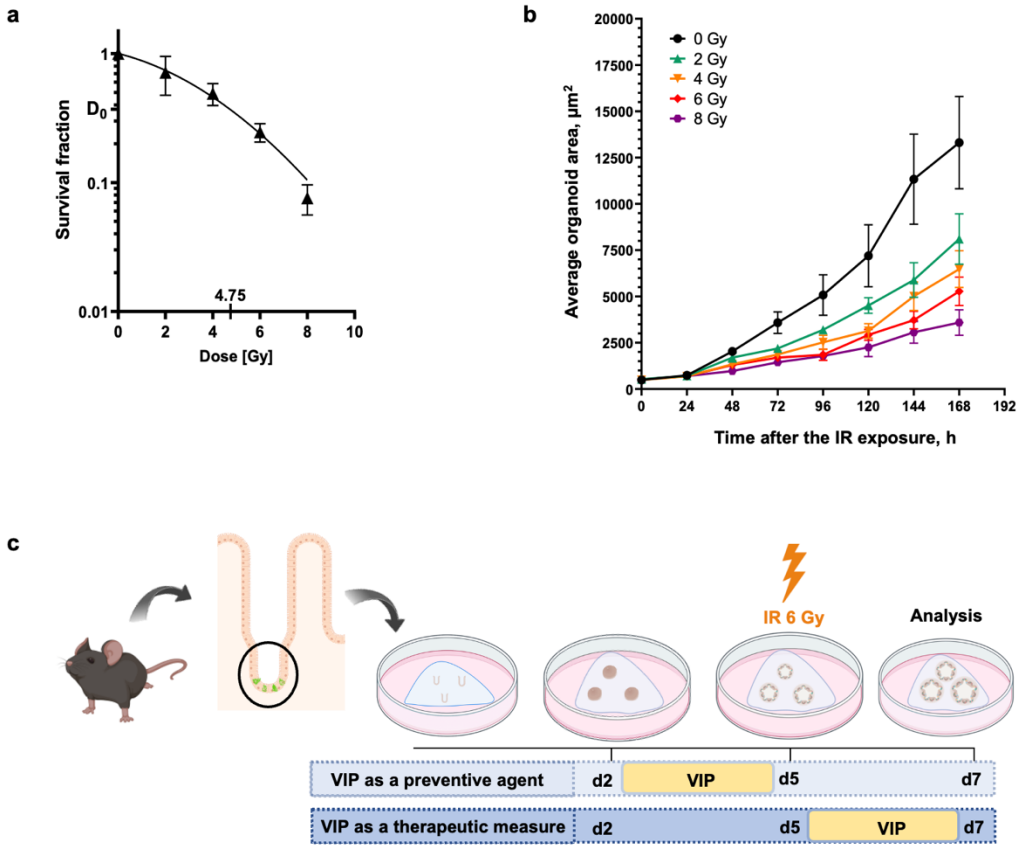

Figure 16. Establishment of the irradiation-based injury models *in vitro.*

a, Mean survival fraction of the murine small intestinal organoids after a single dose of X-ray radiation (2 Gy, 4 Gy, 6 Gy, 8 Gy, or 0 Gy) performed at 24 h after the organoid plating and followed by seven days on culture. Data are shown as means ± SD. The dose-response curve was fitted using the non-linear fit in accordance with the linear-quadratic model (n=4 biological replicates). The radiosensitivity dose, denoted by D0, is 4.75 ± 0.05 Gy. **b,** Organoid growth represented by the mean organoid area in μm^2 after a single dose of X-rays (0, 2, 4, 6, or 8 Gy) measured for 7 days after the IR exposure. The data represents the mean organoid area per dose per sample (0 h, 24 h, 48 h, 72 h, 96 h, 168 h, n = 5; 120 h, 144 h, n = 4). Data are shown as means ± SEM. **c,** Injury models that aimed to identify VIP as a preventive agent or a therapeutic measure.

3.3.2 VIP as a preventive agent

The first model explored whether VIP could trigger cellular mechanisms that would increase organoid resilience to irradiation damage. To assess the preventive capabilities of VIP, we developed an irradiation-based acute injury model in which organoids were first treated with VIP for 72 hours and then exposed to 6 Gy of ionizing irradiation. On day 2 post-irradiation, the organoids were analyzed for the number and progeny of Lgr5-EGFP+ ISCs, as well as for

overall proliferation (Figure 17a). The analysis showed that VIP pre-treatment did not induce significant changes in the number or progeny of Lgr5-EGFP+ ISCs, nor did it affect overall proliferation (Figure 17a-c).

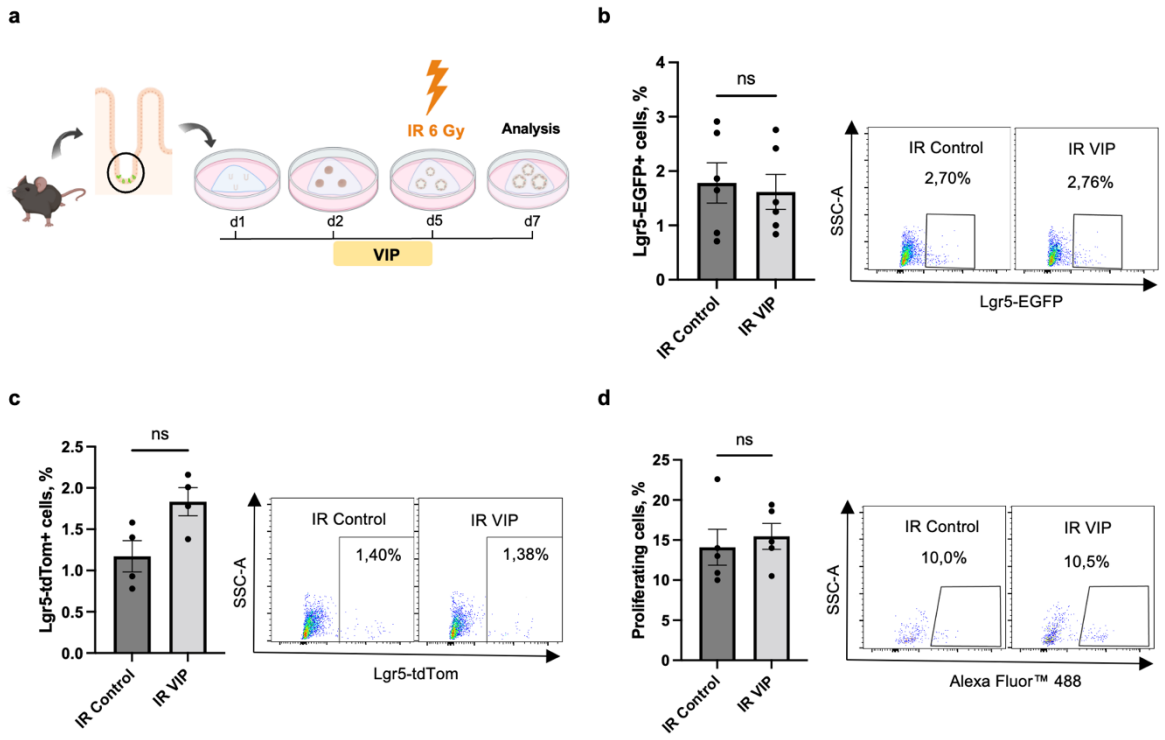

Figure 17. VIP pre-treatment does not protect against radiation-induced damage *in vitro.*

a, Experimental setup and treatment scheme. **b,** Flow cytometry analysis of Lgr5-EGFP+ ISC number in untreated and VIP pre-treated organoids following irradiation (n=6 per group). **c,** Flow cytometry analysis of Lgr5-EGFP+ ISC progeny in untreated and VIP pre-treated organoids following irradiation (n=4 per group). **d,** Analysis of cell proliferation in untreated and VIP pre-treated organoids following irradiation determined by EdU assay (n=5 per group). *$p < 0.05$, **$p < 0.01$, ***$p < 0.001$, ****$p < 0.0001$. Data are shown as means ± SEM, n = number of biological replicates. Statistical analysis was performed using paired Student's *t*-test (**b-d**).

3.3.3 VIP as a therapeutic agent

The second model aimed to evaluate the efficacy of VIP as a therapeutic measure, hypothesizing that VIP could promote recovery and repair following damage induced by irradiation. In this model, we subjected organoids to 6 Gy of ionizing irradiation on day 5 after plating, followed by VIP treatment for the next 48 hours (Figure 18a). Interestingly, in this context, VIP treatment induced a significant expansion of Lgr5-EGFP+ ISCs (Figure 18b). This

expansion, in turn, appeared to trigger a notable increase in the progeny of Lgr5-EGFP+ ISCs (Figure 18c), pointing at the capacity of VIP to mitigate irradiation-induced damage to Lgr5-EGFP+ ISC function. Consistent with these findings, we observed an increase in overall proliferation induced by VIP treatment following irradiation injury, as demonstrated by EdU assay analysis (Figure 18d). Furthermore, VIP treatment also appeared to be associated with a reduction in apoptosis in irradiated organoids (Figure 18e), which supported enhanced cell survival as corroborated by ATP-based CellTiter-Glo® assay (Figure 18f).

To gain additional insights, we performed bulk RNA sequencing analysis of irradiated Lgr5-EGFP+ ISCs in the presence or absence of VIP treatment. This analysis revealed a prominent induction of the hallmark pathway p53 in irradiated, VIP-treated Lgr5-EGFP+ ISCs (Figure 18g). This remains of special interest since the p53 pathway is critically involved in DNA damage response by regulating cell cycle arrest, apoptosis, and repair processes (Abuetabh et al., 2022). The activation of the p53 pathway in VIP-treated Lgr5-EGFP+ ISC post-irradiation suggests that VIP might enhance the intrinsic ability of these ISCs to recover from irradiation-induced damage.

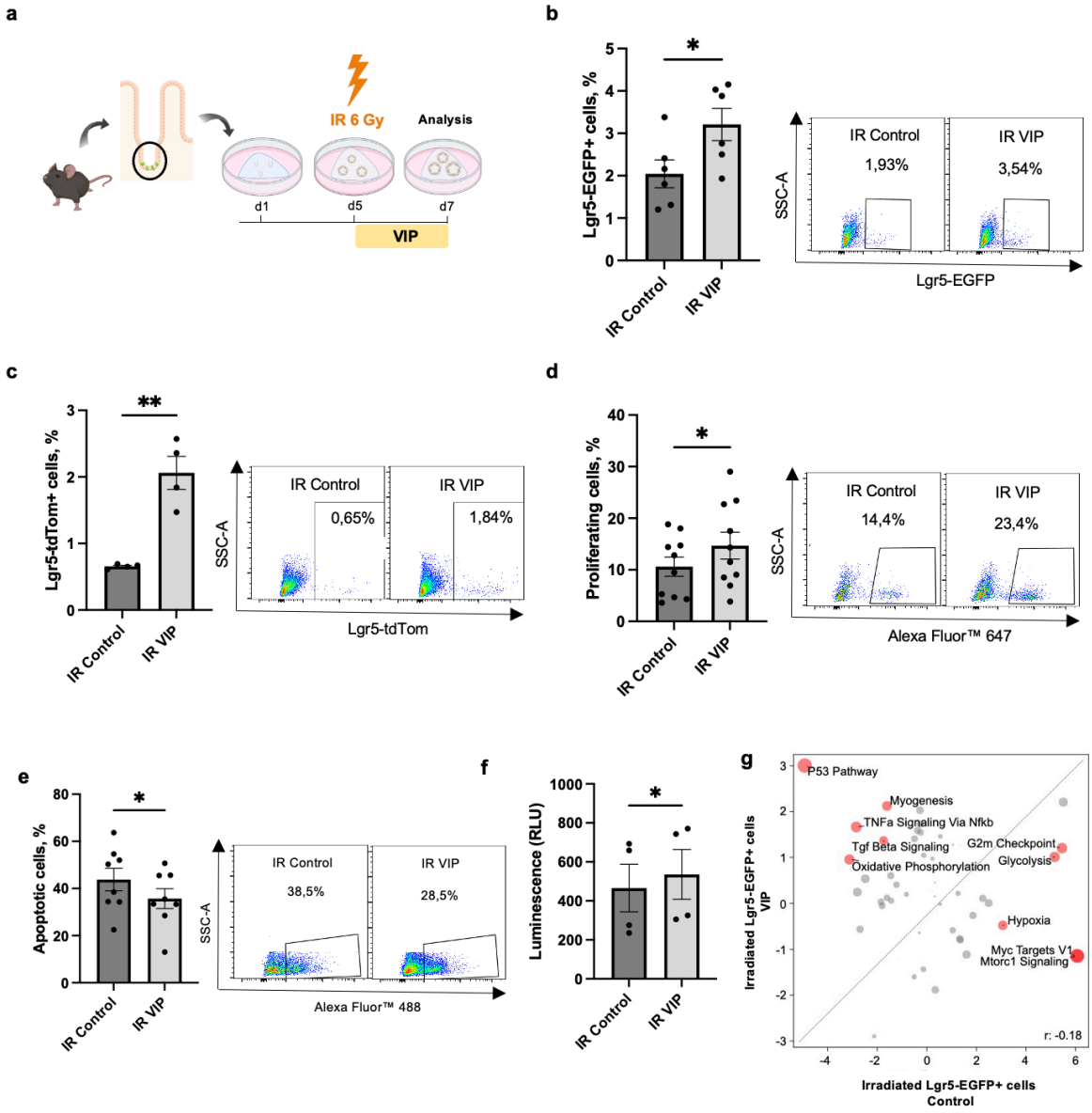

Figure 18. VIP mitigates irradiation-induced injury in intestinal organoids.

a, Experimental setup and treatment scheme. **b,** Flow cytometry analysis of Lgr5-EGFP+ ISC number in irradiated untreated and VIP-treated organoids (n=6 per group). **c,** Flow cytometry analysis of Lgr5-EGFP+ ISC progeny in irradiated untreated and VIP-treated organoids (n=4 per group). **d,** Analysis of cell proliferation in irradiated untreated and VIP-treated organoids determined by EdU assay (n=10 per group). **e,** Quantification of apoptotic cells in irradiated untreated and VIP-treated organoids determined by TUNEL assay (n=8 per group). **f,** Analysis of cell survival of irradiated untreated and VIP-treated organoids determined by ATP-based CellTiter-Glo® assay (n=4 per group). **g,** VIP-induced differential upregulation of hallmark pathways in Lgr5-EGFP+ ISCs in irradiated samples compared to irradiated organoids in the absence of VIP. *$*p < 0.05$, **$p < 0.01$, ***$p < 0.001$, ****$p < 0.0001$.* Data are shown as means ± SEM, n = number of biological replicates. Statistical analysis was performed using paired Student's *t*-test (**b-f**).

Since this treatment scheme differed from treatments of organoids at earlier time points in culture with VIP (Figure 19a), we examined the VIP effects also in sham-irradiated organoids in the current settings. Surprisingly, the onset of VIP treatment at day 5 in sham-irradiated organoids showed no significant change in the number or progeny of Lgr5-EGFP+ ISCs (Figure 19b) nor in the overall cellular proliferation (Figure 19c), which prominently contrasts our previous results (see Figure 13 and Figure 14).

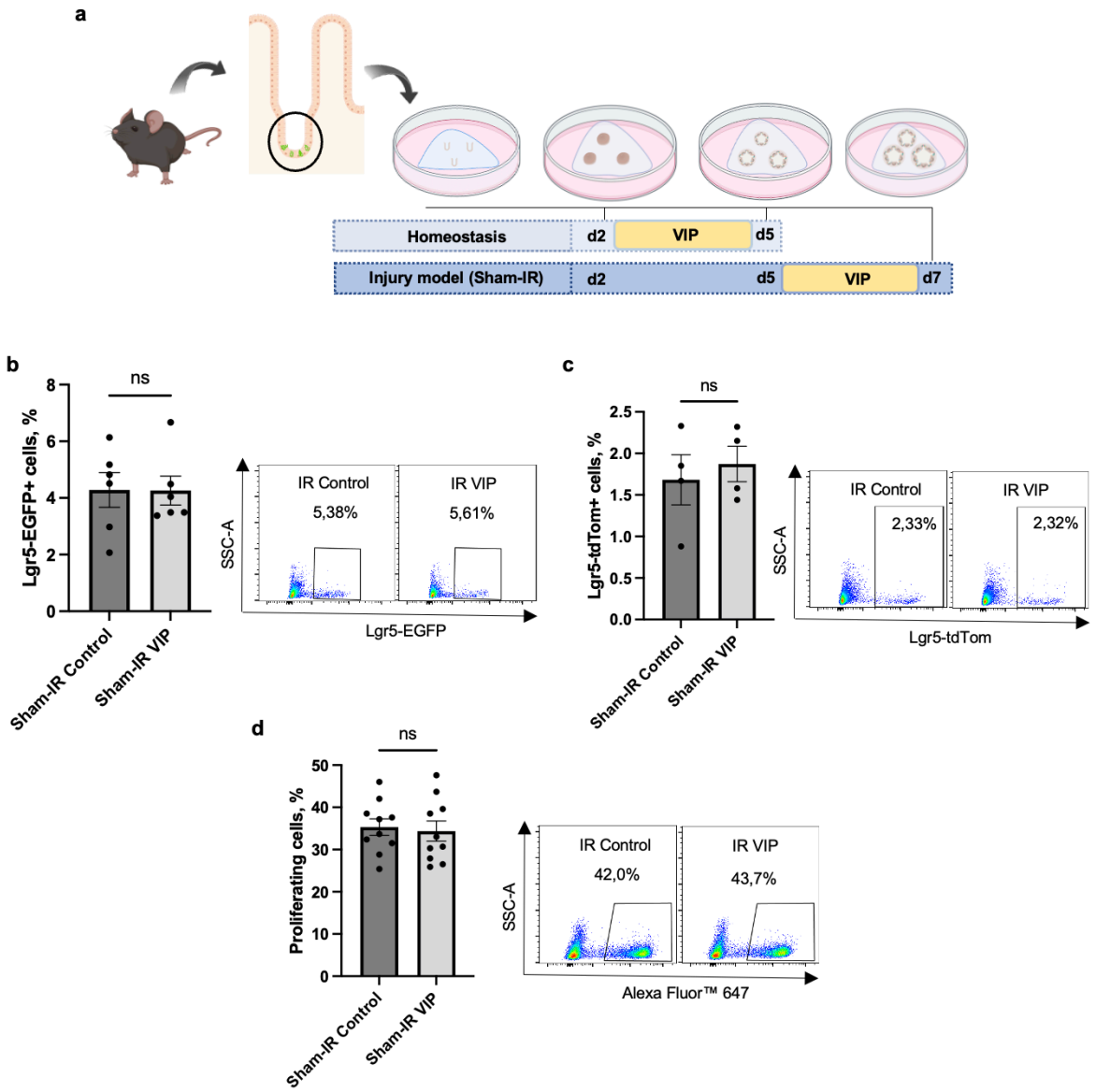

Figure 19. VIP effect on intestinal organoids following VIP treatment initiation at day 5. **a**, Comparison of treatment schemes. **b,** Flow cytometry analysis of Lgr5-EGFP+ ISC number in sham-irradiated untreated and VIP-treated organoids (n=6 per

group). **c,** Flow cytometry analysis of Lgr5-EGFP+ ISC progeny in sham-irradiated untreated and VIP-treated organoids (n=4 per group). **d,** Analysis of cell proliferation in sham-irradiated untreated and VIP-treated organoids determined by EdU assay (n=10 per group). **p < 0.05, **p < 0.01, ***p < 0.001, ****p < 0.0001.* Data are shown as means ± SEM, n = number of biological replicates. Statistical analysis was performed using paired Student's *t*-test (**b-d**).

This outcome can be attributed to the later onset of VIP treatment or the shorter exposure to VIP. However, bulk RNA sequencing analysis of Lgr5-EGFP+ ISC of organoids treated with VIP at this later stage revealed the prominent upregulation of hallmark pathways such as 'Myc targets v1' or 'Mtorc1 signaling' (Figure 20a). When these findings were compared with Lgr5-EGFP+ ISCs of organoids treated with VIP at an earlier time point in culture, it became clear that VIP induced distinct transcriptional changes in Lgr5-EGFP+ ISCs depending on their status in culture. In view of the observed different responses, principal component analysis confirmed the clear separation of the groups by VIP treatment and irradiation (Figure 20b).

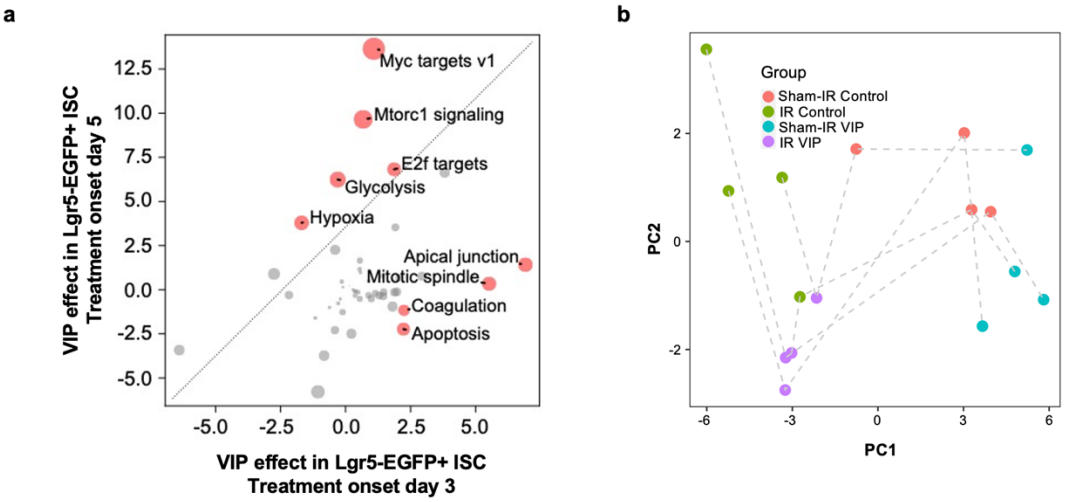

Figure 20. Gene expression profiles of Lgr5-EGFP+ ISCs in organoids treated with VIP at a later time point.
a, VIP-induced differential upregulation of hallmark pathways in Lgr5-EGFP+ ISC in organoids following treatment initiation at day 5 compared to day 3. **b,** Principal component analysis of transformed count data from the bulk RNA sequencing of Lgr5-EGFP+ ISCs isolated from irradiated or sham-irradiated intestinal organoids.

3.4 VIP effects on the intestinal epithelium *in vivo*

3.4.1 VIP in homeostatic conditions

To investigate whether observed VIP effects on intestinal organoids can be translated *in vivo*, we conducted experiments using *Lgr5*-EGFP-IRES-CreER^{T2} mice. These mice received 750 μg/kg VIP via intraperitoneal injections for 5 consecutive days (Figure 21a). Following the treatment period, jejunal crypts were collected and analyzed for the proportion of Lgr5-EGFP+ ISCs by flow cytometry. The analysis revealed an expansion of the Lgr5-EGFP+ ISC pool in the VIP-treated group, suggesting a stimulatory role of VIP on these cells (Figure 21b).

To further validate these findings, we aimed to inhibit VIP signaling by treating mice with a potent VIP receptor antagonist, VIP fragment 6-28, at a dosage of 500 μg/kg through daily i.p. injections over five consecutive days (Figure 21c). This treatment resulted in a significant decrease in Lgr5-EGFP+ ISCs, thereby confirming the role of VIP in expanding the Lgr5-EGFP+ ISC population (Figure 21d).

Next, to determine if VIP treatment *in vivo* exerts an effect on Lgr5-EGFP+ ISC progeny, we treated *Lgr5*-EGFP-IRES-CreER^{T2}/*R26*R-LSL-TdTomato mice with a single dose of 3 mg Tamoxifen via oral gavage, followed by daily i.p. injections of 750 μg/kg VIP (Figure 21e). The analysis of crypt epithelial cells from these mice, however, did not reveal significant differences in Lgr5-EGFP+ ISC progeny between VIP-treated and control mouse cohorts (Figure 21f).

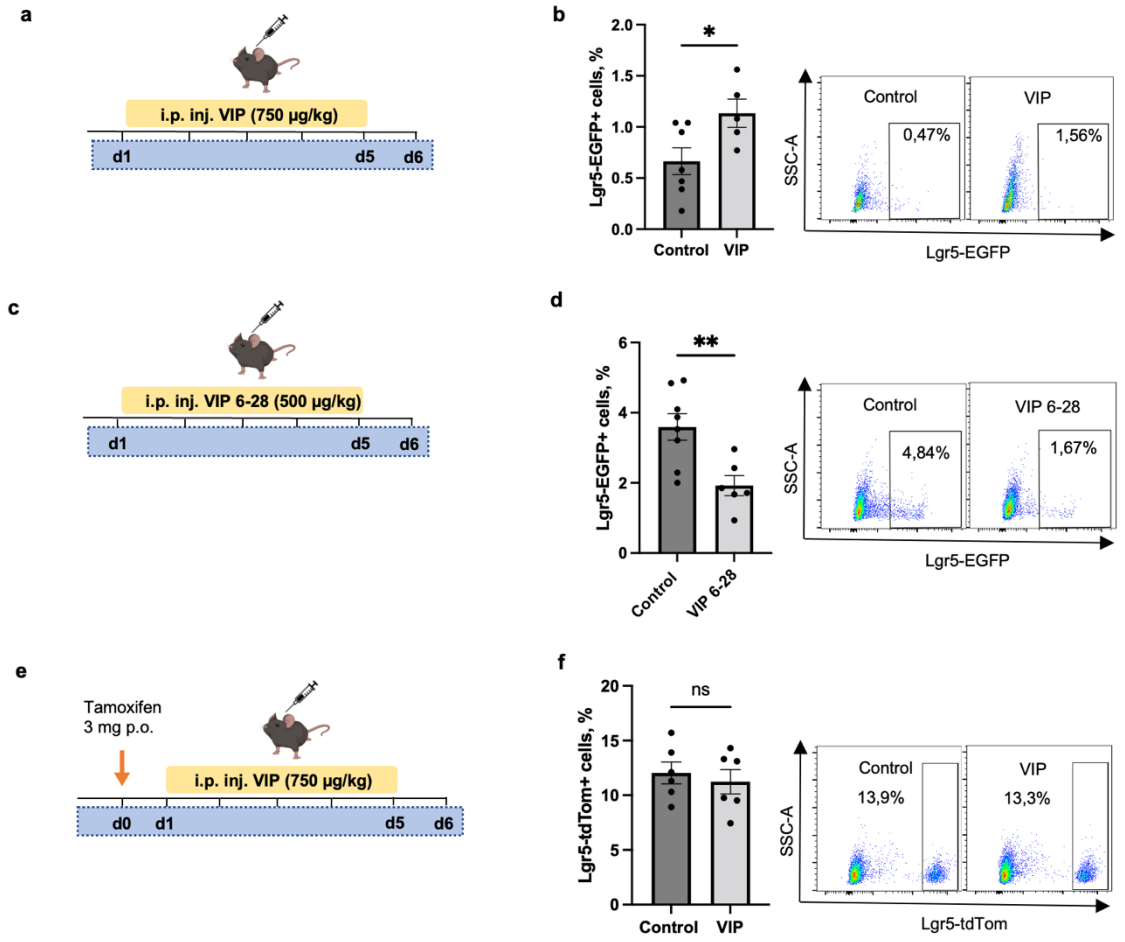

Figure 21. VIP increases Lgr5-EGFP+ ISC number *in vivo.*

a, Experimental outline for administration of VIP in mice. **b,** Flow cytometry analysis of Lgr5-EGFP+ ISC number in jejunal crypts of mice treated with VIP. n=7 (Control), n=5 (VIP). **c,** Experimental outline for administration of VIP receptor antagonist VIP 6-28 in mice. **d,** Flow cytometry analysis of Lgr5-EGFP+ ISC number in jejunal crypts of mice treated with VIP receptor antagonist VIP 6-28. n=7 (Control), n=6 (VIP 6-28). **e,** Experimental outline for administration of VIP in mice following Tamoxifen treatment. **f,** Flow cytometry analysis of Lgr5-EGFP+ ISC progeny in jejunal crypts of mice treated with VIP (n=7 per group). *$*p < 0.05$, $**p < 0.01$, $***p < 0.001$, $****p < 0.0001$.* Data are shown as means ± SEM, n = number of biological replicates. Statistical analysis was performed using unpaired Student's *t*-test (**b, d,** and **f**).

3.4.2 VIP in a model of irradiation-based injury

To further investigate the regenerative potential of VIP *in vivo*, we deployed an abdominal irradiation model in mice. In this model, mice received 12 Gy of abdominal irradiation followed by daily intraperitoneal administration of 750 *µ*g/kg VIP for three consecutive days from day 3 onwards (Figure 22a).

Our prior *in vitro* analyses of gene expression showed that VIP induced the upregulation of several hallmark pathways potentially involved in regeneration, such as 'apical junction' and 'p53 pathway' (Figure 15 and Figure 18). To determine if VIP regulates the same mRNA targets *in vivo*, we performed qPCR experiments on jejunal crypt samples from irradiated and treated mice. This involved the analysis of leading-edge genes for 'apical junction' hallmark pathway: *Acta1 (Actin alpha 1), Gnai2 (G protein subunit alpha I2), Jup (Junction plakoglobin),* and for 'p53 hallmark pathway': *Dcxr (Dicarbonyl and L-xylulose reductase), Cdkn1a (Cyclin-dependent kinase inhibitor 1A), Ccng1 (Cyclin G1).*

The analysis revealed an elevation in the transcription of genes associated with the 'apical junction' pathway following VIP treatment after irradiation exposure, compared to irradiation alone. Although not all genes showed a statistically significant elevation, a clear trend towards increased expression was observed (Figure 22b). Similarly, the expression of genes related to the 'p53 pathway' also showed a trend towards upregulation in the presence of VIP treatment (Figure 22c). Thus, the observed VIP effects align with our *in vitro* findings, suggesting a similar impact of VIP on epithelial regeneration *in vivo*.

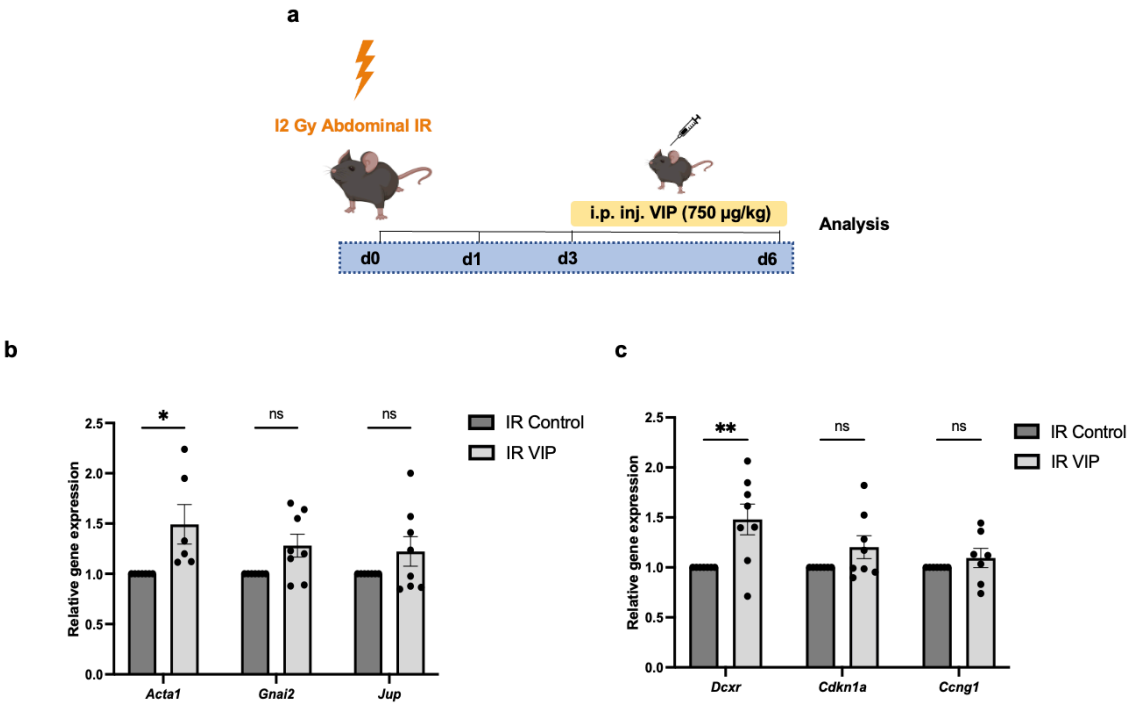

Figure 22. VIP post-irradiation treatment *in vivo* upregulates gene expression profiles similar to those observed *in vitro.*

a, Experimental outline and treatment scheme. **b,** Expression of leading-edge genes of hallmark pathway 'apical junction' in jejunal crypts of irradiated mice determined by qPCR. n=8 (*Acta1* Control), n=6 (*Acta1* VIP), n=8 (*Gnai2* Control), n=8 (*Gnai2* VIP), n=8 (*Jup* Control), n=8 (*Jup* VIP). **c,** Expression of leading-edge genes of the 'p53 pathway' in jejunal crypts of irradiated mice determined by qPCR. n=8 (*Dcxr* Control), n=6 (*Dcxr* VIP), n=8 (*Cdkn1a* Control), n=8 (*Cdkn1a* VIP), n=8 (*Ccng1* Control), n=7 (*Ccng1* VIP). **p < 0.05, **p < 0.01, ***p < 0.001, ****p < 0.0001.* Data are shown as means ± SEM, n = number of biological replicates. Statistical analysis was performed by one-way ANOVA (**b, c**).

High levels of VIP have been reported in patients undergoing radiation therapy (Höckerfelt et al., 2000). In order to determine whether irradiation influences VIP production in our experimental model, we performed an ELISA analysis on samples from the small intestines of mice that were subjected to irradiation, compared with those from sham-irradiated mice. Our results indicate that VIP levels were indeed significantly higher in the small intestine of irradiated mice compared to the sham-irradiated group (Figure 23a). This elevation suggests that VIP could play a role in the response to stress induced by irradiation.

Mice exposed to abdominal irradiation initially exhibited a notable decline in body weight, which stabilized by day 6, leading to a partial recovery by the end of the experimental timeline.

The VIP-treated cohort showed a trend towards faster regeneration from acute injury (Figure 23b). In line with these observations, we detected reduced shrinking of the small intestines (a surrogate marker for structural alterations to the GI tract after IR (Sittipo et al., 2020) (Figure 23c). Furthermore, pathological scoring of intestinal tissue sections post-irradiation revealed that mice treated with VIP displayed significantly reduced signs of intestinal inflammation and epithelial injury, indicating a protective function of VIP after intestinal IR (Figure 23d).

Next, to assess the potential anti-inflammatory effect of VIP, we measured tissue TNF-alpha levels in irradiated and sham-irradiated samples. As expected, ELISA analysis revealed a significantly elevated level of TNF-alpha in the irradiated group compared to sham-irradiated mice due to irradiation-induced inflammation. However, VIP administration resulted in reduced TNF-alpha levels compared to the irradiation-only cohort (Figure 23e), therefore demonstrating the ability of VIP to ameliorate the intestinal inflammatory response induced by abdominal irradiation.

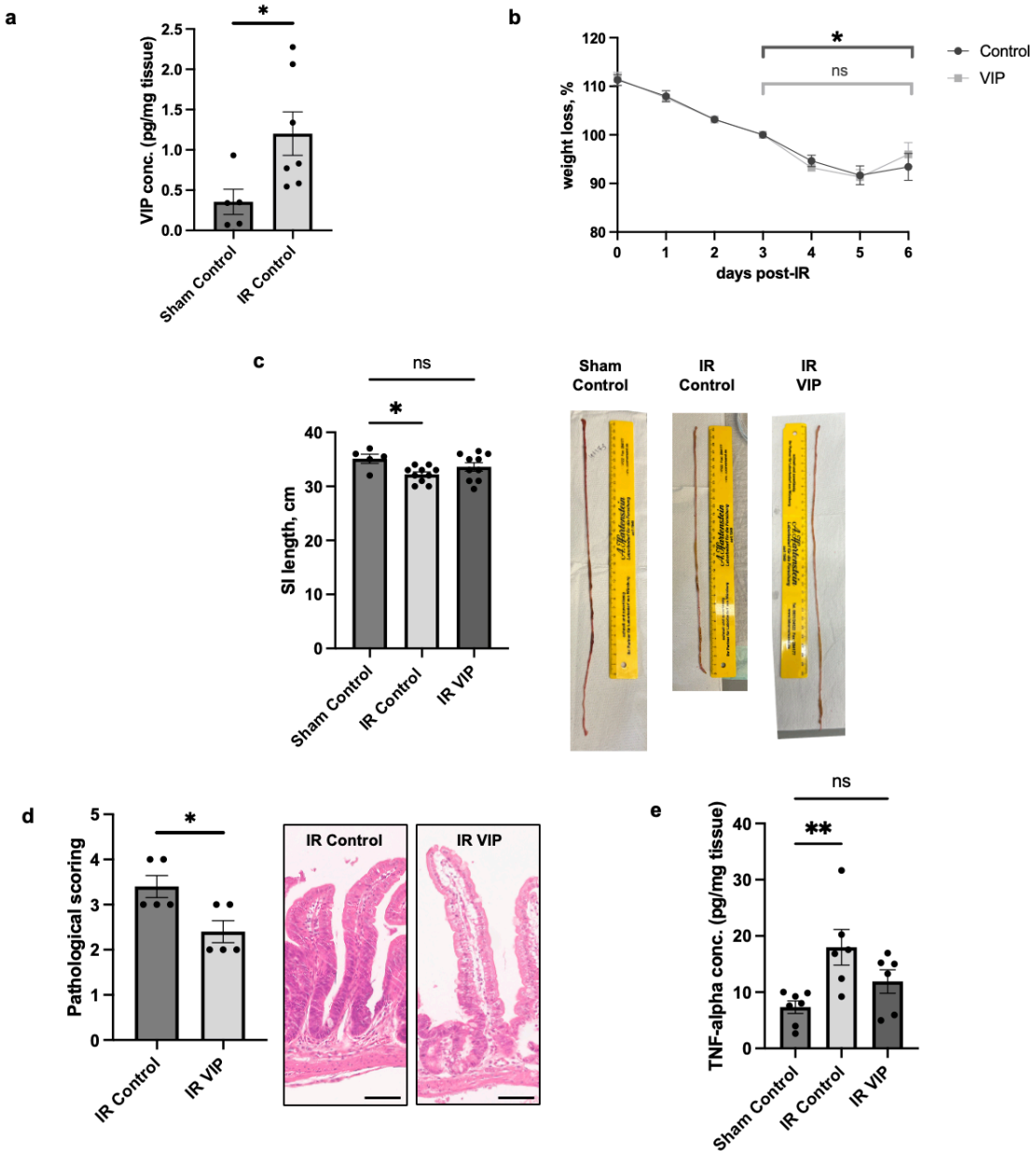

Figure 23. VIP mitigates irradiation-induced injury *in vivo.*

a, ELISA analysis of VIP levels in the intestinal wall on day 6 following acute abdominal irradiation. n=5 (Sham Control), n=7 (IR Control). **b,** Weight analysis in mice after abdominal irradiation. Data are normalized to the time point corresponding to the onset of the VIP treatment (n=6 per group). **c,** Total length of the small intestine in mice after abdominal irradiation. n=5 (Sham Control), n=10 (IR Control; IR VIP). **d,** Pathological scoring of irradiated mouse tissue in the absence or presence of VIP and representative H&E images (Scale bars, 100 μm, n=5 per group). **e,** ELISA analysis of TNF-alpha levels in the intestinal wall of irradiated mice in the absence or presence of VIP. n=7 (Sham Control), n=6 (IR Control; IR VIP). *$*p < 0.05$, $**p < 0.01$, $***p < 0.001$, $****p < 0.0001$.* Data are shown as means ± SEM, n = number of biological replicates. Statistical analysis was

performed using unpaired Student's t-test in (**a, b,** and **d**) and one-way ANOVA (**c, e**).

Finally, we investigated whether the effect of VIP on cellular composition *in vivo* mirrors the trend observed *in vitro*. First, we assessed the numbers of Lgr5-EGFP+ ISCs and observed that VIP did not induce a significant difference in Lgr5-EGFP+ ISC pool sizes (Figure 24b). This suggests that the protective effects of VIP might be mediated through mechanisms that modulate signaling pathways promoting cellular repair and survival without altering the ISC pool size. Next, we detected a significant expansion of Lyz1+ cells in irradiated, VIP-treated mice compared to control groups (Figure 24a). The observed increase in Lyz1+ cells could explain the improved tissue repair in VIP-treated mice following irradiation, as Paneth cells play a crucial role in maintaining the intestinal stem cell niche and producing antimicrobial peptides (Cui et al., 2023). These findings suggest that VIP enhances regeneration from acute injury, potentially by promoting Paneth cell differentiation *in vivo*.

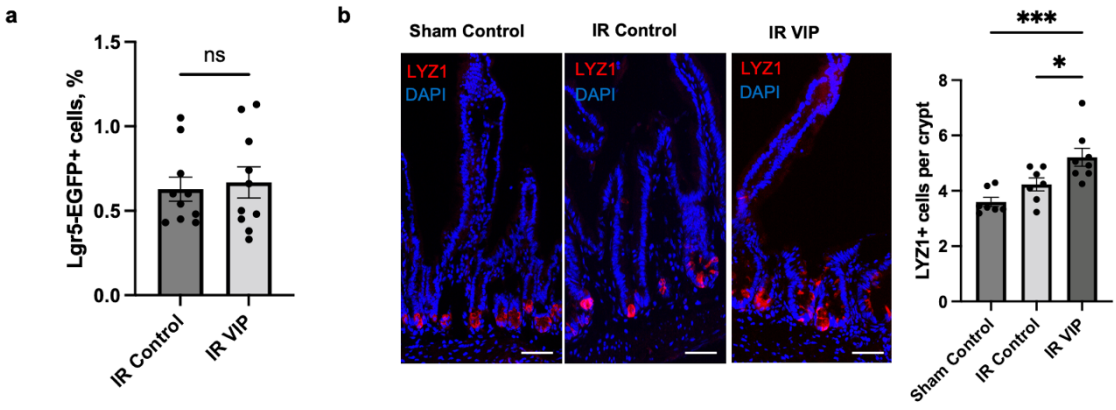

Figure 24. VIP changes cellular composition in the murine intestinal epithelium after abdominal irradiation.
a, Flow cytometry analysis of Lgr5-EGFP+ ISC number in jejunal crypts following acute abdominal irradiation. n=10 per group. **b,** Immunofluorescent analysis of Lyz1 in the murine jejunum following acute abdominal irradiation (Scale bars, 100 μm). n=7 (Sham Control; IR Control), n=8 (IR VIP). Data are shown as means ± SEM, ns = not significant. n = number of biological replicates. Statistical analysis was performed using unpaired Student's t-test (**a**) and one-way ANOVA (**b**).

4. DISCUSSION

Regulating ISC behavior is crucial for maintaining the balance between the generation of new cells and cell loss caused by harsh conditions of the luminal environment and mechanical stress from bowel movements. This regulation becomes even more critical in conditions of injury, where ISCs are essential for replacing damaged cells to ensure proper functioning and sufficient nutrient absorption (Barker, 2014). Damaged stem cell functions can lead to malabsorption and associated illnesses as well as malignant transformation of cells (Vermeulen & Snippert, 2014). Regulation of ISC behavior is achieved by multiple factors that constitute the intestinal stem cell niche, including neuronal mediators originating from the ENS and other non-neuronal sources (Middelhoff et al., 2020). The ENS is the largest component of the peripheral nervous system and regulates a variety of processes within the intestine (M. Rao & Gershon, 2016). While the effects of neuronal mediators on intestinal epithelial secretion and motility are well characterized, their influence on the regulation of ISCs has not been investigated in detail.

In the present study, we aim to determine the involvement of distinct neuronal mediators in the regulation of intestinal stem cell activity and differentiation. Our screening of neuronal mediators identified VIP as a prominent regulator of ISC behavior. We could demonstrate that VIP not only drives cell differentiation towards secretory phenotype but also regulates the number and proliferation of ISCs. Moreover, VIP significantly contributes to cell regeneration and recovery under conditions of injury.

4.1 The role of VIP in intestinal stem cell regulation

Accumulating evidence suggests that VIP plays a significant role in modulating distinct aspects of epithelial cell functions in the small intestine. This is supported by the close proximity of VIPergic nerve fibers to intestinal crypts (Schwerdtfeger & Tobet, 2020; Wu et al., 2015), substantial gene expression of VIP receptors in distinct compartments of the epithelium, including ISC populations (Haber et al., 2017), and protein expression of VPAC1 on the plasma membranes of epithelial cells (Jayawardena et al., 2017).

Previous evidence of VIP effects on cellular differentiation and proliferation has been primarily derived from VIP KO mouse models or 2D cell lines. However, animal models are often too complex to investigate direct effects on ISCs, and 2D cell lines do not fully capture the epithelial cell complexity and three-dimensional interactions. Thus, we employed intestinal

organoids as a model that provides an optimal platform to investigate the direct effects of VIP on the intestinal epithelium, recapitulating its cellular complexity and spatial architecture (Sato et al., 2009).

We have demonstrated that VIP induces a significant change in cell differentiation. Specifically, it increases the expression of *Lyz1*, a well-established marker of Paneth cells. Paneth cells are important members of the stem cell niche, providing essential growth factors necessary for the proper functioning of ISCs (Sato et al., 2011). This finding aligns with a reported reduction in the expression of *Lyz1* and other Paneth cell markers in mice lacking the VIP gene (Yusta et al., 2012). Furthermore, our studies reveal that VIP increases the number of Lyz1+ cells per organoid. VIP operates through GPCRs, primarily by activating G_{α} subunits that stimulate adenylate cyclase to increase cAMP production. Additionally, VIP receptor engagement can also activate $G_{\alpha q/11}$ proteins, leading to the activation of phospholipase C (Lu et al., 2022). Interestingly, the $G_{\alpha q/11}$-mediated pathway is known to play a role in Paneth cell maturation and localization (Watanabe et al., 2016), further supporting our findings.

The published reports about the influence of VIP on goblet cell numbers present conflicting results. While blocking VIP receptors *ex vivo* led to a decrease in epithelial goblet cell numbers in the murine ileum (Schwerdtfeger & Tobet, 2020), a study using VIP KO mice showed an increase in goblet cells across most segments of the small intestine. However, this increase was associated with decreased mucus accumulation in goblet cells, making them dysfunctional (Lelievre et al., 2007). The decreased expression of goblet cell markers was also reported in several other studies employing VIP KO mice or colonic cell lines (Hokari et al., 2005; Wu et al., 2015; Yusta et al., 2012). Here, we confirm the upregulation of typical goblet cell markers and show a trend towards Muc2+ goblet cell expansion upon VIP treatment. These observations suggest that pro-secretory functions of VIP involve not only known effects on increased secretion via the activation of ion channels (Banks et al., 2005) but also the promotion of secretory cell type differentiation associated with the increased expression of secretory markers.

We have shown that the induction of the observed pro-secretory phenotype was mediated mainly by the p38 MAPK pathway. The activation of p38 MAPK downstream of VIP was previously demonstrated in various cell types, including macrophages, keratinocytes, and colonic cells (Harhous et al., 2021; Hokari et al., 2005; X. J. Yu et al., 2010). In colonic cells, p38, as well as MEK/ERK MAPK pathways, were activated downstream of VIP signaling and triggered the expression of *Muc2* (Hokari et al., 2005). Several other studies show the

involvement of p38 MAPK in the regulation of secretory cell differentiation. For instance, treatment of mice with a p38 MAPK antagonist resulted in a decreased number of goblet cells in colonic mucosa (Otsuka et al., 2010). Similarly, deletion of p38 in mice also strongly reduced the goblet cell population (Otsuka et al., 2010). Furthermore, the activation of this pathway has been observed in developing Lyz1+ Paneth cells in intestinal organoids, supporting the hypothesis of p38-mediated secretory cell differentiation (Rodríguez-Colman et al., 2017).

Although the NF-κB pathway is also known to be associated with differentiation of the secretory lineage (Brischetto et al., 2021; Kunze et al., 2020) and seemed to be upregulated in VIP-treated organoids, our data, obtained using distinct antagonists targeting the NF-κB pathway, indicate that the VIP-driven pro-secretory phenotype appeared not mediated via NF-κB signaling.

In view of the significant reduction in the number of Lgr5-EGFP+ ISC progeny following VIP treatment in homeostatic conditions, it appears that increased secretory cell differentiation following VIP treatment originates from early stem cell progeny and/or the transit amplifying cell population independent of Lgr5-EGFP+ ISCs. Indeed, VIPR1, the main receptor for VIP in the intestinal epithelium, was shown to be expressed across different epithelial compartments of the small intestine (Haber et al., 2017).

In homeostatic conditions, we further observed that VIP agonism led to decreased cellular proliferation. Although a study employing a colonic cell line showed a VIP-induced increase in proliferation (Wu et al., 2015), knock-out models demonstrate uncontrolled cellular proliferation in the small bowel of VIP KO and VPAC1 KO mice (Fabricius et al., 2011; Yusta et al., 2012). VIP as an anti-proliferative agent was also identified in a co-culture model consisting of the human submucosa with the submucosal plexus and a human colonic epithelial monolayer (Toumi et al., 2003). These data may, therefore, suggest that VIP in physiological conditions regulates tissue homeostasis by inhibiting excessive cell proliferation. Interestingly, a study investigating the antagonism of p38 MAPK signaling reported not only a decrease in the differentiation of goblet cells but also an increase in the proportion of proliferating cells in the colonic mucosa of mice treated with a p38 MAPK inhibitor (Otsuka et al., 2010). In light of the observed promotion of p38 MAPK signaling in VIP-treated organoids, the effects of VIP on proliferation might also be mediated by p38 MAPK.

We could further extend these data with a detailed analysis of the influence of VIP on Lgr5-EGFP+ ISCs, which appear prominently modulated by VIP in regard to their cell number as well as proliferative activity. Specifically, VIP treatment significantly increased the number of

Lgr5-EGFP+ ISCs, yet, as outlined above, reduced the number of their progeny in the absence of acute tissue injury. This could hint at the modulation of the balance between the capacity of ISCs to undergo self-renewal and differentiation by VIP, which appear essential for maintaining the dynamic homeostasis of intestinal epithelial cells. Therefore, VIP appears to promote the self-renewal of Lgr5-EGFP+ ISCs in intestinal homeostasis, which results in an enlarged ISC pool and a reduction in generated progeny (Yan et al., 2017). Notably, our RNA sequencing analysis of VIP-treated Lgr5-EGFP+ ISCs showed the significant upregulation of the 'apical junction' hallmark pathway (leading edge genes such as *Actb, Gnai2, Ctnnd1*), which has been associated with the regulation of cell proliferation and differentiation (González-Mariscal et al., 2020). A similar trend towards expansion of Lgr5-EGFP+ ISCs was detected in mice treated with a glucagon-like peptide 2 (GLP-2) receptor agonist (Chen et al., 2022). Several studies have shown that GLP-2 can trigger VIP expression and secretion from enteric VIP-expressing neurons (De Heuvel et al., 2012; Sigalet et al., 2007). It appears, therefore, possible that the reported *in vivo* effect of GLP-2 is mediated via VIP signaling in LGR5+ ISCs.

A study employing a VIP KO mouse model showed that while the expression of several key stem cell regulators such as *Notch1, Hes1, Math1, Krüppel-like factor 4 (KLF4), KLF5,* and *Wif1* remained unchanged, the expression of the homeobox transcription factor *Cdx2* was significantly downregulated (Wu et al., 2015). This transcription factor is widely expressed in intestinal epithelial cells and was shown to be important during early developmental stages, as its loss results in abnormal intestinal morphology and excessive proliferation (Gao et al., 2009). The inducible ablation of Cdx2 in Lgr5+ ISCs of intestinal organoids leads to the loss of ISC markers and conversion into a pyloric stem cell phenotype (Simmini et al., 2014). A recent study showed that Cdx2 can facilitate the recruitment of other transcription factors to direct developmental programs in adult intestinal epithelial cells (Lorzadeh et al., 2024). This suggests that VIP may play a role in stabilizing adult stem cell function by supporting Cdx2 expression.

Another potential mechanism that mediates the regulation of ISCs by VIP could involve the modulation of metabolic pathways. VIP inhibits glycolysis in epithelial cells isolated from the rat small intestine (Rossi et al., 1989) and also affects glucose metabolism in various cell types (Maxwell et al., 1988; Merech et al., 2019). Glycolysis in ISCs is critical for the maintenance of ISC function and for controlling their fate (Li et al., 2023). Moreover, VIP may alter nitric oxide (NO) production in intestinal cells (González et al., 1997; Spessert, 1993), which is, in

turn, critical for ISC proliferation and differentiation (Huang et al., 2023; Peñarando et al., 2018).

It is also worth noting that the expansion of Lgr5-EGFP+ ISCs following VIP treatment appeared attenuated in more mature organoids in comparison to those treated earlier in culture. This observation suggests that younger or less mature Lgr5-EGFP+ ISCs are more responsive to VIP-induced regenerative cues than those treated at a later stage. It may be that early in culture, the ISCs and organoids are in a phase where they are more adaptable and responsive to external signals, such as those from VIP, which promote growth and regeneration. In contrast, once these cells reach a certain level of maturity, they might become less receptive to modulation by external factors, including VIP. Indeed, a recent study has shown that during the formation of organoids, cells lose cell specificity and adopt a more 'generic' state through regenerative reprogramming (Lukonin et al., 2020). This might also explain a more prominent effect of VIP under conditions of irradiation. When cells are irradiated, some types of mature cells undergo dedifferentiation, reverting to a more stem-like state, which enhances their plasticity and potential for regeneration (Morral et al., 2024). This more regenerative state might render these cells more responsive to external signals, such as those triggered by VIP.

4.2 The influence of VIP on the intestinal epithelial response to injury

In this study, we utilized acute irradiation injury as a model to induce intestinal damage. Irradiation directly damages DNA by introducing double-stranded breaks and also triggers the formation of free radicals and reactive oxygen species, which further contribute to DNA damage. These events lead to cell apoptosis and mitotic death due to the misrepair of double-strand breaks (Hur & Yoon, 2017).

Several reports showed that VIP demonstrates protective effects when applied as a prophylactic measure before the onset of injury. For instance, it prevented the re-occurrence of TNBS-induced colitis when the mice were pre-treated with VIP (Abad et al., 2003). Another study also demonstrated the beneficial effects of VIP when it was applied before the injections of the neurotoxin 1-methyl-4-phenyl-1,2,3,6-tetrahydropyridine (MPTP) in a model of Parkinson's disease. In this case, however, VIP treatment was more effective when applied up to 3 hours after MPTP administration (Delgado & Ganea, 2003). We also aimed to investigate whether VIP shows any beneficial effects when applied before the onset of injury in our *in vitro* irradiation model. Since dividing cells are more susceptible to radiation-induced DNA damage and we detected a significant anti-proliferative effect of VIP, we hypothesized that VIP may render cells more resistant to irradiation damage. However, VIP pre-treatment did not significantly mitigate the radiation-induced decrease of the Lgr5-EGFP+ ISC pool, their progeny, or the proportion of proliferating cells.

In contrast, when we applied VIP to organoid culture after irradiation, we observed that VIP treatment not only induced the significant expansion of Lgr5-EGFP+ ISCs more prominently than in homeostatic conditions but also markedly promoted the generation of their progeny. Several studies have shown that the acute ablation of Lgr5+ ISCs is well tolerated under homeostatic conditions (Tian et al., 2011) due to the high degree of plasticity of other cell types (Yousefi et al., 2017), yet during injury, when various cell populations are lost, the Lgr5+ ISC presence becomes critical (Metcalfe et al., 2014). Moreover, the constant ablation of Lgr5+ ISCs, including those newly originating from other cell types, compromises intestinal integrity (Tan et al., 2021). Therefore, the VIP-induced expansion of Lgr5-EGFP+ ISCs may contribute to intestinal regeneration and help in withstanding irradiation-induced stress.

Furthermore, acute injury alters the Lgr5-EGFP+ ISC programming in response to VIP treatment, leading to a prominent expansion of Lgr5-EGFP-tdRed+ progeny, which may serve to replace injured or apoptotic early progenitor cell types. Indeed, a recent study revealed that

acute irradiation induces the reprogramming of the intestinal epithelium, which results in the induction of new populations of ISCs (Morral et al., 2024). These cells are characterized by the expression of fetal-like genes and are important contributors to intestinal regeneration after irradiation injury. Importantly, the induction of these cells is mediated by transient p53 expression (Morral et al., 2024). This remains of special interest since VIP treatment appeared to induce the prominent activation of the p53 pathway in irradiated Lgr5-EGFP+ ISCs. In the context of acute intestinal irradiation, the activation of p53 is known to protect from the development of GI syndrome and promote survival (Kirsch et al., 2010). It is, therefore, possible that VIP enhances the induction of irradiation-induced stem cell populations, which contribute to the observed increase in the proportion of proliferative cells in VIP-treated irradiated organoids, in contrast to the VIP-induced decrease in cell proliferation under homeostatic conditions. Moreover, VIP promotes secretory cell lineage differentiation, and secretory cell lineage progenitor cell types have been shown to undergo de-differentiation and contribute to intestinal regeneration (Buczacki et al., 2013; Van Es et al., 2012).

In line with the observed effect on Lgr5-EGFP+ ISCs following irradiation, VIP treatment also reduced apoptosis and enhanced cell survival in irradiated organoids. Similarly, cytoprotective effects of VIP have been reported in cell-line derived cancer stem cells under drug-induced apoptosis, where VIP activated anti-apoptotic signaling, leading to the phosphorylation of proapoptotic protein BAD via the Ras/MAPK and PKA pathways (Sastry et al., 2017). Additionally, VIP significantly increased the survival of corneal endothelial cells exposed to hydrogen peroxidase-induced oxidative stress (Koh & Waschek, 2000). This evidence correlates with the enhanced p53 activation and improved cell survival in VIP-treated irradiated cells, potentially via p53-mediated cell-cycle arrest and DNA double-strand break repair mechanisms.

4.3 The effects of VIP *in vivo*

The observed effects of VIP on the number of Lgr5-EGFP+ ISCs *in vitro* were also reproduced *in vivo*, as we detected a significant increase in the population of Lgr5-EGFP+ ISCs isolated from jejunal crypts of mice receiving i.p. VIP injections. Similarly, antagonizing VIP *in vivo* resulted in a decrease in the numbers of Lgr5-EGFP+ ISCs. These findings indicate that VIP consistently regulates Lgr5-EGFP+ ISC populations in both experimental conditions and biological settings, highlighting its potential role as a key modulator of intestinal integrity.

We next aimed to validate the promotion of intestinal regeneration by VIP following acute irradiation injury *in vivo*. For this purpose, we devised an abdominal irradiation model, which allows for higher abdominal irradiation dosages and the prevention of bone marrow toxicity (Kirsch et al., 2010). Notably, irradiated intestinal tissues showed a significant upregulation of VIP production, suggesting the involvement of VIP in mediating processes triggered by irradiation. An increase in the immunoreactivity of VIP in the rat mucosa damaged by abdominal irradiation was also demonstrated by a previous study (Höckerfelt et al., 2000).

The mechanism underlying acute intestinal irradiation involves significant activation of several signaling pathways related to apoptosis, tight junctions, cell cycle, TNF-alpha cascades, and stimulation of the coagulation system (Mei et al., 2020). Indeed, TNF-alpha levels in the mucosa of irradiated mice were significantly increased, indicating an ongoing inflammatory response following radiation exposure. Interestingly, we observed a prominent reduction in TNF-alpha levels in irradiated VIP-treated mice, consistent with the reported anti-inflammatory properties of VIP (Delgado & Ganea, 2013). It is important to outline, however, that the anti-inflammatory effect of VIP *in vivo* may not be exclusive to the modulation of epithelial cells but also include potential effects on mucosal cell types such as cells of the immune system (Talbot et al., 2020).

Despite a relatively short VIP treatment regimen following abdominal irradiation, we observed significant structural and histopathological improvements in intestinal tissue following VIP treatment. Specifically, VIP alleviated irradiation-induced intestinal shrinkage and significantly improved the parameters of pathological scoring. The shortening of the intestine results partly from impaired regeneration processes and excessive apoptosis following irradiation. This suggests that VIP might expand the pool of Lgr5-EGFP+ ISCs and/or increase cell proliferation, thereby protecting the epithelium from irradiation-induced damage. However, we did not detect a significant increase in Lgr5-EGFP+ ISCs, in contrast to observations *in vitro*

and under homeostatic conditions *in vivo*. This discrepancy might be partly explained by a shorter treatment period compared to the treatment scheme under homeostatic conditions *in vivo*. Furthermore, irradiation may also impair the receptors or downstream signaling pathways through which VIP exerts its effects on the size of the Lgr5-EGFP+ ISC pool. Indeed, a study employing irradiation of the rat colon showed a decrease in VIP receptor expression and reduced cAMP accumulation (Morel et al., 2002). Additionally, as outlined in the previous section, the impact of VIP may vary based on the maturity state of cells, and the timing of VIP administration in relation to the onset of an injury could also play a role. In our *in vivo* injury model, VIP was administered 72 hours post-irradiation, whereas the intestinal organoids were treated with VIP immediately after irradiation. This difference in timing might also account for the different outcomes observed between the two models. Interestingly, we also detected a pronounced increase in Lyz1+ Paneth cells in VIP-treated mice following abdominal irradiation. Paneth cells support ISCs by secreting growth factors (Clevers & Bevins, 2013) and contribute to intestinal regeneration following irradiation-induced ISC loss (S. Yu et al., 2018). Moreover, Paneth cells are essential for protecting the intestinal stem cell niche against bacterial dysbiosis (Cui et al., 2023). The intestinal microbiota plays an important role in tissue regeneration after injury (Ki et al., 2014), and irradiation induces substantial changes in the bacterial compositions in the small and large intestines (Kim et al., 2015). Importantly, increased secretion of antimicrobial peptides by Paneth cells in the context of intestinal irradiation in mice has been described (Gorbunov et al., 2010). It is, therefore, possible that VIP rescues the microenvironmental changes induced by irradiation by promoting the differentiation of cells towards protective secretory cell types. In line, VIP and VIPR1 deficiencies have been associated with significant gut bacterial dysbiosis (Ericsson et al., 2022). However, VIP might also maintain gut microbiota composition through other mechanisms, such as regulating the fucosylation of the epithelium (Lei et al., 2022).

Other possible mechanisms behind observed beneficial effects of VIP *in vivo* following injury may involve VIP-mediated regulation of tight junctions in irradiated tissues. VIP is known to influence epithelial barrier functions by enhancing the expression and assembly of tight junction proteins, which are crucial for maintaining the integrity of the barrier against environmental stressors (Conlin et al., 2009; Morampudi et al., 2015; Seo et al., 2019). In the context of radiation, which typically disrupts cellular structures and promotes inflammation, the role of VIP in stabilizing tight junctions could be particularly beneficial. Additionally, VIP has been shown to protect cells against oxidative stress (Steingart et al., 2000). Oxidative stress

is closely associated with irradiation and is a critical factor in radiation-induced damage to biological tissues (Nuszkiewicz et al., 2020).

Lastly, it is also worth noting that the effects of VIP can be concentration-dependent. A study employing a mouse model of TNBS-induced colitis showed that while very low pharmacological doses show significant beneficial effects, large dosages led to the worsening of mouse health conditions (Abad et al., 2003). This variability in outcomes may be attributed to the activation of different signaling mechanisms leading to various cellular responses (Yang et al., 2009).

4.5 Conclusion and outlook

In this study, we explored the role of VIP in modulating ISC behavior under conditions of stress and homeostasis. We identified VIP as a key factor in promoting cell differentiation towards secretory phenotype and in regulating the number and activity of ISCs. Our findings also demonstrate that VIP significantly enhances the regenerative capabilities of ISCs following injury. This positions VIP as a potent regulator of intestinal integrity, suggesting its application in therapeutic approaches aiming to mitigate the effects of irradiation exposure and other forms of intestinal damage.

However, while the findings are promising, the molecular mechanisms through which VIP impacts the ISC pool and behavior remain unclear, requiring further research to fully elucidate these pathways. Additionally, the observed discrepancies between *in vitro* and *in vivo* results highlight the need for further exploration. Given the timing and concentration-dependent effects of VIP, future studies should focus on establishing optimal dosing and treatment protocols and identifying any potential indirect effects of VIP administration.

Moreover, the experimental conditions used in this study were primarily based on animal models and *in vitro* organoid systems, which may not fully capture the complexity of human physiological responses. This suggests the need for additional studies involving *in vitro* models based on human-derived organoids to better bridge the gap to clinical applications.

Expanding research to examine the effects of VIP on other intestinal regions, such as the colon, could reveal its therapeutic potential in treating pathological conditions such as inflammatory bowel diseases and colon cancer. Furthermore, the role of VIP in modulating the intestinal microbiota represents another promising area of research. Recent studies suggest that VIP can significantly influence the gut microbiome, which is crucial for overall health and disease management.

In conclusion, our study significantly advances the understanding of the role of VIP in intestinal stem cell modulation and suggests its potential as a valuable treatment option in the context of acute GI damage.

References

Abad, C., Gomariz, R., Waschek, J., Leceta, J., Martinez, C., Juarranz, Y., & Arranz, A. (2012). VIP in inflammatory bowel disease: state of the art. *Endocrine, Metabolic & Immune Disorders Drug Targets*, *12*(4), 316–322. https://doi.org/10.2174/187153012803832576

Abad, C., Martinez, C., Juarranz, M. G., Arranz, A., Leceta, J., Delgado, M., & Gomariz, R. P. (2003). Therapeutic effects of vasoactive intestinal peptide in the trinitrobenzene sulfonic acid mice model of Crohn's disease. *Gastroenterology*, *124*(4), 961–971. https://doi.org/10.1053/gast.2003.50141

Abuetabh, Y., Wu, H. H., Chai, C., Al Yousef, H., Persad, S., Sergi, C. M., & Leng, R. (2022). DNA damage response revisited: the p53 family and its regulators provide endless cancer therapy opportunities. *Experimental & Molecular Medicine 2022 54:10*, *54*(10), 1658–1669. https://doi.org/10.1038/s12276-022-00863-4

Angus, H. C. K., Butt, A. G., Schultz, M., & Kemp, R. A. (2020). Intestinal Organoids as a Tool for Inflammatory Bowel Disease Research. *Frontiers in Medicine*, *6*, 499066. https://doi.org/10.3389/FMED.2019.00334/BIBTEX

Azkanaz, M., Corominas-Murtra, B., Ellenbroek, S. I. J., Bruens, L., Webb, A. T., Laskaris, D., Oost, K. C., Lafirenze, S. J. A., Annusver, K., Messal, H. A., Iqbal, S., Flanagan, D. J., Huels, D. J., Rojas-Rodríguez, F., Vizoso, M., Kasper, M., Sansom, O. J., Snippert, H. J., Liberali, P., … van Rheenen, J. (2022). Retrograde movements determine effective stem cell numbers in the intestine. *Nature 2022 607:7919*, *607*(7919), 548–554. https://doi.org/10.1038/s41586-022-04962-0

Banks, M. R., Farthing, M. J. G., Robberecht, P., & Burleigh, D. E. (2005). Antisecretory actions of a novel vasoactive intestinal polypeptide (VIP) antagonist in human and rat small intestine. *British Journal of Pharmacology*, *144*(7), 994–1001. https://doi.org/10.1038/sj.bjp.0706128

Barker, N. (2014). Adult intestinal stem cells: critical drivers of epithelial homeostasis and regeneration. *Nature Reviews. Molecular Cell Biology*, *15*(1), 19–33. https://doi.org/10.1038/NRM3721

Barker, N., Van Es, J. H., Kuipers, J., Kujala, P., Van Den Born, M., Cozijnsen, M., Haegebarth, A., Korving, J., Begthel, H., Peters, P. J., & Clevers, H. (2007). Identification of stem cells in small intestine and colon by marker gene Lgr5. *Nature 2007 449:7165*, *449*(7165), 1003–1007. https://doi.org/10.1038/nature06196

Beumer, J., & Clevers, H. (2021). Cell fate specification and differentiation in the adult mammalian intestine. *Nature Reviews Molecular Cell Biology*, *22*(1), 39–53. https://doi.org/10.1038/s41580-020-0278-0

Bevins, C. L., & Salzman, N. H. (2011). Paneth cells, antimicrobial peptides and maintenance of intestinal homeostasis. *Nature Reviews Microbiology 2011 9:5*, *9*(5), 356–368. https://doi.org/10.1038/nrmicro2546

Brischetto, C., Krieger, K., Klotz, C., Krahn, I., Kunz, S., Kolesnichenko, M., Mucka, P., Heuberger, J., Scheidereit, C., & Schmidt-Ullrich, R. (2021). NF-κB determines Paneth versus goblet cell fate decision in the small intestine. *Development (Cambridge, England)*, *148*(21). https://doi.org/10.1242/DEV.199683

Buch, K., Peters, T., Nawroth, T., Sänger, M., Schmidberger, H., & Langguth, P. (2012). Determination of cell survival after irradiation via clonogenic assay versus multiple MTT Assay - A comparative study. *Radiation Oncology*, *7*(1), 1–6. https://doi.org/10.1186/1748-717X-7-1/FIGURES/4

Buczacki, S. J. A., Zecchini, H. I., Nicholson, A. M., Russell, R., Vermeulen, L., Kemp, R., & Winton, D. J. (2013). Intestinal label-retaining cells are secretory precursors expressing

Lgr5. *Nature*, *495*(7439), 65–69. https://doi.org/10.1038/NATURE11965

Chen, M. E., Naeini, S. M., Srikrishnaraj, A., Drucker, D. J., Fesler, Z., & Brubaker, P. L. (2022). Glucagon-Like Peptide-2 Stimulates S-Phase Entry of Intestinal Lgr5+ Stem Cells. *Cellular and Molecular Gastroenterology and Hepatology*, *13*(6), 1829. https://doi.org/10.1016/J.JCMGH.2022.02.011

Clevers, H. C., & Bevins, C. L. (2013). Paneth cells: Maestros of the small intestinal crypts. *Annual Review of Physiology*, *75*, 289–311. https://doi.org/10.1146/annurev-physiol-030212-183744

Conlin, V. S., Wu, X., Nguyen, C., Dai, C., Vallance, B. A., Buchan, A. M. J., Boyer, L., & Jacobson, K. (2009). Vasoactive intestinal peptide ameliorates intestinal barrier disruption associated with Citrobacter rodentium-induced colitis. *American Journal of Physiology - Gastrointestinal and Liver Physiology*, *297*(4). https://doi.org/10.1152/ajpgi.90551.2008

Cui, C., Wang, X., Zheng, Y., Li, L., Wang, F., Wei, H., & Peng, J. (2023). Paneth cells protect intestinal stem cell niche to alleviate deoxynivalenol-induced intestinal injury. *Ecotoxicology and Environmental Safety*, *264*(August), 115457. https://doi.org/10.1016/j.ecoenv.2023.115457

De Heuvel, E., Wallace, L., Sharkey, K. A., & Sigalet, D. L. (2012). Glucagon-like peptide 2 induces vasoactive intestinal polypeptide expression in enteric neurons via phophatidylinositol 3-kinase-7 signaling. *American Journal of Physiology - Endocrinology and Metabolism*, *303*(8), 994–1005. https://doi.org/10.1152/ajpendo.00291.2012

Delgado, M., & Ganea, D. (2003). Neuroprotective effect of vasoactive intestinal peptide (VIP) in a mouse model of Parkinson's disease by blocking microglial activation. *The FASEB Journal : Official Publication of the Federation of American Societies for Experimental Biology*, *17*(8), 944–946. https://doi.org/10.1096/fj.02-0799fje

Delgado, M., & Ganea, D. (2013). Vasoactive intestinal peptide: a neuropeptide with pleiotropic immune functions. *Amino Acids*, *45*(1), 25–39. https://doi.org/10.1007/S00726-011-1184-8

Deng, S., Xi, Y., Wang, H., Hao, J., Niu, X., Li, W., Tao, Y., & Chen, G. (2010). Regulatory effect of vasoactive intestinal peptide on the balance of Treg and Th17 in collagen-induced arthritis. *Cellular Immunology*, *265*(2), 105–110. https://doi.org/10.1016/J.CELLIMM.2010.07.010

Dickson, L., & Finlayson, K. (2009). VPAC and PAC receptors: From ligands to function. *Pharmacology and Therapeutics*, *121*(3), 294–316. https://doi.org/10.1016/J.PHARMTHERA.2008.11.006

Ericsson, A. C., Bains, M., McAdams, Z., Daniels, J., Busi, S. B., Waschek, J. A., & Dorsam, G. P. (2022). The G Protein-Coupled Receptor, VPAC1, Mediates Vasoactive Intestinal Peptide-Dependent Functional Homeostasis of the Gut Microbiota. *Gastro Hep Advances*, *1*(2), 253–264. https://doi.org/10.1016/J.GASTHA.2021.11.005

Fabricius, D., Karacay, B., Shutt, D., Leverich, W., Schafer, B., Takle, E., Thedens, D., Khanna, G., Raikwar, S., Yang, B., Desmond, M. E., & O'Dorisio, M. S. (2011). Characterization of intestinal and pancreatic dysfunction in VPAC1-Null mutant mouse. *Pancreas*, *40*(6), 861–871. https://doi.org/10.1097/MPA.0b013e318214c783

Farin, H. F., Van Es, J. H., & Clevers, H. (2012). Redundant Sources of Wnt Regulate Intestinal Stem Cells and Promote Formation of Paneth Cells. *Gastroenterology*, *143*(6), 1518-1529.e7.

Gao, N., White, P., & Kaestner, K. H. (2009). Establishment of Intestinal Identity and Epithelial-Mesenchymal Signaling by Cdx2. *Developmental Cell*, *16*(4), 588–599. https://doi.org/10.1016/j.devcel.2009.02.010

Gehart, H., & Clevers, H. (2019). Tales from the crypt: new insights into intestinal stem cells. *Nature Reviews Gastroenterology and Hepatology*, *16*(1), 19–34.

https://doi.org/10.1038/s41575-018-0081-y

González-Mariscal, L., Miranda, J., Gallego-Gutiérrez, H., Cano-Cortina, M., & Amaya, E. (2020). Relationship between apical junction proteins, gene expression and cancer. *Biochimica et Biophysica Acta. Biomembranes*, *1862*(9). https://doi.org/10.1016/J.BBAMEM.2020.183278

González, C., Barroso, C., Martín, C., Gulbenkian, S., & Estrada, C. (1997). Neuronal nitric oxide synthase activation by vasoactive intestinal peptide in bovine cerebral arteries. *Journal of Cerebral Blood Flow and Metabolism*, *17*(9), 977–984. https://doi.org/10.1097/00004647-199709000-00007/ASSET/IMAGES/LARGE/10.1097_00004647-199709000-00007-FIG5.JPEG

Goode, T., O'Connor, T., Hopkins, A., Moriarty, D., O'Sullivan, G. C., Collins, J. K., O'Donoghue, D., Baird, A. W., O'Connell, J., & Shanahan, F. (2003). Neurokinin-1 Receptor (NK-1R) Expression Is Induced in Human Colonic Epithelial Cells by Proinflammatory Cytokines and Mediates Proliferation in Response to Substance P. *Journal of Cellular Physiology*, *197*(1), 30–41. https://doi.org/10.1002/jcp.10234

Gorbunov, N. V., Garrison, B. R., & Kiang, J. G. (2010). Response of crypt paneth cells in the small intestine following total-body gamma-irradiation. *International Journal of Immunopathology and Pharmacology*, *23*(4), 1111–1123. https://doi.org/10.1177/039463201002300415

Gross, E. R., Gershon, M. D., Margolis, K. G., Gertsberg, Z. V., & Cowles, R. A. (2012). Neuronal serotonin regulates growth of the intestinal mucosa in mice. *Gastroenterology*, *143*(2), 408-417.e2. https://doi.org/10.1053/j.gastro.2012.05.007

Gustafsson, J. K., & Johansson, M. E. V. (2022). The role of goblet cells and mucus in intestinal homeostasis. *Nature Reviews Gastroenterology & Hepatology 2022 19:12*, *19*(12), 785–803. https://doi.org/10.1038/s41575-022-00675-x

Haber, A. L., Biton, M., Rogel, N., Herbst, R. H., Shekhar, K., Smillie, C., Burgin, G., Delorey, T. M., Howitt, M. R., Katz, Y., Tirosh, I., Beyaz, S., Dionne, D., Zhang, M., Raychowdhury, R., Garrett, W. S., Rozenblatt-Rosen, O., Shi, H. N., Yilmaz, O., … Regev, A. (2017). A single-cell survey of the small intestinal epithelium. *Nature 2017 551:7680*, *551*(7680), 333–339. https://doi.org/10.1038/nature24489

Harhous, Z., Faour, W. H., & El Zein, N. (2021). VIP modulates human macrophages phenotype via FPRL1 via activation of RhoA-GTPase and PLC pathways. *Inflammation Research : Official Journal of the European Histamine Research Society ... [et Al.]*, *70*(3), 309–321. https://doi.org/10.1007/S00011-021-01436-3

Höckerfelt, U., Franzén, L., Kjörell, U., & Forsgren, S. (2000). Parallel increase in substance P and VIP in rat duodenum in response to irradiation. *Peptides*, *21*(2), 271–281. https://doi.org/10.1016/S0196-9781(99)00200-4

Hokari, R., Lee, H., Crawley, S. C., Yang, S. C., Gum, J. R., Miura, S., & Kim, Y. S. (2005). Vasoactive intestinal peptide upregulates MUC2 intestinal mucin via CREB/ATF1. *American Journal of Physiology-Gastrointestinal and Liver Physiology*, *289*(5), G949–G959. https://doi.org/10.1152/ajpgi.00142.2005

Hua, G., Thin, T. H., Feldman, R., Haimovitz-Friedman, A., Clevers, H., Fuks, Z., & Kolesnick, R. (2012). Crypt Base Columnar Stem Cells in Small Intestines of Mice Are Radioresistant. *Gastroenterology*, *143*(5), 1266. https://doi.org/10.1053/J.GASTRO.2012.07.106

Huang, L., Xu, Z., Lei, X., Huang, Y., Tu, S., Xu, L., Xia, J., & Liu, D. (2023). Paneth cell-derived iNOS is required to maintain homeostasis in the intestinal stem cell niche. *Journal of Translational Medicine*, *21*(1). https://doi.org/10.1186/S12967-023-04744-W

Hur, W., & Yoon, S. K. (2017). Molecular Pathogenesis of Radiation-Induced Cell Toxicity in Stem Cells. *International Journal of Molecular Sciences 2017, Vol. 18, Page 2749*, *18*(12), 2749. https://doi.org/10.3390/IJMS18122749

Ireland, H., Houghton, C., Howard, L., & Winton, D. J. (2005). Cellular inheritance of a Cre-activated reporter gene to determine Paneth cell longevity in the murine small intestine. *Developmental Dynamics : An Official Publication of the American Association of Anatomists*, *233*(4), 1332–1336. https://doi.org/10.1002/DVDY.20446

Iwasaki, M., Akiba, Y., & Kaunitz, J. D. (2019). Recent advances in vasoactive intestinal peptide physiology and pathophysiology: Focus on the gastrointestinal system [version 1; peer review: 4 approved]. In *F1000Research* (Vol. 8, p. 1629). F1000 Research Ltd. https://doi.org/10.12688/f1000research.18039.1

Jayawardena, D., Guzman, G., Gill, R. K., Alrefai, W. A., Onyuksel, H., & Dudeja, P. K. (2017). Expression and localization of VPAC1, the major receptor of vasoactive intestinal peptide along the length of the intestine. *American Journal of Physiology - Gastrointestinal and Liver Physiology*, *313*(1), G16–G25. https://doi.org/10.1152/ajpgi.00081.2017

Jönsson, M., Norrgård, Ö., & Forsgren, S. (2012). Epithelial expression of vasoactive intestinal peptide in ulcerative colitis: Down-regulation in markedly inflamed colon. *Digestive Diseases and Sciences*, *57*(2), 303–310. https://doi.org/10.1007/S10620-011-1985-3/FIGURES/4

Kaur, P., & Potten, C. S. (1986). Cell Migration Velocities In the Crypts of the Small Intestine After Cytotoxic Insult Are Not Dependent On Mitotic Activity. *Cell Proliferation*, *19*(6), 601–610. https://doi.org/10.1111/J.1365-2184.1986.TB00761.X

Ki, Y., Kim, W., Cho, H., Ahn, K., Choi, Y., & Kim, D. (2014). The Effect of Probiotics for Preventing Radiation-Induced Morphological Changes in Intestinal Mucosa of Rats. *Journal of Korean Medical Science*, *29*(10), 1372–1378. https://doi.org/10.3346/JKMS.2014.29.10.1372

Kim, Y. S., Kim, J., & Park, S. J. (2015). High-throughput 16S rRNA gene sequencing reveals alterations of mouse intestinal microbiota after radiotherapy. *Anaerobe*, *33*, 1–7. https://doi.org/10.1016/J.ANAEROBE.2015.01.004

Kirsch, D. G., Santiago, P. M., Di Tomaso, E., Sullivan, J. M., Hou, W. S., Dayton, T., Jeffords, L. B., Sodha, P., Mercer, K. L., Cohen, R., Takeuchi, O., Korsmeyer, S. J., Bronson, R. T., Kim, C. F., Haigis, K. M., Jain, R. K., & Jacks, T. (2010). p53 controls radiation-induced gastrointestinal syndrome in mice independent of apoptosis. *Science (New York, N.Y.)*, *327*(5965), 593–596. https://doi.org/10.1126/SCIENCE.1166202

Kittikulsuth, W., Nakano, D., Kitada, K., Uyama, T., Ueda, N., Asano, E., Okano, K., Matsuda, Y., & Nishiyama, A. (2023). Vasoactive intestinal peptide blockade suppresses tumor growth by regulating macrophage polarization and function in CT26 tumor-bearing mice. *Scientific Reports 2023 13:1*, *13*(1), 1–12. https://doi.org/10.1038/s41598-023-28073-6

Koh, S. W. M., & Waschek, J. A. (2000). Corneal endothelial cell survival in organ cultures under acute oxidative stress: Effect of VIP. *Investigative Ophthalmology and Visual Science*, *41*(13), 4085–4092.

Koon, H. W., Zhao, D., Na, X., Moyer, M. P., & Pothoulakis, C. (2004). Metalloproteinases and transforming growth factor-α mediate substance p-induced mitogen-activated protein kinase activation and proliferation in human colonocytes. *Journal of Biological Chemistry*, *279*(44), 45519–45527. https://doi.org/10.1074/jbc.M408523200

Korotkevich, G., Sukhov, V., Budin, N., Shpak, B., Artyomov, M. N., & Sergushichev, A. (2021). Fast gene set enrichment analysis. *BioRxiv*, 060012. https://doi.org/10.1101/060012

Kunze, B., Wein, F., Fang, H. Y., Anand, A., Baumeister, T., Strangmann, J., Gerland, S., Ingermann, J., Münch, N. S., Wiethaler, M., Sahm, V., Hidalgo-Sastre, A., Lange, S., Lightdale, C. J., Bokhari, A., Falk, G. W., Friedman, R. A., Ginsberg, G. G., Iyer, P. G., … Quante, M. (2020). Notch Signaling Mediates Differentiation in Barrett's Esophagus and Promotes Progression to Adenocarcinoma. *Gastroenterology*, *159*(2), 575–590. https://doi.org/10.1053/J.GASTRO.2020.04.033

Langer, I., Jeandriens, J., Couvineau, A., Sanmukh, S., & Latek, D. (2022). Signal Transduction by VIP and PACAP Receptors. *Biomedicines*, *10*(2), 406. https://doi.org/10.3390/BIOMEDICINES10020406/S1

Leceta, J., Martinez, C., Delgado, M., Garrido, E., & Gomariz, R. P. (1996). Expression of vasoactive intestinal peptide in lymphocytes: a possible endogenous role in the regulation of the immune system. *Advances in Neuroimmunology*, *6*(1), 29–36. https://doi.org/10.1016/S0960-5428(96)00001-0

Lee, M., Hadi, M., Halldén, G., & Aponte, G. W. (2005). Peptide YY and neuropeptide Y induce villin expression, reduce adhesion, and enhance migration in small intestinal cells through the regulation of CD63, matrix metalloproteinase-3, and Cdc42 activity. *Journal of Biological Chemistry*, *280*(1), 125–136. https://doi.org/10.1074/jbc.M408858200

Lei, C., Sun, R., Xu, G., Tan, Y., Feng, W., McClain, C. J., & Deng, Z. (2022). Enteric VIP-producing neurons maintain gut microbiota homeostasis through regulating epithelium fucosylation. *Cell Host & Microbe*, *30*(10), 1417-1434.e8. https://doi.org/10.1016/J.CHOM.2022.09.001

Lelievre, V., Favrais, G., Abad, C., Adle-Biassette, H., Lu, Y., Germano, P. M., Cheung-Lau, G., Pisegna, J. R., Gressens, P., Lawson, G., & Waschek, J. A. (2007). Gastrointestinal dysfunction in mice with a targeted mutation in the gene encoding vasoactive intestinal polypeptide: A model for the study of intestinal ileus and Hirschsprung's disease. *Peptides*, *28*(9), 1688–1699. https://doi.org/10.1016/J.PEPTIDES.2007.05.006

Levy, A., Gal, R., Granoth, R., Dreznik, Z., Fridkin, M., & Gozes, I. (2002). In vitro and in vivo treatment of colon cancer by VIP antagonists. *Regulatory Peptides*, *109*(1–3), 127–133. https://doi.org/10.1016/S0167-0115(02)00195-7

Li, C., Zhou, Y., Wei, R., Napier, D. L., Sengoku, T., Alstott, M. C., Liu, J., Wang, C., Zaytseva, Y. Y., Weiss, H. L., Wang, Q., & Evers, B. M. (2023). Glycolytic Regulation of Intestinal Stem Cell Self-Renewal and Differentiation. *Cellular and Molecular Gastroenterology and Hepatology*, *15*(4), 931. https://doi.org/10.1016/J.JCMGH.2022.12.012

Liberzon, A., Birger, C., Thorvaldsdóttir, H., Ghandi, M., Mesirov, J. P., & Tamayo, P. (2015). The Molecular Signatures Database (MSigDB) hallmark gene set collection. *Cell Systems*, *1*(6), 417–425. https://doi.org/10.1016/J.CELS.2015.12.004

Lopez-Garcia, C., Klein, A. M., Simons, B. D., & Winton, D. J. (2010). Intestinal stem cell replacement follows a pattern of neutral drift. *Science*, *330*(6005), 822–825. https://doi.org/10.1126/SCIENCE.1196236/SUPPL_FILE/LOPEZ.SOM.PDF

Lorzadeh, A., Ye, G., Sharma, S., & Jadhav, U. (2024). DNA methylation-dependent and -independent binding of CDX2 directs activation of distinct developmental and homeostatic genes. *BioRxiv*, 2024.02.11.579850. https://doi.org/10.1101/2024.02.11.579850

Love, M. I., Huber, W., & Anders, S. (2014). Moderated estimation of fold change and dispersion for RNA-seq data with DESeq2. *Genome Biology*, *15*(12), 1–21. https://doi.org/10.1186/S13059-014-0550-8/FIGURES/9

Lu, J., Piper, S. J., Zhao, P., Miller, L. J., Wootten, D., & Sexton, P. M. (2022). Targeting VIP and PACAP Receptor Signaling: New Insights into Designing Drugs for the PACAP Subfamily of Receptors. *International Journal of Molecular Sciences*, *23*(15). https://doi.org/10.3390/ijms23158069

Lukonin, I., Serra, D., Challet Meylan, L., Volkmann, K., Baaten, J., Zhao, R., Meeusen, S., Colman, K., Maurer, F., Stadler, M. B., Jenkins, J., & Liberali, P. (2020). Phenotypic landscape of intestinal organoid regeneration. *Nature*, *586*(7828), 275–280. https://doi.org/10.1038/S41586-020-2776-9

Macosko, E. Z., Basu, A., Satija, R., Nemesh, J., Shekhar, K., Goldman, M., Tirosh, I., Bialas, A. R., Kamitaki, N., Martersteck, E. M., Trombetta, J. J., Weitz, D. A., Sanes, J. R., Shalek, A. K., Regev, A., & McCarroll, S. A. (2015). Highly Parallel Genome-wide

Expression Profiling of Individual Cells Using Nanoliter Droplets. *Cell*, *161*(5), 1202–1214. https://doi.org/10.1016/J.CELL.2015.05.002

Madisen, L., Zwingman, T. A., Sunkin, S. M., Oh, S. W., Zariwala, H. A., Gu, H., Ng, L. L., Palmiter, R. D., Hawrylycz, M. J., Jones, A. R., Lein, E. S., & Zeng, H. (2009). A robust and high-throughput Cre reporting and characterization system for the whole mouse brain. *Nature Neuroscience 2009 13:1*, *13*(1), 133–140. https://doi.org/10.1038/nn.2467

Maiti, A. K., Sharba, S., Navabi, N., Lindén ID, S. K., Nordisk, N., Julin, R., Wiberg, Å., Lundgren, M., & Wallenberg Foundations, A. (2018). Colonic levels of vasoactive intestinal peptide decrease during infection and exogenous VIP protects epithelial mitochondria against the negative effects of IFNγ and TNFα induced during Citrobacter rodentium infection. *PLOS ONE*, *13*(9), e0204567. https://doi.org/10.1371/JOURNAL.PONE.0204567

Martinez, P. S., Giuranno, L., Vooijs, M., & Coppes, R. P. (2021). The radiation-induced regenerative response of adult tissue-specific stem cells: Models and signaling pathways. *Cancers*, *13*(4), 1–18. https://doi.org/10.3390/cancers13040855

Maxwell, R. J., Prysor-Jones, R. A., Jenkens, J. S., & Griffiths, J. R. (1988). Vasoactive intestinal peptide stimulates glycolysis in pituitary tumours; 1H-NMR detection of lactate in vivo. *BBA - Molecular Cell Research*, *968*(1), 86–90. https://doi.org/10.1016/0167-4889(88)90047-X

McCarthy, N., Manieri, E., Storm, E. E., Saadatpour, A., Luoma, A. M., Kapoor, V. N., Madha, S., Gaynor, L. T., Cox, C., Keerthivasan, S., Wucherpfennig, K., Yuan, G. C., de Sauvage, F. J., Turley, S. J., & Shivdasani, R. A. (2020). Distinct Mesenchymal Cell Populations Generate the Essential Intestinal BMP Signaling Gradient. *Cell Stem Cell*, *26*(3), 391-402.e5. https://doi.org/10.1016/j.stem.2020.01.008

McCauley, H. A., Matthis, A. L., Enriquez, J. R., Nichol, J. T., Sanchez, J. G., Stone, W. J., Sundaram, N., Helmrath, M. A., Montrose, M. H., Aihara, E., & Wells, J. M. (2020). Enteroendocrine cells couple nutrient sensing to nutrient absorption by regulating ion transport. *Nature Communications*, *11*(1), 1–10. https://doi.org/10.1038/s41467-020-18536-z

McMahon, S. J. (2019). The linear quadratic model: Usage, interpretation and challenges. *Physics in Medicine and Biology*, *64*(1), 0–24. https://doi.org/10.1088/1361-6560/aaf26a

Merech, F., Soczewski, E., Hauk, V., Paparini, D., Ramhorst, R., Vota, D., & Pérez Leirós, C. (2019). Vasoactive Intestinal Peptide induces glucose and neutral amino acid uptake through mTOR signalling in human cytotrophoblast cells. *Scientific Reports 2019 9:1*, *9*(1), 1–12. https://doi.org/10.1038/s41598-019-53676-3

Metcalfe, C., Kljavin, N. M., Ybarra, R., & De Sauvage, F. J. (2014). Lgr5+ stem cells are indispensable for radiation-induced intestinal regeneration. *Cell Stem Cell*, *14*(2), 149–159. https://doi.org/10.1016/j.stem.2013.11.008

Middelhoff, M., Nienhüser, H., Valenti, G., Maurer, H. C., Hayakawa, Y., Takahashi, R., Kim, W., Jiang, Z., Malagola, E., Cuti, K., Tailor, Y., Zamechek, L. B., Renz, B. W., Quante, M., Yan, K. S., & Wang, T. C. (2020). Prox1-positive cells monitor and sustain the murine intestinal epithelial cholinergic niche. *Nature Communications*, *11*(1), 1–14. https://doi.org/10.1038/s41467-019-13850-7

Morampudi, V., Conlin, V. S., Dalwadi, U., Wu, X., Marshall, K. C., Nguyen, C., Vallance, B. A., & Jacobson, K. (2015). Vasoactive intestinal peptide prevents PKCε-induced intestinal epithelial barrier disruption during EPEC infection. *American Journal of Physiology - Gastrointestinal and Liver Physiology*, *308*(5), G389–G402. https://doi.org/10.1152/AJPGI.00195.2014/ASSET/IMAGES/LARGE/ZH30041568350007.JPEG

Morel, E., Dublineau, I., Lebrun, F., & Griffiths, N. M. (2002). Alterations of the VIP-stimulated cAMP pathway in rat distal colon after abdominal irradiation. *American Journal of*

Physiology. Gastrointestinal and Liver Physiology, *282*(5). https://doi.org/10.1152/AJPGI.00457.2001

Morral, C., Ayyaz, A., Kuo, H. C., Fink, M., Verginadis, I. I., Daniel, A. R., Burner, D. N., Driver, L. M., Satow, S., Hasapis, S., Ghinnagow, R., Luo, L., Ma, Y., Attardi, L. D., Koumenis, C., Minn, A. J., Wrana, J. L., Lee, C. L., & Kirsch, D. G. (2024). p53 promotes revival stem cells in the regenerating intestine after severe radiation injury. *Nature Communications*, *15*(1). https://doi.org/10.1038/S41467-024-47124-8

Nezami, B. G., & Srinivasan, S. (2010). Enteric Nervous System in the Small Intestine: Pathophysiology and Clinical Implications. *Current Gastroenterology Reports*, *12*(5), 358. https://doi.org/10.1007/S11894-010-0129-9

Nuszkiewicz, J., Woźniak, A., & Szewczyk-Golec, K. (2020). Ionizing radiation as a source of oxidative stress—the protective role of melatonin and vitamin d. *International Journal of Molecular Sciences*, *21*(16), 1–22. https://doi.org/10.3390/ijms21165804

Otsuka, M., Kang, Y. J., Ren, J., Jiang, H., Wang, Y., Omata, M., & Han, J. (2010). Distinct Effects of p38α Deletion in Myeloid Lineage and Gut Epithelia in Mouse Models of Inflammatory Bowel Disease. *Gastroenterology*, *138*(4), 1255-1265.e9. https://doi.org/10.1053/j.gastro.2010.01.005

Parekh, S., Ziegenhain, C., Vieth, B., Enard, W., & Hellmann, I. (2016). The impact of amplification on differential expression analyses by RNA-seq. *Scientific Reports 2016 6:1*, *6*(1), 1–11. https://doi.org/10.1038/srep25533

Pellegrinet, L., Rodilla, V., Liu, Z., Chen, S., Koch, U., Espinosa, L., Kaestner, K. H., Kopan, R., Lewis, J., & Radtke, F. (2011). Dll1- and Dll4-Mediated Notch Signaling Are Required for Homeostasis of Intestinal Stem Cells. *Gastroenterology*, *140*(4), 1230-1240.e7. https://doi.org/10.1053/J.GASTRO.2011.01.005

Peñarando, J., López-Sánchez, L. M., Mena, R., Guil-Luna, S., Conde, F., Hernández, V., Toledano, M., Gudiño, V., Raponi, M., Billard, C., Villar, C., Díaz, C., Gómez-Barbadillo, J., De la Haba-Rodríguez, J., Myant, K., Aranda, E., & Rodríguez-Ariza, A. (2018). A role for endothelial nitric oxide synthase in intestinal stem cell proliferation and mesenchymal colorectal cancer. *BMC Biology*, *16*(1), 1–14. https://doi.org/10.1186/S12915-017-0472-5/FIGURES/6

Petsakou, A., Liu, Y., Liu, Y., Comjean, A., Hu, Y., & Perrimon, N. (2023). Cholinergic neurons trigger epithelial Ca2+ currents to heal the gut. In *Nature* (Vol. 623, Issue 7985). Springer US. https://doi.org/10.1038/s41586-023-06627-y

Potten, C. S. (1990). A comprehensive study of the radiobiological response of the murine (BDF1) small intestine. *International Journal of Radiation Biology*, *58*(6), 925–973. https://doi.org/10.1080/09553009014552281/ASSET//CMS/ASSET/4ED7E0A3-BF58-4CC0-A3C8-DA91D1ECB728/09553009014552281.FP.PNG

Prosser, S. L., & Pelletier, L. (2017). Mitotic spindle assembly in animal cells: A fine balancing act. *Nature Reviews Molecular Cell Biology*, *18*(3), 187–201. https://doi.org/10.1038/nrm.2016.162

Raingeaud, J., Gupta, S., Rogers, J. S., Dickens, M., Han, J., Ulevitch, R. J., & Davis, R. J. (1995). Pro-inflammatory cytokines and environmental stress cause p38 mitogen-activated protein kinase activation by dual phosphorylation on tyrosine and threonine. *The Journal of Biological Chemistry*, *270*(13), 7420–7426. https://doi.org/10.1074/JBC.270.13.7420

Rao, I. H., Waller, E. K., Dhamsania, R. K., & Chandrasekaran, S. (2023). Gene Expression Analysis Links Autocrine Vasoactive Intestinal Peptide and ZEB1 in Gastrointestinal Cancers. *Cancers*, *15*(13). https://doi.org/10.3390/CANCERS15133284/S1

Rao, M., & Gershon, M. D. (2016). The bowel and beyond: the enteric nervous system in neurological disorders. *Nature Reviews. Gastroenterology & Hepatology*, *13*(9), 517. https://doi.org/10.1038/NRGASTRO.2016.107

Ritsma, L., Ellenbroek, S. I. J., Zomer, A., Snippert, H. J., De Sauvage, F. J., Simons, B. D., Clevers, H., & Van Rheenen, J. (2014). Intestinal crypt homeostasis revealed at single-stem-cell level by in vivo live imaging. *Nature 2014 507:7492*, *507*(7492), 362–365. https://doi.org/10.1038/nature12972

Rodrat, M., Wongdee, K., Teerapornpuntakit, J., Thongbunchoo, J., Id, D. T., Aeimlapa, R., Thammayon, N., Thonapan, N., Wattano, P., & Charoenphandhu Id, N. (2022). *Vasoactive intestinal peptide and cystic fibrosis transmembrane conductance regulator contribute to the transepithelial calcium transport across intestinal epithelium-like Caco-2 monolayer*. https://doi.org/10.1371/journal.pone.0277096

Rodríguez-Colman, M. J., Schewe, M., Meerlo, M., Stigter, E., Gerrits, J., Pras-Raves, M., Sacchetti, A., Hornsveld, M., Oost, K. C., Snippert, H. J., Verhoeven-Duif, N., Fodde, R., & Burgering, B. M. T. (2017). Interplay between metabolic identities in the intestinal crypt supports stem cell function. *Nature 2017 543:7645*, *543*(7645), 424–427. https://doi.org/10.1038/nature21673

Rossi, I., Monge, L., & Feliu, J. E. (1989). Short-term regulation of glycolysis by vasoactive intestinal peptide in epithelial cells isolated from rat small intestine. *The Biochemical Journal*, *262*(2), 397–402. https://doi.org/10.1042/BJ2620397

Said, S. I., & Mutt, V. (1972). Isolation from Porcine-Intestinal Wall of a Vasoactive Octacosapeptide Related to Secretin and to Glucagon. *European Journal of Biochemistry*, *28*(2), 199–204. https://doi.org/10.1111/j.1432-1033.1972.tb01903.x

Sailaja, B. S., He, X. C., & Li, L. (2016). The regulatory niche of intestinal stem cells. *The Journal of Physiology*, *594*(17), 4827. https://doi.org/10.1113/JP271931

Sanlioglu, A. D., Karacay, B., Balci, M. K., Griffith, T. S., & Sanlioglu, S. (2012). Therapeutic potential of VIP vs PACAP in diabetes. *Journal of Molecular Endocrinology*, *49*(3), R157–R167. https://doi.org/10.1530/JME-12-0156

Sastry, K. S., Chouchane, A. I., Wang, E., Kulik, G., Marincola, F. M., & Chouchane, L. (2017). Cytoprotective effect of neuropeptides on cancer stem cells: vasoactive intestinal peptide-induced antiapoptotic signaling. *Cell Death & Disease*, *8*(6), e2844. https://doi.org/10.1038/CDDIS.2017.226

Sato, T., Van Es, J. H., Snippert, H. J., Stange, D. E., Vries, R. G., Van Den Born, M., Barker, N., Shroyer, N. F., Van De Wetering, M., & Clevers, H. (2011). Paneth cells constitute the niche for Lgr5 stem cells in intestinal crypts. *Nature*, *469*(7330), 415–418. https://doi.org/10.1038/NATURE09637

Sato, T., Vries, R. G., Snippert, H. J., Van De Wetering, M., Barker, N., Stange, D. E., Van Es, J. H., Abo, A., Kujala, P., Peters, P. J., & Clevers, H. (2009). Single Lgr5 stem cells build crypt-villus structures in vitro without a mesenchymal niche. *Nature*, *459*(7244), 262–265. https://doi.org/10.1038/NATURE07935

Schmitt, M., Schewe, M., Sacchetti, A., Feijtel, D., van de Geer, W. S., Teeuwssen, M., Sleddens, H. F., Joosten, R., van Royen, M. E., van de Werken, H. J. G., van Es, J., Clevers, H., & Fodde, R. (2018). Paneth Cells Respond to Inflammation and Contribute to Tissue Regeneration by Acquiring Stem-like Features through SCF/c-Kit Signaling. *Cell Reports*, *24*(9), 2312-2328.e7. https://doi.org/10.1016/j.celrep.2018.07.085

Schneider, C., O'Leary, C. E., & Locksley, R. M. (2019). Regulation of immune responses by tuft cells. *Nature Reviews Immunology 2019 19:9*, *19*(9), 584–593. https://doi.org/10.1038/s41577-019-0176-x

Schulz, S., Röcken, C., Mawrin, C., Weise, W., Höllt, V., & Schulz, S. (2004). Immunocytochemical identification of VPAC1, VPAC2, and PAC1 receptors in normal and neoplastic human tissues with subtype-specific antibodies. *Clinical Cancer Research*, *10*(24), 8235–8242. https://doi.org/10.1158/1078-0432.CCR-04-0939

Schwerdtfeger, L. A., & Tobet, S. A. (2020). Vasoactive intestinal peptide regulates ileal goblet cell production in mice. *Physiological Reports*, *8*(3).

https://doi.org/10.14814/PHY2.14363

Seo, S., Miyake, H., Alganabi, M., Janssen Lok, M., O'Connell, J. S., Lee, C., Li, B., & Pierro, A. (2019). Vasoactive intestinal peptide decreases inflammation and tight junction disruption in experimental necrotizing enterocolitis. *Journal of Pediatric Surgery*, *54*(12), 2520–2523. https://doi.org/10.1016/J.JPEDSURG.2019.08.038

Sharkey, K. A., & Mawe, G. M. (2023). The enteric nervous system. *Physiological Reviews*, *103*(2), 1487–1564. https://doi.org/10.1152/PHYSREV.00018.2022

Sigalet, D. L., Wallace, L. E., Holst, J. J., Martin, G. R., Kaji, T., Tanaka, H., & Sharkey, K. A. (2007). Enteric neural pathways mediate the anti-inflammatory actions of glucagon-like peptide 2. *American Journal of Physiology - Gastrointestinal and Liver Physiology*, *293*(1), 211–221. https://doi.org/10.1152/AJPGI.00530.2006/ASSET/IMAGES/LARGE/ZH300707480500 06.JPEG

Simmini, S., Bialecka, M., Huch, M., Kester, L., Van De Wetering, M., Sato, T., Beck, F., Van Oudenaarden, A., Clevers, H., & Deschamps, J. (2014). Transformation of intestinal stem cells into gastric stem cells on loss of transcription factor Cdx2. *Nature Communications*, *5*. https://doi.org/10.1038/NCOMMS6728

Sittipo, P., Pham, H. Q., Park, C. E., Kang, G. U., Zhi, Y., Ji, H. J., Jang, A., Seo, H. S., Shin, J. H., & Lee, Y. K. (2020). Irradiation-Induced Intestinal Damage Is Recovered by the Indigenous Gut Bacteria Lactobacillus acidophilus. *Frontiers in Cellular and Infection Microbiology*, *10*, 540279. https://doi.org/10.3389/FCIMB.2020.00415/BIBTEX

Snippert, H. J., van der Flier, L. G., Sato, T., van Es, J. H., van den Born, M., Kroon-Veenboer, C., Barker, N., Klein, A. M., van Rheenen, J., Simons, B. D., & Clevers, H. (2010). Intestinal crypt homeostasis results from neutral competition between symmetrically dividing Lgr5 stem cells. *Cell*, *143*(1), 134–144. https://doi.org/10.1016/j.cell.2010.09.016

Snoeck, V., Goddeeris, B., & Cox, E. (2005). The role of enterocytes in the intestinal barrier function and antigen uptake. *Microbes and Infection*, *7*(7–8), 997–1004. https://doi.org/10.1016/J.MICINF.2005.04.003

Spessert, R. (1993). Vasoactive intestinal peptide stimulation of cyclic guanosine monophosphate formation: further evidence for a role of nitric oxide synthase and cytosolic guanylate cyclase in rat pinealocytes. *Endocrinology*, *132*(6), 2513–2517. https://doi.org/10.1210/ENDO.132.6.7684978

Steingart, R. A., Solomon, B., Brenneman, D. E., Fridkin, M., & Gozes, I. (2000). VIP and peptides related to activity-dependent neurotrophic factor protect PC12 cells against oxidative stress. *Journal of Molecular Neuroscience*, *15*(3), 137–145. https://doi.org/10.1385/JMN:15:3:137/METRICS

Sternini, C., Anselmi, L., & Rozengurt, E. (2008). Enteroendocrine cells: a site of 'taste' in gastrointestinal chemosensing. *Current Opinion in Endocrinology, Diabetes, and Obesity*, *15*(1), 73. https://doi.org/10.1097/MED.0B013E3282F43A73

Subramanian, A., Tamayo, P., Mootha, V. K., Mukherjee, S., Ebert, B. L., Gillette, M. A., Paulovich, A., Pomeroy, S. L., Golub, T. R., Lander, E. S., & Mesirov, J. P. (2005). Gene set enrichment analysis: a knowledge-based approach for interpreting genome-wide expression profiles. *Proceedings of the National Academy of Sciences of the United States of America*, *102*(43), 15545–15550. https://doi.org/10.1073/PNAS.0506580102

Tackett, J. J., Gandotra, N., Bamdad, M. C., Muise, E. D., & Cowles, R. A. (2017). Enhanced serotonin signaling stimulates ordered intestinal mucosal growth. *Journal of Surgical Research*, *208*, 198–203. https://doi.org/10.1016/j.jss.2016.09.036

Talbot, J., Hahn, P., Kroehling, L., Nguyen, H., Li, D., & Littman, D. R. (2020). Feeding-dependent VIP neuron-ILC3 circuit regulates the intestinal barrier. *Nature*, *579*(7800), 575–580. https://doi.org/10.1038/S41586-020-2039-9

Tan, S. H., Phuah, P., Tan, L. T., Yada, S., Goh, J., Tomaz, L. B., Chua, M., Wong, E., Lee,

B., & Barker, N. (2021). A constant pool of Lgr5+ intestinal stem cells is required for intestinal homeostasis. *Cell Reports*, *34*(4), 108633. https://doi.org/10.1016/j.celrep.2020.108633

Tang, B. O., Yong, X., Xie, R., Li, Q. W., & Yang, S. M. (2014). Vasoactive intestinal peptide receptor-based imaging and treatment of tumors (review). *International Journal of Oncology*, *44*(4), 1023–1031. https://doi.org/10.3892/IJO.2014.2276/HTML

ten Hove, A. S., Mallesh, S., Zafeiropoulou, K., de Kleer, J. W. M., van Hamersveld, P. H. P., Welting, O., Hakvoort, T. B. M., Wehner, S., Seppen, J., & de Jonge, W. J. (2023). Sympathetic activity regulates epithelial proliferation and wound healing via adrenergic receptor α2A. *Scientific Reports*, *13*(1), 1–16. https://doi.org/10.1038/s41598-023-45160-w

Tetteh, P. W., Basak, O., Farin, H. F., Wiebrands, K., Kretzschmar, K., Begthel, H., Van Den Born, M., Korving, J., De Sauvage, F., Van Es, J. H., Van Oudenaarden, A., & Clevers, H. (2016). Replacement of Lost Lgr5-Positive Stem Cells through Plasticity of Their Enterocyte-Lineage Daughters. *Cell Stem Cell*, *18*(2), 203–213. https://doi.org/10.1016/j.stem.2016.01.001

Tian, H., Biehs, B., Chiu, C., Siebel, C. W., Wu, Y., Costa, M., De Sauvage, F. J., & Klein, O. D. (2015). Opposing activities of notch and wnt signaling regulate intestinal stem cells and gut homeostasis. *Cell Reports*, *11*(1), 33–42. https://doi.org/10.1016/j.celrep.2015.03.007

Tian, H., Biehs, B., Warming, S., Leong, K. G., Rangell, L., Klein, O. D., & De Sauvage, F. J. (2011). A reserve stem cell population in small intestine renders Lgr5-positive cells dispensable. *Nature 2011 478:7368*, *478*(7368), 255–259. https://doi.org/10.1038/nature10408

Toumi, F., Neunlist, M., Cassagnau, E., Parois, S., Laboisse, C. L., Galmiche, J. P., & Jarry, A. (2003). Human submucosal neurones regulate intestinal epithelial cell proliferation: Evidence from a novel co-culture model. *Neurogastroenterology and Motility*, *15*(3), 239–242. https://doi.org/10.1046/j.1365-2982.2003.00409.x

Tutton, P. J. M. (1974). The influence of serotonin on crypt cell proliferation in the jejunum of rat. *Virchows Archiv B Cell Pathology*, *16*(1), 79–87. https://doi.org/10.1007/BF02894066

Van Es, J. H., Sato, T., Van De Wetering, M., Lyubimova, A., Yee Nee, A. N., Gregorieff, A., Sasaki, N., Zeinstra, L., Van Den Born, M., Korving, J., Martens, A. C. M., Barker, N., Van Oudenaarden, A., & Clevers, H. (2012). Dll1+ secretory progenitor cells revert to stem cells upon crypt damage. *Nature Cell Biology*, *14*(10), 1099–1104. https://doi.org/10.1038/NCB2581

VanDussen, K. L., Carulli, A. J., Keeley, T. M., Patel, S. R., Puthoff, B. J., Magness, S. T., Tran, I. T., Maillard, I., Siebel, C., Kolterud, Å., Grosse, A. S., Gumucio, D. L., Ernst, S. A., Tsai, Y. H., Dempsey, P. J., & Samuelson, L. C. (2012). Notch signaling modulates proliferation and differentiation of intestinal crypt base columnar stem cells. *Development (Cambridge, England)*, *139*(3), 488–497. https://doi.org/10.1242/DEV.070763

Vermeulen, L., & Snippert, H. J. (2014). Stem cell dynamics in homeostasis and cancer of the intestine. *Nature Reviews Cancer*, *14*(7), 468–480. https://doi.org/10.1038/nrc3744

Vu, J. P., Million, M., Larauche, M., Luong, L., Norris, J., Waschek, J. A., Pothoulakis, C., Pisegna, J. R., & Germano, P. M. (2014). Inhibition of Vasoactive Intestinal Polypeptide (VIP) Induces Resistance to Dextran Sodium Sulfate (DSS)-Induced Colitis in Mice. *Journal of Molecular Neuroscience*, *52*(1), 37–47. https://doi.org/10.1007/S12031-013-0205-3)

Walsh, K. T., & Zemper, A. E. (2019). The Enteric Nervous System for Epithelial Researchers: Basic Anatomy, Techniques, and Interactions With the Epithelium. *Cellular and Molecular Gastroenterology and Hepatology*, *8*(3), 369–378. https://doi.org/10.1016/J.JCMGH.2019.05.003

Watanabe, N., Mashima, H., Miura, K., Goto, T., Yoshida, M., Goto, A., & Ohnishi, H. (2016). Requirement of Gαq/Gα11 Signaling in the Preservation of Mouse Intestinal Epithelial Homeostasis. *CMGH*, *2*(6), 767-782.e6. https://doi.org/10.1016/j.jcmgh.2016.08.001

Wu, X., Conlin, V. S., Morampudi, V., Ryz, N. R., Nasser, Y., Bhinder, G., Bergstrom, K. S., Yu, H. B., Waterhouse, C. C. M., Buchan, A. M. J., Popescu, O. E., Gibson, W. T., Waschek, J. A., Vallance, B. A., & Jacobson, K. (2015). Vasoactive intestinal polypeptide promotes intestinal barrier homeostasis and protection against colitis in mice. *PLoS ONE*, *10*(5), e0125225. https://doi.org/10.1371/journal.pone.0125225

Xu, C. L., Guo, Y., Qiao, L., Ma, L., & Cheng, Y. Y. (2018). Recombinant expressed vasoactive intestinal peptide analogue ameliorates TNBS-induced colitis in rats. *World Journal of Gastroenterology*, *24*(6), 706. https://doi.org/10.3748/WJG.V24.I6.706

Yam, C. Q. X., Lim, H. H., & Surana, U. (2022). DNA damage checkpoint execution and the rules of its disengagement. *Frontiers in Cell and Developmental Biology*, *10*. https://doi.org/10.3389/FCELL.2022.1020643

Yan, K. S., Janda, C. Y., Chang, J., Zheng, G. X. Y., Larkin, K. A., Luca, V. C., Chia, L. A., Mah, A. T., Han, A., Terry, J. M., Ootani, A., Roelf, K., Lee, M., Yuan, J., Li, X., Bolen, C. R., Wilhelmy, J., Davies, P. S., Ueno, H., … Kuo, C. J. (2017). Non-equivalence of Wnt and R-spondin ligands during Lgr5+ intestinal stem-cell self-renewal. *Nature*, *545*(7653), 238–242. https://doi.org/10.1038/NATURE22313

Yang, K., Trepanier, C. H., Li, H., Beazely, M. A., Lerner, E. A., Jackson, M. F., & MacDonald, J. F. (2009). Vasoactive intestinal peptide acts via multiple signal pathways to regulate hippocampal NMDA receptors and synaptic transmission. *Hippocampus*, *19*(9), 779–789. https://doi.org/10.1002/hipo.20559

Yousefi, M., Li, L., & Lengner, C. J. (2017). Hierarchy and Plasticity in the Intestinal Stem Cell Compartment. *Trends in Cell Biology*, *27*(10), 753–764. https://doi.org/10.1016/j.tcb.2017.06.006

Yu, H. B., Yang, H., Allaire, J. M., Ma, C., Graef, F. A., Mortha, A., Liang, Q., Bosman, E. S., Reid, G. S., Waschek, J. A., Osborne, L. C., Sokol, H., Vallance, B. A., & Jacobson, K. (2021a). Vasoactive intestinal peptide promotes host defense against enteric pathogens by modulating the recruitment of group 3 innate lymphoid cells. *Proceedings of the National Academy of Sciences of the United States of America*, *118*(41), e2106634118. https://doi.org/10.1073/PNAS.2106634118/SUPPL_FILE/PNAS.2106634118.SAPP.PDF

Yu, H. B., Yang, H., Allaire, J. M., Ma, C., Graef, F. A., Mortha, A., Liang, Q., Bosman, E. S., Reid, G. S., Waschek, J. A., Osborne, L. C., Sokol, H., Vallance, B. A., & Jacobson, K. (2021b). Vasoactive intestinal peptide promotes host defense against enteric pathogens by modulating the recruitment of group 3 innate lymphoid cells. *Proceedings of the National Academy of Sciences of the United States of America*, *118*(41). https://doi.org/10.1073/PNAS.2106634118/-/DCSUPPLEMENTAL

Yu, S., Tong, K., Zhao, Y., Balasubramanian, I., Yap, G. S., Ferraris, R. P., Bonder, E. M., Verzi, M. P., & Gao, N. (2018). Paneth Cell Multipotency Induced by Notch Activation following Injury. *Cell Stem Cell*, *23*(1), 46-59.e5. https://doi.org/10.1016/J.STEM.2018.05.002

Yu, X. J., Ren, X. H., Xu, Y. H., Chen, L. M., Zhou, C. L., & Li, C. Y. (2010). Vasoactive intestinal peptide induces vascular endothelial growth factor production in human HaCaT keratinocytes via MAPK pathway. *Neuropeptides*, *44*(5), 407–411. https://doi.org/10.1016/J.NPEP.2010.05.002

Yusta, B., Holland, D., Waschek, J. A., & Drucker, D. J. (2012). Intestinotrophic glucagon-like peptide-2 (GLP-2) activates intestinal gene expression and growth factor-dependent pathways independent of the vasoactive intestinal peptide gene in mice. *Endocrinology*, *153*(6), 2623–2632. https://doi.org/10.1210/en.2012-1069

Zhong, H. L., Li, P. Z., Li, D., Guan, C. X., & Zhou, Y. (2023). The role of vasoactive intestinal peptide in pulmonary diseases. *Life Sciences*, *332*, 122121. https://doi.org/10.1016/J.LFS.2023.122121

Acknowledgments

First and foremost, I would like to thank my supervisor, Dr. Moritz Middelhoff, for giving me the opportunity to start a project in his new lab. I am very grateful for your support, patience, and constant willingness to spread your infectious enthusiasm for science and research. Thank you for always being available for discussions and offering assistance and guidance in the research and writing process of the manuscript, abstracts, and this thesis. I am truly happy to see how the lab has grown over these years, and I wish you and the team a lot of success in the future.

I would like to thank Prof. Dr. Michael Quante for adopting me in his lab at the very beginning of my PhD journey and for making me feel a part of the team. Your expertise and insightful suggestions were invaluable in shaping my project.

I am grateful to the members of my thesis committee, Prof. Dr. Ekin Demir and Prof. Dr. Dieter Saur, for their time and constructive feedback during the meetings, as well as Prof. Dr. Roland Schmid for creating an excellent research environment in the II Med department.

I thank Dr. Rupert Öllinger and Dr. Carlo Maurer for their help with performing and analyzing RNA sequencing experiments. I extend my gratitude to Max Giller from AG Fischer, who taught me how to perform *in vivo* irradiation studies. Thanks to members of CFCA, Linda Bachmann and Ritu Mishra, for their assistance in cell sorting and flow cytometry experiments. Thank you to all other collaborators involved in my project.

Special thanks go to my lab members, Caro, Mohab, Anneke, and Fabian, for being a great team in the final stage of the PhD journey. Thanks a lot to Anastasia for bringing her expertise in irradiation and helping establish *in vitro* irradiation models. I thank Jessica for sharing with me all these long lab days, sharing mouse guts, sharing weekend medium change duties, and sharing our sports passion.

Thanks a lot to Junika, Sebastian, Juliane, and Enric for being the best office mates and for all the chats, advice, and great times together. Thanks to Sebastian and Fabian Kortum for being my teammates in organizing Wednesday seminars and the best PhD retreat.

I would like to thank all members of AG Quante who welcomed me into the lab when I started my PhD. Big thanks go to Theresa and Akanksha for explaining everything, providing all the protocols, showing all the techniques, and for all the fun times we had together. Huge thanks

go to Marcos and Donja, who started in the lab at the same time as me, brightened my working days with all these countless laughs, went together through different struggles, and even shared bib writing sessions at the very end.

Thanks to Kevin, Nirav, Nan, Leeanne, Karyna, Thorsten, Kıvanç, Fränze, Bailing, Ali, Christina, Julia, Lina, Derya, Ludwig, Miguel, Valentina, Li, Andrea, Marie, and other members of II Med for always being friendly, helpful, willing to share advice, lunch, afternoon beer, volleyball or poker game, or a floor Christmas party and for making my time unforgettable and enjoyable.

Last but not least, I am thankful to my friends who are always there for me despite distances, adult life struggles, and world cataclysms. Thanks to my family, my mother, my sister, and бабуся, for all the love and support. Thank you to my fiancé Misha for always being my best example, my best supporter, and my best motivation all these years.